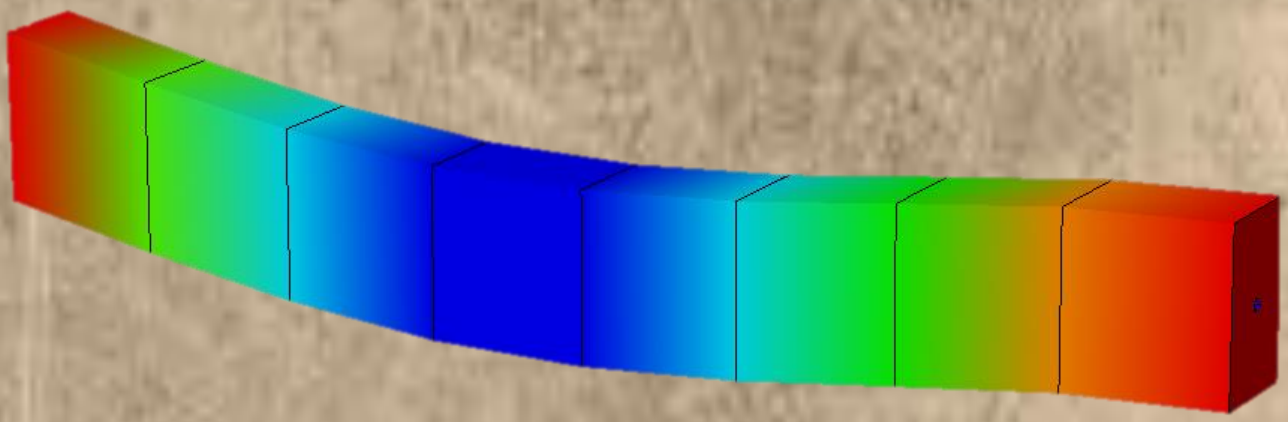

Reliability assessment of ‘simple’ statically indeterminate structures

Master of Science Thesis

Justin de Jong

March 6th, 2018

TU Delft

Reliability assessment of ‘simple’ statically indeterminate structures

By

J. de Jong
4316835

in partial fulfilment of the requirements for the degree of

Master of Science
in Civil Engineering

at the Delft University of Technology,
to be defended publicly on Tuesday March 6, 2018 at 4:00 PM.

The contents of this thesis is solely under the responsibility of the author.

Thesis committee:

Dr. ir. M.A.N. Hendriks, (Chair)	TU Delft
Prof. dr. ir. J.G Rots,	TU Delft
Prof. dr. ir. R.D.J.M. Steenbergen,	TNO
Dr. Ir. Y. Yang,	TU Delft
Ir. P. Evangeliou,	TNO
Ir. A. Roy	TU Delft

This thesis is confidential and cannot be made public until March 6, 2018.

An electronic version of this thesis is available at http://repository.tudelft.nl/.

Preface

This document lays out the Master thesis of Justin de Jong. This Master thesis is a compulsory part of the Master programme Structural Engineering at Delft University of Technology.

This master thesis project was started in April 2017. The inspiration for this subject came from other master theses done by Robin van der Have and Panagiotis Evangeliou. Both of their theses involve probabilistic procedures and where dealing with statically determinate structures. The idea that came to mind was to try to combine probabilistic calculation with statically indeterminate structures.

I would like to thank my entire committee for the useful feedback and input provided during the process. Especially the supervision by dr. Ir. Max Hendriks helped me to keep focussed. I would like to thank Panagiotis Evangeliou for his support during my entire process and help regarding the Finite Element implementation. As well, Anindya Roy has been very helpful for keeping track of the probabilistic calculations and documentation. Therefore, I would like to thank him.

Finally, I would like to express my gratitude towards my family and friends for their support throughout the entire project. Especially, my girlfriend has continuously encouraged me to finalize this thesis.

Delft, March 6, 2018
Justin de Jong

Contents

Abstract

Probability calculations are used to determine the possible failure of civil structures which includes bridges. The Eurocode uses a conservative form of these probability calculations and this could have a negative economic impact. Having said this, more advanced probability calculation methods are developed to decrease the negative economic impact this could have.

Nowadays structural analysis in daily practise is mostly done through the finite element method. The finite element method uses either linear or non-linear structural analysis. The latter mentioned analysis is used for the analysis of materials in which the nonlinear effects have significant impact. However not only finite element analyses are used to determine structural behaviour. Analytical models remain an important tool to examine civil structures. Since the analytical models cannot address all the influences of the nonlinear parameters, conservative assumptions were made.

On the one hand the modern design code uses semi-probabilistic in combination with the analytical model. Finite element analysis together with semi-probabilistic assessment is a possible use for design purposes as well. On the other hand full-probabilistic assessments, are not possible to execute in combination with nonlinear, finite element analyses. The reason for that the computation time becomes too large.

The research question that is tried to answer in this thesis: *"How does a semi-probabilistic compare to a full-probabilistic safety assessment for a statically indeterminate beam structure?"*

The 2-span statically indeterminate reinforced concrete beams that are studied in this thesis find their origin from the research done by Monnier between 1965 and 1970. This research had as goal to see what the influence of shear force would be on the bending capacity. This specific research is chosen because here statically indeterminate beams are dealt with. The experiments' data generated during the execution of the four-point bending test is the starting point of this thesis.

To answer the research question, the components of a reliability model have been investigated. The levels of model approximation (LoA) as stated in the model code 2010 together with the level of reliability calculations (Steenbergen 2011) were used. Two combinations between LoA and reliability methods have been analysed to assess their strengths and weaknesses. These two reliability analyses were both were based on an analytical model (LoA I). The reliability level I and III, the so called semi-probabilistic and full-probabilistic, calculations were used.

In conclusion, the full-probabilistic reliability calculation is all cases applicable to determine the probability of failure of a statically indeterminate structure. However, semi-probability reliability are useful as well but it does allow only partly redistribution of forces. In case of statically indeterminate structures this can have significant impact on the failure load. The best reliability method for a statically indeterminate structure is dependent on the amount of redistribution of forces.

The semi-probabilistic calculations treat structures, where a lot of redistribution can occur, conservatively. For instance, the semi-probabilistic calculation procedure that is used in this

thesis allows for only partly redistribution of forces. The full-probabilistic calculation procedure is therefore beneficial to use for structures where a lot of redistribution can occur in the ultimate limit state.

It turned out that the full-probabilistic calculation determines a higher reliability of the structure. In the full-probabilistic analysis, the limit state function is used in its analytical form. Whereas in the semi-probabilistic analysis is made with the use of approximations of the limit state function. However, when the cross-section of a statically indeterminate structure is designed in such a way that little redistribution will take place, the difference between the full- and semi-probabilistic is insignificant.

Nomenclature

Notation

$\Delta \cdot$	Difference
$\delta \cdot$	Increment

Greek symbols

α	ratio between the length of field and the offset of the force
α_i	weight or sensitivity factor of random variable i
β	reliability index
β_u	arm length of the force in the concrete compressive zone
γ_S	partial factor of the solicitation on the structure
γ_R	partial factor of the resistance of the structure
δ	moment reduction coefficient
ε_{cu2}	ultimate strain in the compressive zone of the concrete
ε'_s	strain of the reinforcement in the compressive zone of the concrete
θ	angle of displaced structure
λ	ratio between the hogging and sagging moment capacity
μ_z	mean value of the limit state function Z
ρ_l	longitudinal reinforcement ratio
σ_z	standard deviation of the limit state function Z
φ	angle of displace structure/rotation capacity
$\Phi(\cdot)$	cumulative density function of the standard normal distribution

Latin symbols

A'_s	cross-sectional area of the top reinforcement in the compressive zone of the concrete

A_s	cross-sectional area of the bottom reinforcement in the compressive zone of the concrete
b	width of the beam
c	uncertainty factor in the shear capacity
d'	concrete cover of the reinforcement in the concrete compressive zone
d	effective depth of the concrete cross-section
E_c	Young's modulus of concrete
E_s	Young's modulus of reinforcement steel
f_{av}	average concrete compressive strength in the concrete compressive zone
f_c	concrete's compressive strength
f_y	yield stress of the reinforcement steel
F_c	internal force of the concrete compressive zone
F_p	external force acting on the structure
F'_s	internal force of the reinforcement in the concrete compressive zone
F_s	internal tensile force of the reinforcement
I	moment of inertia
l	span length
M_{ED}	design moment caused by the external forces
M_f	segging moment capacity at the span of the structure
M_{rd}	design moment capacity of the cross-section
M_s	hogging moment capacity at the mid-support of the structure
$P(F)$	probability of F
Pf	probability of failure
F_X	variable F with the probability density function of X
$Var[F]$	variance of F
$V_{P(F)}$	coefficient of variation of probability of F
R_k	characteristic value of the resistance part of the limit state function
S_k	characteristic value of the solicitation part of the limit state function
V_{rd_c}	the design force capacity of shear force resistance without shear force reinforcement
$V_{rd_{max}}$	the maximum design resistance for shear failure
x_u	height of the concrete compressive zone

Z	limit state function

Abbreviations

cdf	cumulative density function
cov	coefficient of variation
DIANA	Displacement Analyzer, finite element programme
FE	finite element
FEA	finite element analysis
FEM	finite element method
FORM	first order reliability method
MCS	Monte Carlo Simulation
NLFEA	nonlinear finite element analysis
PDE	partial differential equation
PDF	probability density function
SLS	Serviceability limit state
SORM	second order reliability method
ULS	Ultimate Limit State

1 Introduction

1.1 Background

Probability calculations are used to determine the possible failure of civil structures which includes bridges. The Eurocode uses a conservative form of probability calculations and this could have a negative economic impact. Having said this, more advanced probability calculation methods are developed to likely decrease this economic impact.

Concrete bridges, build in The Netherlands after the Second World War, were made with a life expectancy of approximately 100 years. In general, large civil structures are designed to have this lifespan. It is hard to predict on forehand what the condition will be of the structure after such a long time. At the time the concrete bridges were designed, people knew that cars would become the main form of transportation . Additionally, the weight of the vehicles would increase during the lifetime of these bridges.

The last statement is support by the website: https://www.autosnelwegen.nl/index.php/geschiedenis/7-1959-1973-massamotorisatie. In Figure 1.1 the expected development of transportation by people in 1950 is from this website. It displays the forecast of the development of transportation made in 1950. More specifically Figure 1.1 focusses on the transportation by car, bike, motorbike, public transport and walking.

Figure 1.2 shows the travelled kilometres in the year 2002 and the forecast of the travelled kilometres in 2040 based upon certain economical scenarios. Figure 1.2 shows that the prognosis of the traffic intensity in 2002 was already higher than expected. Note: in Figure 1.1 and Figure 1.2 use different categories to divided the groups of travellers.

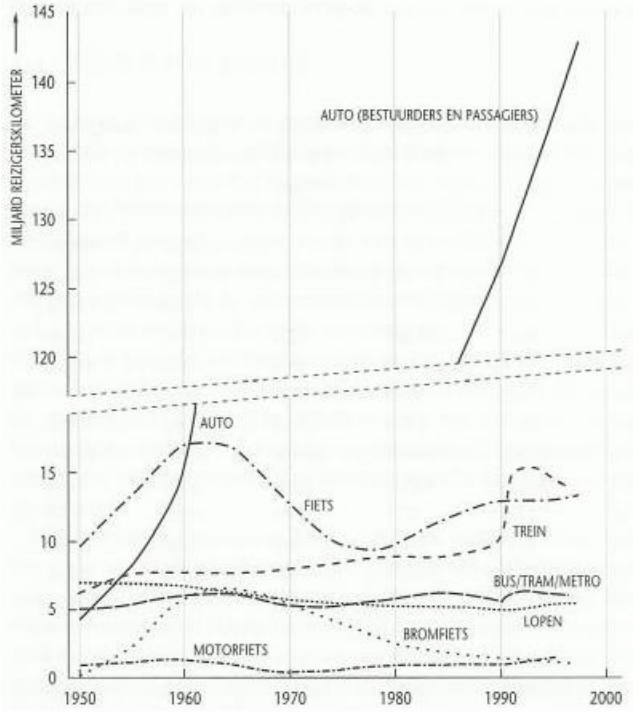

Figure 1.1 expected development of transportation of people in 1950

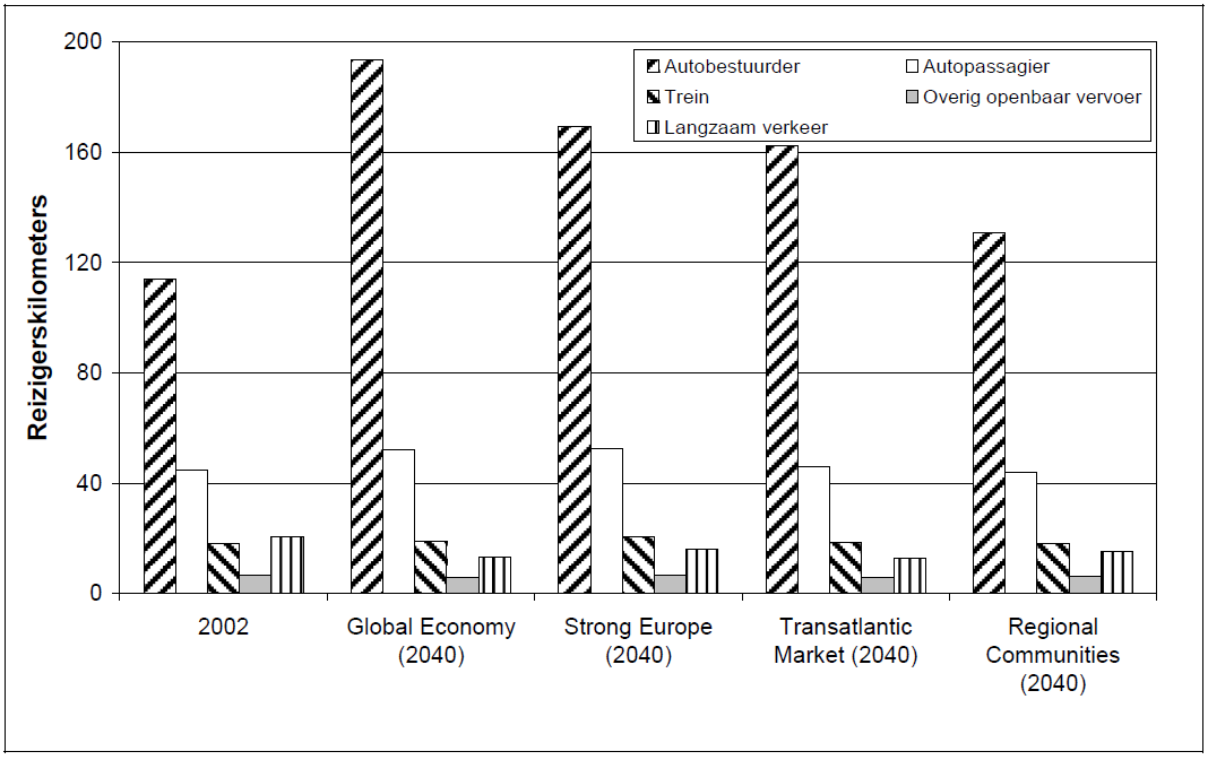

Figure 1.2 prognosis of the mobility, based on different scenarios (billion travel kilometres) (Janssen, Okker et al. 2006)

"Rijkswaterstaat" published a survey in 2007, which stated the results of a four-year investigation into the Dutch bridges' conditions. Out of 654 bridges that were investigated in the period of 2002-2005, 21% of the bridges were not sufficiently safe according to the specified safety rules. ("Inventarisatie kunstwerken", RWS, 2007). As of today, a large number of Dutch bridges have reached the point where the safety is not sufficient any longer according to the specified safety rules. Hasten to add that in the near future the expected traffic load on bridges is to increase even further. In April 2017 "Kennisinstituut voor mobiliteitsbeleid" (transl. English: "the knowledge centre for mobility policy") has published a report with the expectations for the coming 5 years. Based on the increasing economically position of the Netherlands, an rise of traffic intensity of 6.3% on average is expected and even 8.2% on the motorways in 2022 ("Trendprognose wegverkeer" 2017-2022 voor RWS, KIM, 2017). In Figure 1.2 is a prognosis presented, which is based on various scenarios. (Janssen, Okker et al.) expect an increase of 100% in 2040 in the most extreme case.

The lack of knowledge about the urge of maintaining or replacing the bridges in a critical state has been the motivation to start researches in this specific field. At the same time, this lack of knowledge causes a lot of uncertainties in the asset management of "Rijkswaterstaat" (RWS). RWS does not know whether to reserve funds towards the replacement of the bridges or not to. To start the research in the latter mentions field of interest, researchers have touched upon several topics with respect to the reliability calculations. The model approximation and the reliability calculation method have tried to obtain optimal results. The focus of the investigations was mainly on statically determinate structures.

1.2 Motivation

As introduced in paragraph 1.1 , the former investigations in regards to reliability calculation were mainly focussed on statically determinate structures. Not only are there statically determinate structures but statically indeterminate structures as well. Therefore, statically indeterminate structures will be looked at. The goal is to provide more information about the reliability calculations for statically indeterminate structures.

More specifically, this will be concentrated on two span beams. The force flow in such a structure is still simple to check with hand calculations. As a matter of fact, the spans of a bridge are modelled in a similar way. This means, the design of a bridge deck is more sophisticated, although the approximation of a multiple span beam is getting the model closer to reality.

Hand-calculations are extremely important in the engineering field, it gives the engineer a quick check of the calculation that has been done. The most part of the design calculation of complex structures are done by computer. These computer calculations are done with finite element software. Both analytical and finite element analyses are investigated and in this thesis the following research question will be answered:

"How does a semi-probabilistic compare to a full-probabilistic safety assessment for a statically indeterminate beam structure?"

To state how the two safety assessments differ, "Python" is used to simulate an experiment. "Python" is a numerical software package capable of executing given algorithms. The simulated experiment is based upon another experiment which was done in a laboratory. The laboratory experiment was done by Monnier between 1965 and 1970 and this experiment is chosen as a stepping stone, since the tested structure was a statically indeterminate beam. These experiments are rarely performed and that is why this experiment will be investigated in this thesis. In chapter 3 of this thesis, Monnier's experiment is summarised since it has significant importance for this thesis.

1.3 Scope of the thesis

This thesis' objective is to compare a full-probabilistic safety assessment with a semi-probabilistic one. There will be looked computation time and accuracy of the safety assessment.
The experiment in this master thesis has the following boundaries:

- Only statically indeterminate beams in reinforced concrete, with the same dimensions as the beams in the experiment done by Monnier will be looked at;
- Bending failure and shear failure will be investigated independent from each other;
- The material parameters will not differ along the beam;
- The material properties are the same as specified in Monnier's experiment;
- Only sensitivity calculations will be used in combination with the NLFEA;
- The analytical model will be evaluated with reliability calculation procedures;
- The load acting on the structure is not simulated as a random variable but as a deterministic value.

1.4 Approach & outline of thesis

To answer the research question, two different approaches will be followed in this project: an analytical one and a numerical one. The analytical approach is based on a study of reliability methods explained by (Jonkman, Steenbergen et al. 2015) and structural approximations given in (MC2010). The reliability methods are used for the general evaluation of structures and are adopted in the European construction code as well. The structural approximations are used in this thesis as guideline for the mechanical simplification in the structural model. In particular, the constitutive relations of the material parameters are simplified in the model approximations. The analytical model is built in “Anacoda’s Python”. “Python” is specifically used for modelling the statically indeterminate reinforced concrete beam and evaluating its failure modes.

The numerical approach consists of building a model like the one in “Python”. With “FEA DIANA” (a finite element programme) it is possible to analyse several non-linear effects. These non-linear effects are complicated to implement in the “Python” code. “FEA DIANA” has convenient tools for taking into account nonlinear effects. Furthermore, a sensitivity analysis is carried out to state the influences of the nonlinear effect on the beam. At the end of the investigation, the results obtained with the analytical model and the numerical model are compared. These results are compared with the Eurocode.

The comparison between the analytical and the numerical model in combination with reliability methods are fundamental to give a well-thought out answer to the research question.
The report of the project is structured in the following chapters:

Chapter 2 presents a detailed description of the reliability methods described by (Jonkman, Steenbergen et al. 2015) on which both the numerical and the analytical reliability models are based. The fundamental differences between the statically determinate structure types and the statically indeterminate beams types are studied.

Chapter 3 consists of a summary of the fundamental experimental done by Monnier in 1970 which is used as a stepping stone for the set-up of the analytical and numerical model. The results of the Monnier’s experiments are explained.

Chapter 4 presents the analytical model build in “Python” this includes: assumptions, model boundaries, and results generated by the model. The results are given by a parameter study and calculating the maximum deterministic force. After this the results are compared with the governing Eurocode.

Chapter 5 presents assumptions and the model boundaries that are used in “FEA DIANA”. The results of the numerical model are reported in this chapter. The results of the sensitivity study are presented in this chapter.

Chapter 6 reports the interpretation of the results and it provides answers to the research question.

Chapter 7 contains several concluding comments and suggestions for future work.

2 Methods

Chapter 2 is build up out of four main topics: statically indeterminate structures, level of approximation, reliability calculations and uncertainties. First statically indeterminate structures are defined as well as the differences between statically indeterminate and determinate structures in plasticity calculations. Thereafter levels of approximation of structural models and reliability calculations are discussed. The combination between model approximation and reliability calculation gives the calculation methods. At the end of this chapter uncertainties in the calculations that will be done are discussed.

2.1 Statically determinate and statically indeterminate structures

Statically determined structures are characterised by their force distribution which follows directly from the equilibrium equations. Meaning that there is an equal amount of equilibrium equations and unknown reaction forces. The reaction forces are calculated by solving the system of equations. In the case a structure with less unknown forces than equilibrium equations, this is called kinematical indeterminate and is by definition not stable. In the last possible case the number of known reaction forces is bigger than the number of equilibrium equations. This type of structure is called statically indeterminate which entails that having only the equilibrium equations are not enough to determine the force flow in the structure. (Hartsuijker and Welleman 2003)
An example of a statically indeterminate structure is a continuous beam over multiple (more than two) supports. To calculate the reaction forces for a statically indeterminate structure, the stiffness relations have to be taken into account.

To clarify the behaviour of structures before collapsing, the theory of plasticity is necessary. In plasticity, the assumption is that all rotations are captured in so-called plastic hinges and the rest of the structure remains rigid. A plastic hinge develops at a point in a beam structure where the yield strength is reached. After the yield strength has been reached, the stress does not increases further, however the strain keeps increasing. When this kind of hinge occurs, this hinge is called a plastic hinge. When the structure has developed more plastic hinges then the degree of internal indeterminacy, it will fail. Since statically determined structures have a degree of internal indeterminacy of zero, it means that the first plastic hinge causes failure. For statically indeterminate structures this is much more complex.

Firstly, if there is a statically indeterminate structure with a degree of internal indeterminacy equal to one and there are two plastic hinges developed, the structure fails. Moreover, when the first plastic hinge occurs, the maximum moment capacity of the structure in that specific point is reached. In order to carry more load, the structure has to redistribute the internal forces. Since the structure cannot allow more stress when the steel in the reinforced beam starts to yield. This means that the deformation/rotation increases, but the resistance capacity stays the same. The steel needs to have yield capacity, only then the forces can be redistributed. The load can be increased until the second plastic hinge has fully developed and at this time the structure fails. When this process happens, assumption is that the rotation capacity of the plastic hinge is ensured. Rotation capacity will be further explained in chapter 2.3.

Secondly, there is a possibility that a local failure mechanism can occur as well. However in this thesis the attention is focussed only on two span continuous beams. Local failure is highly unlikely to happen in this type of structures.

This characteristic behaviour of redistribution of forces when a plastic hinge develops is very useful in ultimate limit state (ULS). Nonetheless this phenomenon does not only help to increase the magnitude of the collapse load but, it also makes the non-linear computer calculations rather complex. Yet, it is vital that the model has a very accurate representation of the real situation because the redistribution of forces can be totally different if one part of the structure is made too strong or weak. This will be one of the main challenges in the master thesis.

2.2 Levels of approximation for structural analyses

An engineering model is always intended to simulate the physical reality. The more physical effects and aspects are considered, the more sophisticated the model will be. Levels-of-approximation are developed for engineers by (MC2010) to consistently use different model accuracies. There are four Levels-of-Approximation (LoA) for structural analyses according to the (MC2010). The higher the LoA is, the better it simulates reality.

LoA I is an approximation which is mostly simple and conservative therefore it is often used for preliminary designs. The hypotheses of the physical parameters are safe although realistic as well. Besides the approximation being simple and conservative it is low time consuming, which is an advantage. The disadvantage is that the structure is often over-designed and therefore not economic.

LoA II and LoA III are not used in this thesis, but they will be touched upon briefly. These LoAs are still low time-consuming and have simplified formulas for physical parameters. Additionally, these LoA have simplified analytical formulas for internal forces, geometrical- and other mechanical parameters. This makes these LoAs slightly more accurate than LoA I.

LoA IV is mainly based on numerical procedures. It is the best estimation of reality and is therefore advised for the final design of very complex structures. Although LoA IV is the most accurate, it is at the same time the most time consuming. This latter addressed drawback should be considered before performing such an analysis. In Figure 2.1 we see the relationship between the devoted time versus accuracy. This figure is taken from the Model Code 2010.

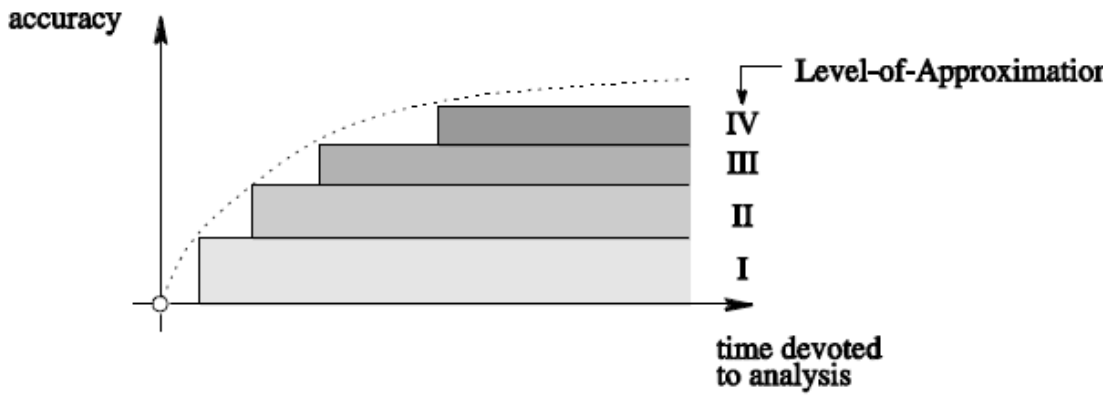

Figure 2.1:Accuracy on the estimate of the actual behaviour as a function of time devoted to the analysis for various Levels-of-Approximation (Model Code 2010)

The chosen LoA together with the reliability methods, that will be discussed in the next paragraph, form the analysis procedure followed in this thesis. In regards to the LoA, only Level I and IV will be used in the thesis.

2.2.1 Hand calculation's analysis

LoA I is used to perform a hand calculation. This hand calculation is extremely useful to keep track of the force flow within the structure. Having a comparison makes the verification of a numerical model much easier. In addition this hand calculation will use the stress-strain assumptions applied in the Eurocode. Not only is the assumption very accessible, because the relation is simple to derive, but it is consistent with the governing rules in structural design as well.

2.2.2 Finite element analysis

Even though a (nonlinear) finite element analysis (Level IV of approximation) is rather time consuming, it provides a more accurate result. This way it is easy to incorporate nonlinear behaviour in the calculation. To perform a finite element analysis, "DIANA" is used. "DIANA " is a software programme able to evaluate given models by using the finite element method.

The finite element method (FEM) is a numerical method for solving partial differential equations. It is particularly suited for solving partial differential equations on complex geometries, as are commonly encountered in solid and structural mechanics. The procedure can be largely automated making it well suited to efficient computer implementation. The application of the finite element method leads to systems of linear equations which can be solved using a computer. (Wells 2006)

The partial differential equation (PDE) that describes the behaviour of the structure is solved in the following way:

First, the strong form of the PDE must be known. The strong form describes the behaviour of the solid body precisely.
Second, by reducing the number of derivatives, the weak form can be derived. The weak form of the PDE is convenient to solve numerically.

Third, the domain of the PDE is divided into small parts, finite elements. This finite element mesh is the discretised form of the PDE. The PDE can now be solved for the nodes of the finite elements. By using shape functions, the solution is extended over the entire model.
Fourth, the displacement field is the fundamental unknown in the PDE and therefore the minimising of errors in the displacement field is crucial. This method is called the Galerkin approximation.
Fifth, when the displacements are known, all other internal forces can be derived from there.

$$\boldsymbol{Ku - f = 0} \qquad (2.1)$$

For nonlinear analyses incremental displacements and -forces are used. The constitutive relation in every increment can be updated because of this. Through this the nonlinear effects are evaluated in a consistent way.

$$\boldsymbol{K\Delta u = f_{ext}^{t+\Delta t} - f_{int}^{t}} \qquad (2.2)$$

Published literature indicates that nonlinear effects have to be taken into account. There is stated that:
The linear elastic material behaviour of the structural analysis is a gross simplification, especially for concrete structures. This can lead to a modelled structural response and internal force distribution that deviates significantly from reality. (Schlune, Plos et al. 2012)

Non-linear analysis are widely used, mostly this refers to the non-linear stress-strain relation. The yielding of the steel and cracking of the concrete is considered during this type of analysis. To better take into account, the real physical behaviour of reinforced concrete, non-linear finite element analyses (NLFEA) could be carried out. The results of such analyses are global in nature due to all sections contributing to the load carrying capacity. (Engen, Hendriks et al. 2017)

2.3 Reliability methods

This paragraph talks about the 5 different levels of reliability methods. However, just three out of five methods are used in this this thesis. In this paragraph the mathematical procedure behind the different reliability calculations is derived.

Reliability methods are procedures used to determine the probability of failure of structures. To use reliability methods input parameters are necessary. The parameters which are expected to vary are:

- Geometry;
- Material parameters;
- Loading.

In this theses $\underline{x}$ is denoted a set of all random variables and $\boldsymbol{R}$ would be the structural response to these input.

$$\boldsymbol{R} = \boldsymbol{R}(\underline{x}) \tag{2.3}$$

The structural response is used to determine the probability of failure. A limit state function (LSF) is introduced as g. The following condition of the LSF will indicated the safety of the structure.

- $Z = g(\boldsymbol{R}) > 0$, no failure
- $Z = g(\boldsymbol{R}) \leq 0$, failure

The probability of failure (P_f) is then found by using:

$$P_f = \int_{g(\boldsymbol{R})<0} f_x(\boldsymbol{R}) * d\boldsymbol{R} \tag{2.4}$$

In which, $f_x(\boldsymbol{R})$ is the joint probability density function (PDF).

The levels for reliability methods are divided in five levels and they will be addressed briefly:

- **Level IV**: risk based method, here the economic impact is also considered;
- **Level III**: the most accurate method, in this level one of the following analysis procedures is used: analytical integration (if possible), numerical integration or Monte Carlo simulation;
- **Level II**: calculations for this level are characterised by the approximation of the limit state function, probability function or other component of the calculation. The approximation of the limit state function is mainly done by Taylor series;
- **Level I**: semi-probabilistic methods, using characteristic values, level I calculations are used in the Eurocode. The most well-known aspect of these calculations are the partial factors;
- **Level 0**: deterministic calculation, this is not really a reliability calculation since probabilistic methods are not considered.

The levels I, II and III will be used in the thesis and therefore these levels will be explained in more detail. The Levels will be explained in descending order because in this way the approximation by decreasing one level is better understandable.

2.3.1 Level III reliability calculations

Level III reliability calculations are the most accurate reliability calculations used in this thesis. Monte Carlo simulation is an example of a level III reliability calculation. The Monte Carlo simulation is used to generate random draws from each parameter's distribution. If the analytical expressions contain independent normally distributed variables for resistance and acting force, then the explicit method can be used:

$$\mu_z = \mu_r - \mu_s \tag{2.5}$$

$$\sigma_z = \sqrt{\sigma_r^2 + \sigma_s^2} \tag{2.6}$$

$$\beta = \frac{\mu_z}{\sigma_z} \tag{2.7}$$

$$P_f = P[z < 0] = \Phi\left[\frac{0 - \mu_z}{\sigma_z}\right] = \Phi[-\beta] \tag{2.8}$$

The explicit method evaluated the safety of the structure much faster. The Monte Carlo simulation makes use more sophisticated method of random draws from the distributions of each parameter.

$$\begin{aligned} F_X(X) &= X_u \\ X &= F_x^{-1}(X_u) \end{aligned} \tag{2.9}$$

Where: F_X^{-1} is the inverse of the cumulative density function of random variable X. X_u is a uniformly distribute random variable between (0-1).

If the limit state function has n random variables, then:
$X_i = Vector(X_1, \dots, X_n)$

And we assume N simulations:
$j = set(1, .., N)$

This gives the limit state function of $z_j(\underline{x})$:
$z_j(\underline{x}) = z(x_{1j}, x_{2j}, \dots, x_{nj})$

In case ($Z_j < 0$) then, N_f is increased by one. And therefore:

$$P_f = \frac{N_f}{N} = \frac{1}{N} * \sum_{j=1}^{N} I\left[z_j(\underline{x}) < 0\right] \tag{2.10}$$

Theoretically, an infinite amount of simulations is necessary to create an exact solution. Infinite simulations are not possible to perform. The accuracy of the probability of failure can be calculated by approximating the coefficient of variation. To do this, the variation of the probability of failure needs to be known.

$$Var[P_f] = \frac{1}{N} * P_f * (1 - P_f) \qquad (2.11)$$

When the variation of the probability of failure are known, the variation coefficient can then be determined.

$$V_{P_f} = \frac{\sqrt{Var[P_f]}}{P_f} = \sqrt{\frac{1 - P_f}{N * P_f}} \qquad (2.12)$$

If the probability of failure is small, expression (2.12) can be approximated by:

$$V_{P(F)} \cong \sqrt{\frac{1}{N * P_f}} \qquad (2.13)$$

2.3.2 Level II reliability calculations

In **level II** methods only the mean values of the basic variables and the moments of first and second order (covariance matrix) are used in most cases. The joint probability density function is simplified, and the limit state function is linearized in the design point, i.e. the point on the hyperplane ($Z = g(\boldsymbol{R}) = 0$) in normal space where with the highest probability density (FORM or SORM). The FORM elaboration will be explained in more detail. If the limit state function is a linear function of random variables, then the level II calculation can represent the limit function exact, namely:

$$Z = a_1 * X_1 + a_2 * X_2 + \cdots + a_n * X_n + b \tag{2.14}$$

With the following mean value and standard deviation:

$$\mu_Z = a_1 * \mu_1 + a_2 * \mu_2 + \cdots + a_n * \mu_n + b \tag{2.15}$$

$$\sigma_Z = \sqrt{\sum_{i=1}^{n}\sum_{j=1}^{n} \sigma_i * a_i * \sigma_j * a_j * COV(X_i, X_j)} \tag{2.16}$$

However, when the limit state function is not linear, the Taylor series is used. It is very common to use the mean values of the random variable as initial guess of the design point. The design point is the point on the limit state function with the highest probability of failure. This point is not as easy to find as it is for linear limit state functions. When the mean values are used as guess this will result in the following equation:

$$z(\underline{X}) = Z \cong z(\mu_1, \mu_2, \dots, \mu_n) + \sum_{i=1}^{n} \frac{\partial z\left(\underline{\mu}\right)}{\partial X_i} * (X_i - \mu_i) \tag{2.17}$$

With:

$$\mu_Z \cong z(\mu_1, \mu_2, \dots, \mu_n) \tag{2.18}$$

$$\sigma_Z \cong \sqrt{\sum_{i=1}^{n}\sum_{j=1}^{n} \frac{\partial z\left(\underline{\mu}\right)}{\partial X_i} * \sigma_i * \frac{\partial z\left(\underline{\mu}\right)}{\partial X_j} * \sigma_j * COV(X_i, X_j)} \tag{2.19}$$

With the mean value and the standard deviation of the random variables, the probability of failure can be calculated. In (2.17) the Taylor series has only 2 terms which implies that the approximation is linear. If the limit state function turns out to be linear, the probability of failure can be determined exactly. However, a non-linear limit state equation should be approximated by the Taylor series and an initial guess of the location of the design point must be done. The first elaboration of FORM will probably is not be sufficient. But after updating the guess of the design point, the later elaborations will give better results.

$$\beta = \frac{\mu_z}{\sigma_z} \tag{2.20}$$

$$\alpha_i = \frac{\partial z\left(\underline{\mu}\right)}{\partial X_i} * \frac{\sigma_i}{\sigma_Z} \tag{2.21}$$

With this alpha value, the new guess of the design point can be done. This new guess will be indicated with μ_i^*.

$$\mu_i^* = \mu_i - \alpha_i * \beta * \sigma_i \tag{2.22}$$

After this the procedure continues with the following loop (all updated values will be indicated with a star):

$$Start;$$

$$\mu_Z^* \cong z(\mu_1^*, \mu_2^*, \dots, \mu_n^*) + \sum_{i=1}^{n} \frac{\partial z\left(\underline{\mu^*}\right)}{\partial X_i} * (X_i - \mu_i^*) \tag{2.23}$$

$$\sigma_Z^* \cong \sqrt{\sum_{i=1}^{n}\sum_{j=1}^{n} \frac{\partial z\left(\underline{\mu^*}\right)}{\partial X_i} * \sigma_i * \frac{\partial z\left(\underline{\mu^*}\right)}{\partial X_j} * \sigma_j * COV(X_i, X_j)} \tag{2.24}$$

$$\beta^* = \frac{\mu_z^*}{\sigma_z^*} \tag{2.25}$$

$$\alpha_i^* = \frac{\partial z\left(\underline{\mu^*}\right)}{\partial X_i} * \frac{\sigma_i}{\sigma_Z^*} \tag{2.26}$$

$$\mu_i^* = \mu_i - \alpha_i^* * \beta^* * \sigma_i \tag{2.27}$$

$$stop\ criterium\ satisfied?\ Yes => Stop;\ No => Go\ To\ Start;$$

After having determine the new design point, the whole procedure must be done over again with the new guess. The procedure keeps repeating until the difference between the guess of the design point and the updated point is sufficient small. Sufficient small should be defined by the user of the method. Furthermore, the probability of failure can be calculated from the last obtained beta value by using equation:

$$P_f = \Phi[-\beta^*] \tag{2.28}$$

2.3.3 Level I reliability calculations

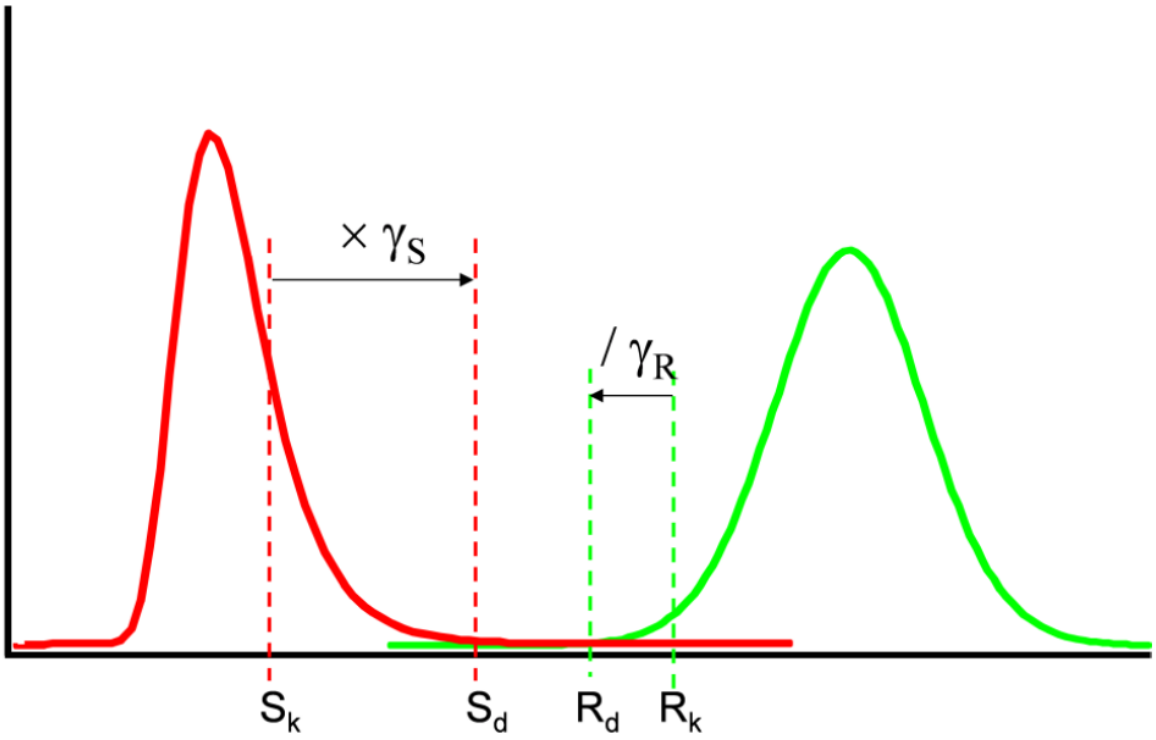

Figure 2.2 Probability density functions showing the variations in load (red, left) and resistance (green, right)

The last level of reliability method explained in detail in this thesis is **level I** also known as semi-probabilistic reliability method. This level I method aims to evaluated the reliability of a structure with limited analyses. These reliability calculations make use of characteristic values and partial factors based on level II calculations. There is a mutation of the limit state function used in this semi-probabilistic approach, namely:

$$\frac{R_k}{\gamma_R} > \gamma_s * S_k \qquad (2.29)$$

In this inequality the subscript 'k' indicates that the parameter contains the characteristic value. The characteristic values of the resistance are defined as the value with a non-exceeding probability of 5%. The characteristic value of the solicitation is defined as the value with a non-exceeding probability of 95%. The gamma values are the earlier introduced as partial factors. These partial factors are depending on the target reliability and the coefficient of variation. The effect of the characteristic and partial factors is graphically showed in Figure 2.2. The characteristic values are determinate according to the following formulas:

$$R_k = \mu_R - k_R * \sigma_R \qquad (2.30)$$

$$S_k = \mu_S - k_S * \sigma_S \qquad (2.31)$$

With:

$$k_i = \alpha_i * \beta \qquad (2.32)$$

Formulae (2.30) and (2.31) are similar to formula (2.22) in the level II calculation. However, the alpha values and the reliability index needs to be known beforehand. The current Eurocode recommend the following alpha values for the dominant variables:

$$\alpha_R = 0.8$$
$$\alpha_S = -0.7$$

The beta value (reliability index) has the same definition as in the level III and level II calculations, in fact the reliability index is a target value from the Eurocode. In the Eurocode, there are several consequent classes which give the corresponding beta values. The partial factors account for the reliability index in the different consequent classes. Furthermore, there are gamma values for both the resistance and solicitation part of inequality (2.29). The resistance gamma factor is based on the material(s) used in the structure. Examples are:

$$\gamma_c = 1.5\ (concrete)$$
$$\gamma_s = 1.15\ (steel)$$

These numerical values for the resistance partial factors come from several tests done with multiple specimens with different properties. The model uncertainty is considered and it is accounted for in the resistance partial factor. The values are conservative because the values need to hold in several situations. The gamma values at the solicitation side are based on the level II method. For instance, the partial factor for a permanent load: (assumed CC2 designed for 50 years, coefficient of variation of 8% according Eurocode)

$$\gamma_g = \frac{g^*}{G_k} = \frac{\mu_G - \alpha_S * \beta * \sigma_G}{\mu_G} = 1 + 0.7 * 3.8 * V_G = 1 + 2.66 * V_G = 1 + 2.66 * 0.08 = 1.2$$

In a similar way the partial factor for the variable loads can be derived. Moreover, it is important to be aware of which partial factors should be used in which situation. When all the partial factors are known, inequality (2.29) must be satisfied. The probability of failure is based on the beta value which already given in the Eurocode. Therefore, the probability of failure is known before hand and the check is whether the inequality holds.

2.4 System analysis of a two-span beam

Besides the possible reliability methods, one must look at the system failure. Considering that this thesis will be deal with a statically indeterminate structure, the failure modes will include multiple events. The event tree and the corresponding limit state function are introduced at the end of this paragraph.

The focus of this thesis is on the reliability calculations of a statically indeterminate structure. Reliability calculations are based upon the failure probability of a system. The components of such a system can be displayed in a fault tree. But before a fault tree analysis can be performed, the possible ways in which the system can fail has to be clarified. In order to do that, it is useful to start off with a system analysis. Thereafter the failure modes and effects are analysed. When all of the previous parts are completed, the final fault tree with the probability of failure can be determined. (Jonkman, Steenbergen et al. 2015)

The failure system of a statically indeterminate beam is quite complex. In principle, the beam fails when the solicitation force is bigger than the resisting force. From this observation the limit state function, $Z = R - S$ where the structure fails if Z is smaller than zero, is used to determine whether this happens or not, see also Figure 2.3 the compound event. There are 2 main categories that must be investigated: the solicitation and the resistance denoted respectively as, S and R.

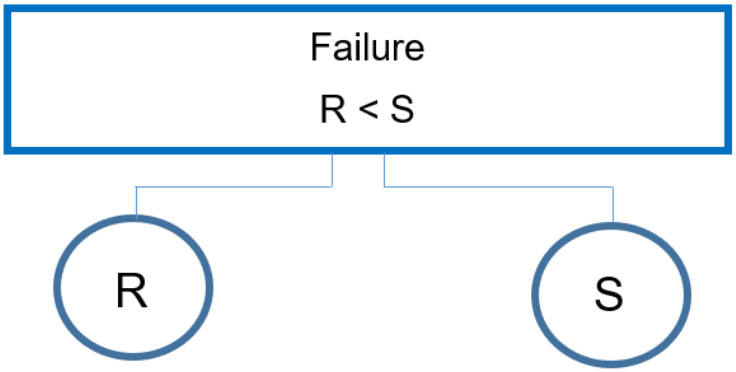

Figure 2.3 the compound event of failure

The resistance and the solicitation are depending on input parameters. The probability of failure of the beam in Figure 2.4 is depending on certain events that must happen. Assumed is that the beam can develop plastic hinges at only three locations along the beam (as indicated in Figure 2.4). On top of that, the beam can fail when the shear force exceeds the shear capacity.

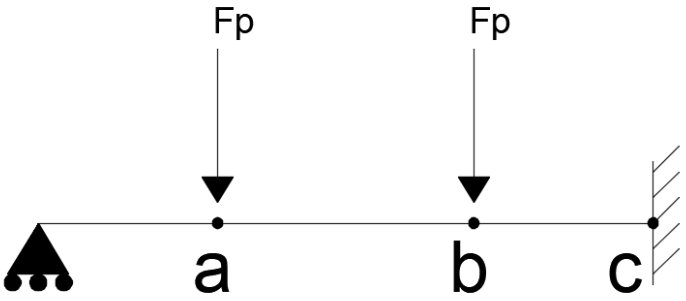

Figure 2.4 possible locations of plastic hinges

The beam will fail when either the shear force is exceeded, or more than one plastic hinge will develop. Therefore, the following system can be made.

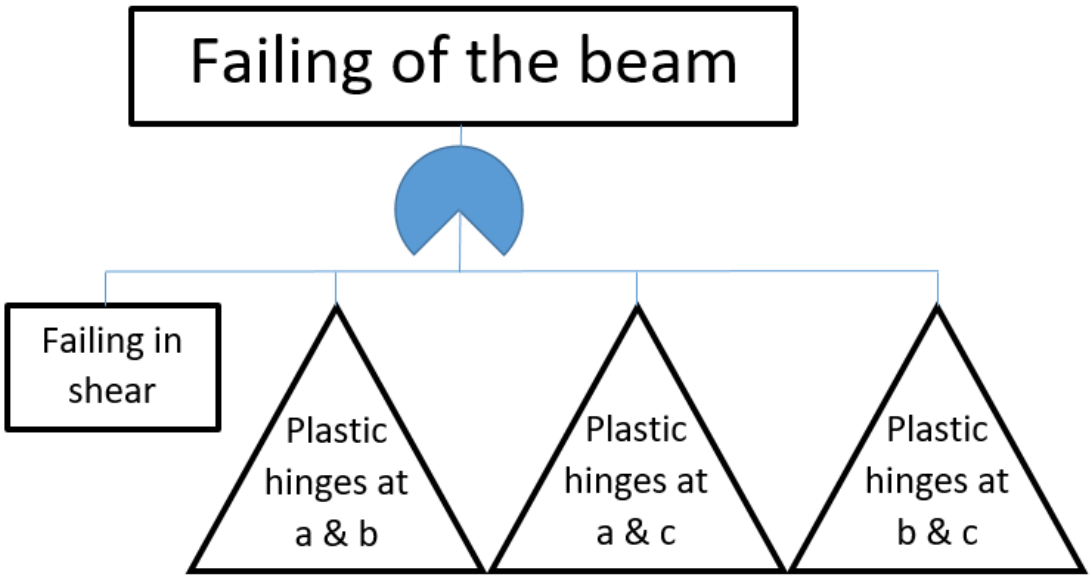

Figure 2.5 fault tree

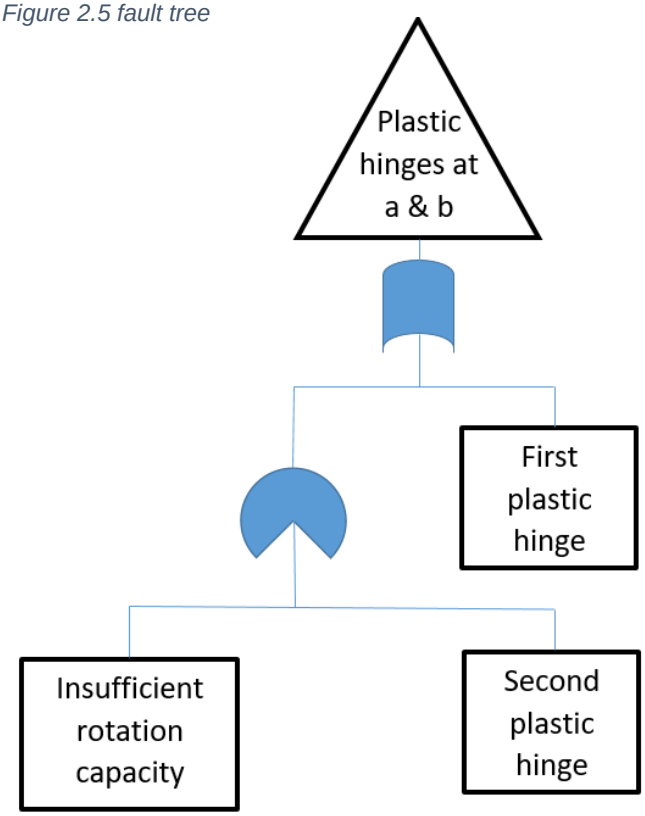

Figure 2.6 fault tree

Throughout the system presented in Figure 2.5 and Figure 2.6, the probability of system failure can be determined. The assumption that there is no correlation between shear and bending failure is made. This simplification avoids interaction between the failure modes. When there is a correlation coefficient unequal to zero, the reliability index is harder to determine. The Gaussian copula is used to describe the behaviour of the interaction between the failure modes. Often the Ditlevsen method is used to determine the upper and lower bound of the reliability index.

It will turn out that the location where the bending moment exceeds its capacity is different from the location of shear force capacity exceedance. Therefore the parameters in the locations is different from each other and thus there is no correlation.

Note that the three reference symbols in Figure 2.5 all have the same continuation as presented in Figure 2.6. In expression (2.33) the letter P is used to indicate the probability of developing a plastic hinge and the letter in brackets after the P indicates the location along the beam according Figure 2.4. Moreover, there is one exception because with P(s) the probability of failure in shear is meant. Furthermore, Pf stands for probability of system failure.

$$Pf = P(s) \cup \big(P(a) \cap P(c)\big) \cup \big(P(b) \cap P(c)\big) \cup \big(P(a) \cap P(b)\big) \tag{2.33}$$

2.4.1 Parallel system failure

There are three events with respect to bending in the system, these events have a certain probability. In this paragraph the possible relationship between the occurrence of the events is pointed out.

The three possible parallel systems are:

- Plastic hinges at a and c (Figure 2.7)
- Plastic hinges at b and c (Figure 2.8)
- Plastic hinges at a and b (Figure 2.9)

The probability of failure in case of one of these events occurs, is determinate in the following way:

Case 1 plastic hinge at a and c

In this calculation M_f is the moment capacity in the positive or field moment and M_s is the moment capacity of the negative or support moment.

$$\delta\theta * \alpha l = \delta\varphi * l * (1-\alpha)$$
$$\delta\varphi = \delta\theta * \frac{\alpha}{1-\alpha} \quad (2.34)$$

$$\lambda = \frac{M_f}{M_s} \quad (2.35)$$
$$M_f = \lambda * M_s$$

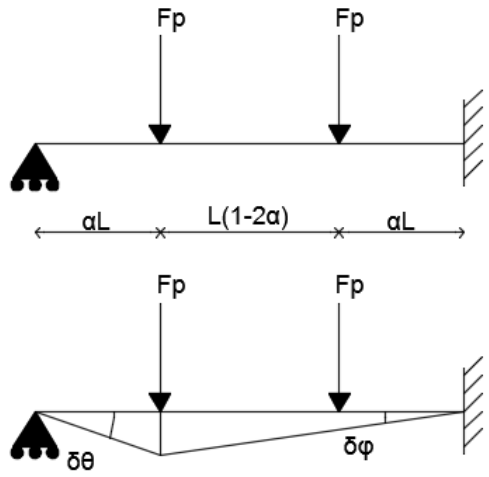

Figure 2.7 Plastic hinge at a and c

Virtual work:

$$F_p * \delta\theta * \alpha l + F_p * \delta\varphi * \alpha l = \lambda * M_s * (\delta\theta + \delta\varphi) + M_s * \delta\varphi$$

$$F_p * \delta\theta * \alpha l * \left(1 + \frac{\alpha}{1-\alpha}\right) = M_s * \delta\theta * \left(\frac{\alpha}{1-\alpha} + \lambda * \left(1 + \frac{\alpha}{1-\alpha}\right)\right)$$

$$F_p * \alpha l * \left(\frac{1}{1-\alpha}\right) = M_s * \left(\frac{\alpha+\lambda}{1-\alpha}\right) \quad (2.36)$$

$$F_p = M_s * \left(\frac{\alpha+\lambda}{\alpha l}\right)$$

The limit state function is stated as follows:

$$Z = M_s * \left(\frac{\alpha}{1-\alpha}\right) + M_f * \left(1 + \frac{\alpha}{1-\alpha}\right) - F_p * \alpha l * \left(\frac{1}{1-\alpha}\right) \quad (2.37)$$

Case 2 plastic hinge at b and c

$$\delta\theta * l * (1-\alpha) = \delta\varphi * \alpha l$$
$$\delta\varphi = \delta\theta * \frac{1-\alpha}{\alpha} \tag{2.38}$$

$$\lambda = \frac{M_f}{M_s}$$
$$M_f = \lambda * M_s \tag{2.39}$$

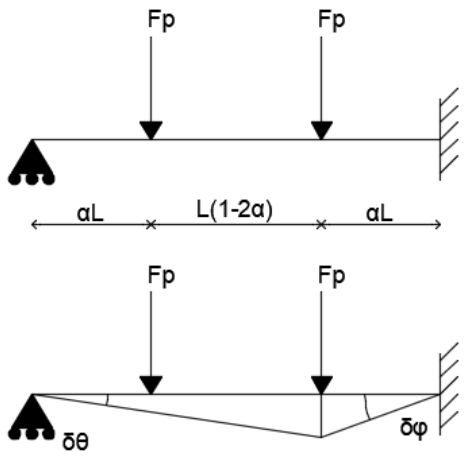

Figure 2.8 Plastic hinge at b and c

Virtual work:

$$F_p * \delta\varphi * \alpha l + F_p * \delta\theta * \alpha l = \lambda * M_s * (\delta\theta + \delta\varphi) + M_s * \delta\varphi$$

$$F_p * \delta\theta * \alpha l * \left(1 + \frac{(1-\alpha)}{\alpha}\right) = M_s * \delta\theta * \left(\frac{(1-\alpha)}{\alpha} + \lambda * \left(1 + \frac{1-\alpha}{\alpha}\right)\right)$$

$$F_p * \alpha l * \left(\frac{1}{\alpha}\right) = M_s * \left(\frac{1-\alpha+\lambda}{\alpha}\right) \tag{2.40}$$

$$F_p = M_s * \left(\frac{1-\alpha+\lambda}{\alpha l}\right)$$

The limit state function is stated as follows:

$$Z = M_s * \frac{1-\alpha}{\alpha} + M_f * \left(\frac{1}{\alpha}\right) - F_p * \alpha l * \left(1 + \frac{(1-\alpha)}{\alpha}\right) \tag{2.41}$$

Case 3 plastic hinge at a and b

$$\delta\theta * \alpha l = \delta\varphi * l * (1 - 2 * \alpha)$$
$$\delta\varphi = \delta\theta * \frac{\alpha}{1 - 2 * \alpha} \tag{2.42}$$

$$\lambda = \frac{M_f}{M_s}$$
$$M_f = \lambda * M_s \tag{2.43}$$

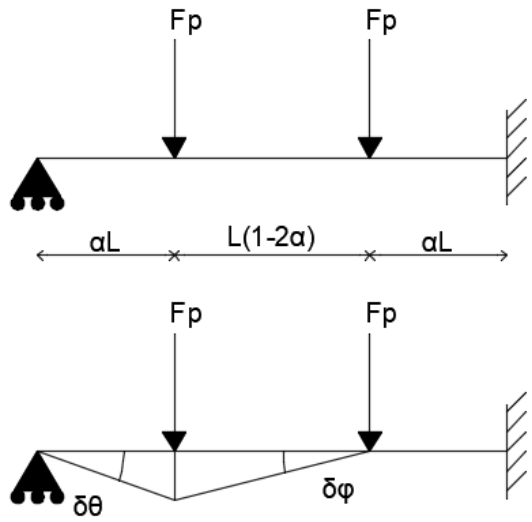

Figure 2.9 Plastic hinge at a and b

Virtual work:

$$F_p * \delta\theta * \alpha l = \lambda * M_s * (\delta\theta + \delta\varphi) + M_s * \delta\varphi$$

$$F_p * \delta\theta * \alpha l *= M_s * \delta\theta * \left(\frac{\alpha}{1 - 2 * \alpha} + \lambda * \left(1 + \frac{\alpha}{1 - 2 * \alpha}\right)\right)$$

$$F_p * \alpha l = M_s * \left(\frac{\alpha - \alpha * \lambda + \lambda}{1 - 2 * \alpha}\right) \tag{2.44}$$

$$F_p = M_s * \left(\frac{\alpha - \alpha * \lambda + \lambda}{\alpha l * (1 - 2 * \alpha)}\right)$$

The limit state function is stated as follows:

$$Z = M_s * \left(\frac{\alpha}{1 - 2 * \alpha}\right) + M_f * \left(1 + \frac{\alpha}{1 - 2 * \alpha}\right) - F_p * \alpha l \tag{2.45}$$

The limit state functions of the failure modes are summarised in Table 1. With the limit state functions and the properties of the random variables, the mean and the standard deviation of the limit state function can be determined.

Table 1 limit state functions of the failure mechanisms

Case:	Limit state functions
1	$Z = M_s * \left(\frac{\alpha}{1-\alpha}\right) + M_f * \left(1 + \frac{\alpha}{1-\alpha}\right) - F_p * \alpha l * \left(\frac{1}{1-\alpha}\right)$
2	$Z = M_s * \frac{1-\alpha}{\alpha} + M_f * \left(\frac{1}{\alpha}\right) - F_p * \alpha l * \left(1 + \frac{(1-\alpha)}{\alpha}\right)$
3	$Z = M_s * \left(\frac{\alpha}{1-2*\alpha}\right) + M_f * \left(1 + \frac{\alpha}{1-2*\alpha}\right) - F_p * \alpha l$

When the explicit method is used, the probability of failure can be determined in the following way:

$$\beta = \frac{\mu(Z)}{\sigma(Z)} \tag{2.46}$$

$$P(F) = \Phi(-\beta) \tag{2.47}$$

Whether or not the relation between the failure of the different parts is correlated will be discussed in the fourth chapter. In that chapter the first calculations are done with numerical values. For the system there are two failure modes which are investigated as introduced earlier; shear failure and bending failure. Since the structure in this case is statically indeterminate, the bending failure can be extended into two subcomponents:

1) insufficient rotation capacity of a plastic hinge;
2) plastic failure due to the forming of a mechanism.

If the shear capacity is insufficient the system will fail before a mechanism of plastic hinges occurs. However, if the shear capacity has extremely small probability of failure during the experiment then, the focus is on bending failure.

2.4.2 Rotation capacity

Rotation capacity is an important aspect in statically indeterminate structures that are developing a plastic mechanism. Dealing with a statically indeterminate structure brings about several difficulties. It is showed before that rotation capacity is a very important aspect with respect to the failure mode. In most plasticity calculations, it is assumed that the rotation capacity is sufficient. Moreover, since rotation capacity is an important part of the system in failure, this topic will be explored in more depth. The basic principle of capacity is that the resistance must be larger than the acting solicitation. In this case, the required rotation capacity to form a mechanism should be smaller than the present rotation capacity in the beam. Keeping in mind that rotation capacity of reinforced concrete is very complex, and this topic is not the main focus of the thesis, this topic will be discussed briefly.

To start off, the required rotation capacity is calculated by making use of the “forget-me-nots” (in Dutch: “vergeet-me-nietjes”) given in Figure 2.10. By using a superposition of three known basic situations the quite complex structure in Figure 2.4 can be calculated.

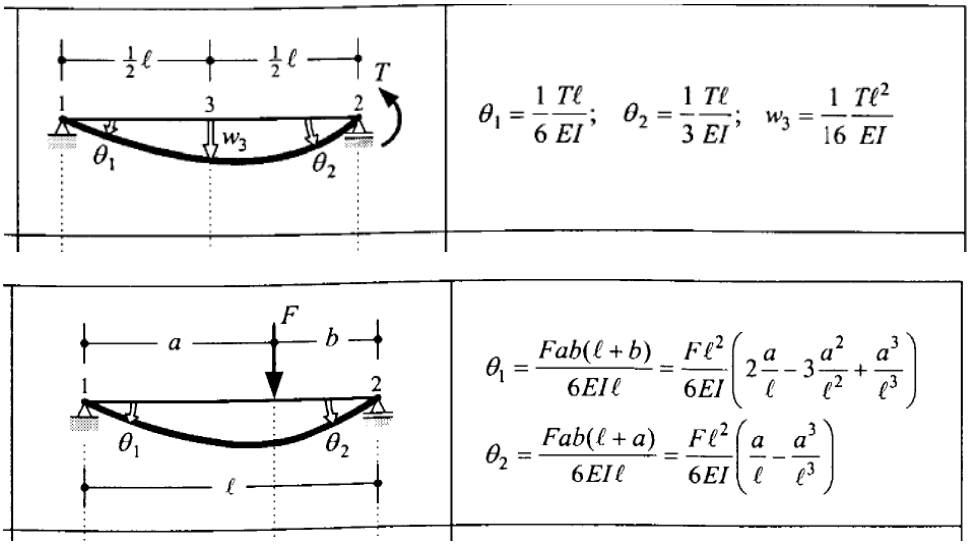

Figure 2.10 forget me nots; simply supported beam with a moment acting at one side and simply supported beam with one vertical point at distance ‘a’ from the left-hand side.

As stated in paragraph 2.4.1 parallel system failure, the first possible mechanism that can occur is a plastic hinge at the middle support or at the clamped end when a symmetric beam is used and a plastic hinge at the point where the point load nearest to the free end of beam acts. This mechanism is chosen as an example. When the moment distribution before failure is drawn, Figure 2.11 will be obtained.

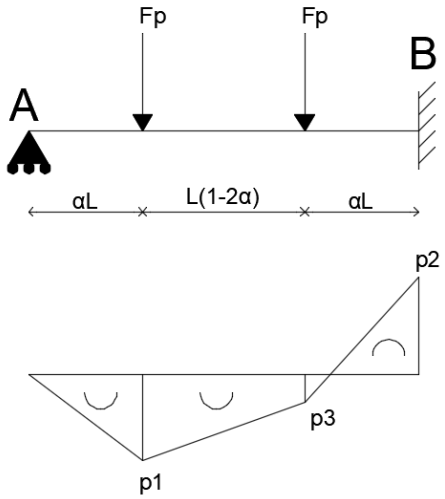

Magnitude of the moment:

$$P1 = M_f$$

$$P2 = M_s$$

$$P3 = \left(M_f * \frac{1-\alpha}{\alpha} - F_p * (1 - 2 * \alpha) * L\right)$$

Figure 2.11 moment distribution just before collapsing

From the moment distribution before failure, to rotation capacity is a small step. According to the linear-elastic theory the first plastic hinge will develop at the clamp end as located in Figure 2.11. The following question arises, does this plastic hinge have enough rotation capacity? This problem will be broken down into two phases: the first phase before the plastic hinge at the clamped end is developed and the phase from the plastic hinge development till failure. In

the first phase there is per definition no rotation at the clamped end. The second phase is more interesting since there is already force on the structure and any increase of this force will cause plastic rotation. To determine whether the structure provide enough rotation capacity, two things must be known. The plastic rotation required to let the mechanism develop and the available rotation capacity.

It turns out that the plastic hinge has occurred at the clamped end when:

$$Fp_{first\ plastic\ hinge} = \frac{2 * M_s}{3 * (1 - \alpha) * \alpha * L} \quad (2.48)$$

And the collapse load:

$$Fp_{collapse} = \frac{M_s * (\alpha + \lambda)}{\alpha * L} \quad (2.49)$$

Thus, the load increase between the first plastic hinge and collapse is:

$$\Delta Fp = Fp_{collapse} - Fp_{first\ plastic\ hinge} \quad (2.50)$$

During the second state in which the rotation capacity is necessary, the moment at the clamped end stays constant (M_s).

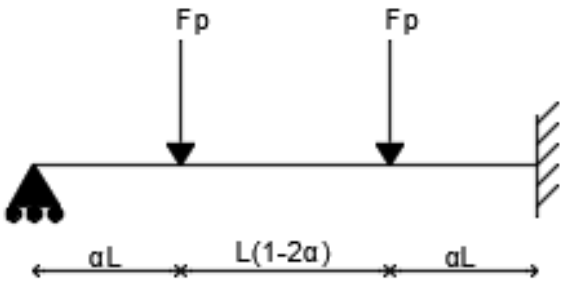

Figure 2.12 mechanic schema of the symmetric part of the continues beam

Figure 2.12 is equal to the superposition of the following three statically determinate structures as presented in Figure 2.13:

“Forget-me-nots” for rotation at RHS of the structure:

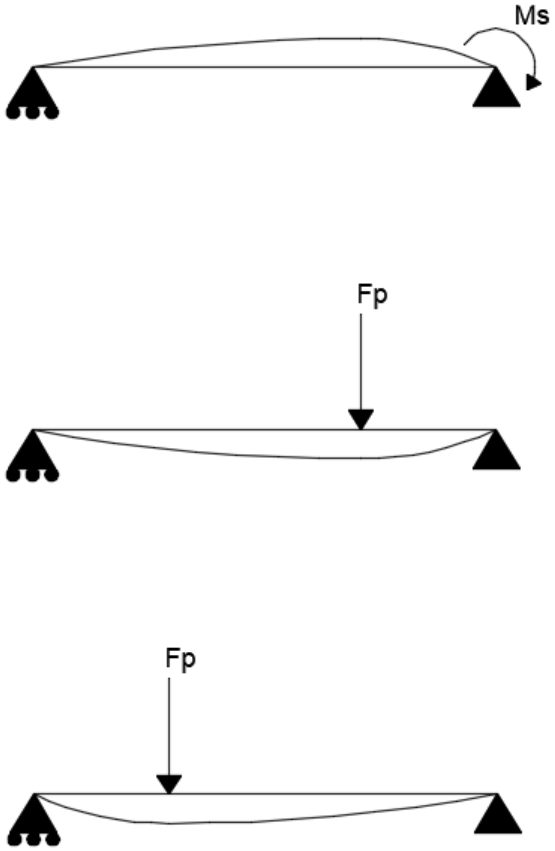

$$\varphi_c = -\frac{M_s * L}{3 * EI}$$

$$\varphi_c = \frac{F_p * L^2}{6 * EI} * (2 * (1-\alpha) - 3 * (1-\alpha)^2 + (1-\alpha)^3)$$

$$\varphi_c = \frac{F_p * L^2}{6 * EI} * ((1-\alpha) - (1-\alpha)^3)$$

Figure 2.13 Superposition of the statically indeterminate structure

With these expressions it is possible to set-up an equation for the required rotation capacity: At the moment that the first plastic hinge develops, the rotation at point c is zero.

$$\varphi_{c_1} = -\frac{M_s * L}{3 * EI} + \frac{Fp_{first\ plastic\ hinge} * L^2}{2 * EI} * \left((1-\alpha) - (1-\alpha)^2\right) = 0 \qquad (2.51)$$

At the moment that the second plastic hinge develops and the structure fails, the magnitude of the rotation at point c is the following:

$$\varphi_{c_2} = -\frac{M_s * L}{3 * EI} + \frac{Fp_{collapse} * L^2}{2 * EI} * \left((1-\alpha) - (1-\alpha)^2\right) \qquad (2.52)$$

The plastic rotation therefore is:

$$\Delta\varphi_c = \varphi_{c_2} - \varphi_{c_1} \qquad (2.53)$$

thus

$$\Delta\varphi_c = \frac{\Delta F_p * L^2}{2 * EI} * \left((1-\alpha) - (1-\alpha)^2\right) \qquad (2.54)$$

Someone could argue about the possible failure mechanisms. However, it can be proven that the mechanism in Figure 2.7 Plastic hinge at a and c is the governing failure mechanism. This prove makes use of Prager's theorem which is used in plasticity to show the uniqueness of a failure mechanism. This theorem shortly sees: "if the moment distribution line nowhere exceeds the maximum moment capacity, this mechanism is an upper bound for the failure load". For simple beam structure can be shown that the lower bound is equal to the upper bound.(Hartsuijker and Welleman 2003)

The last part of the rotation capacity is to find an expression for the available rotation capacity. As said earlier, the rotation capacity of a reinforce concrete beam is rather complex. In the year 1999 A. Bigaj did a very extended investigation of the structural dependence of rotation capacity in reinforce concrete beams and slabs. His formulas will be discussed in the remainder of this paragraph.

The formulas found in the thesis done by A. Bigaj maps all the formulas back to a simply supported beam with a slenderness of (span length / height of the beam) 12 [-]. First the "c" value (aka material reinforcement ratio) must be determinate and from that number the rotation capacity can be looked up in an empirical graph (Figure 2.14).

$$c = \omega * \frac{f_y}{f_c'} \qquad (2.55)$$

In which:

- ω is the geometrical reinforcement ratio;
- f_y is the reinforcement yield stress;
- f_c' is the value of the average concrete compressive stress in the compressive zone.

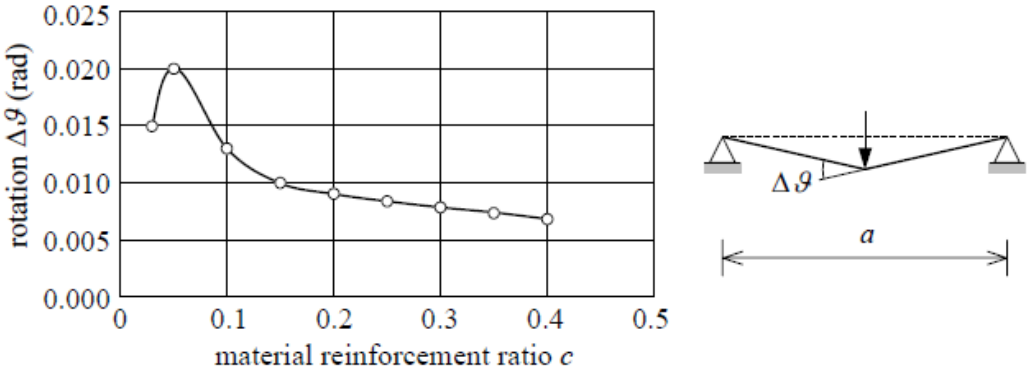

Figure 2.14 empirical relation between the material reinforcement ratio and the plastic rotation capacity of a beam with a slenderness (a/h) of 12

The rotation capacity (red in Figure 2.14) is the equivalent rotation capacity of a simply supported beam with a slenderness of 12. However, in the investigation done in the year 1999 also a formula to map back to the initial situation was derived empirically.

$$\Delta\varphi_{a/h} = \left[\frac{\frac{a}{h}}{12}\right]^{0.85} * \Delta\varphi_{12} \qquad (2.56)$$

With expression (2.56) the rotation capacity can be determined as well as the required rotation capacity. If the required rotation capacity is smaller than the available rotation capacity, the rotation capacity is ensured. This check will be done numerically in chapter 4.

2.5 Uncertainties

In this paragraph the three most common uncertainties in modelling civil structures are discussed:

- Material uncertainty
- Geometrical uncertainty
- Model uncertainty

2.5.1 Material uncertainty

The material uncertainty is depending on the stochastic variables that describe the material behaviour/properties. If the limit state function is a linear function of the stochastic variables, the calculation is rather simple. However, complexity starts when non-linear effects are considered.

Not all the non-linear probabilistic functions have a closed form with an analytical solution. For the full probabilistic analysis this is not a problem. Level III calculations like MCS is making use of multiple calculations which is expensive in terms of computation time. To reduce the computation time, semi-probabilistic calculations or level II calculations can be performed.
FORM or SORM are two of the widely used level II methods. These methods try to obtain the design point through an optimization algorithm. The optimization algorithm usually calculates the gradient of the LSF. If the LSF is available in analytical form, application of FORM or SORM is simpler. But when the LSF is not available in its explicit form, FORM or SORM can be difficult to implement.

Ideally, the physical uncertainty on structural level should be assessed by performing a large number of experiments on nominally equivalent components. (Engen, Hendriks et al. 2017) Unfortunately, for this master thesis there are only 4 types of experiments which are performed just once. It is very hard to conclude things with such little experimental background.

In level I reliability methods, by applying the partial factors to the material strengths instead of the sectional resistance, the partial factors can still be used for this kind of analysis. Furthermore, it must be noted that that the design material parameters are only used to calculate the capacity of sections with respect to bending moments and normal forces.
It is a drawback to this approach that in accounting for all types of uncertainties by reducing the material parameters, very low material parameters must be used. In non-linear analysis of statically indeterminate structures, **the use of reduced material parameters can lead to an unrealistic load distribution.** Which means that, due to reduction of for example the stiffness of the statically indeterminate structure an unexpected failure mode with initially a very low probability of failure can become dominant. Furthermore, for structures in which the structural behaviour is influenced by second-order effects, the very low material parameters can result in an over-conservative and uneconomical design (Schlune, Plos et al. 2012)

For reinforced concrete, the material model for concrete is considered the largest source of modelling uncertainties! (Engen, Hendriks et al. 2017) Because, concrete is reacting more heterogeneous than for instance steel. On top of that, the geometrical uncertainty is less of an issue because of the boarding in which the concrete is casted.

2.5.2 Geometrical uncertainty

All literature agrees upon the fact that the geometrical uncertainty of reinforced concrete is usually rather small. On top of that, the type of structure that will be investigated in this thesis is not sensitive to small imperfections. According to the safety formats for non-linear analysis of concrete structures a geometrical uncertainty of approximately 5% is reasonable. Stability will not be investigated an is out of the scope.
However, it will be looked at small geometrical deviations with respect to the effective depth of the concrete cross-section. When the effective depth of a cross-section changes, this has a mayor influence of the internal liver arm.

2.5.3 Model uncertainty

The model used to obtain the LSF be it analytical form or FE model, introduces an additional component of uncertainty to the reliability calculation. A very accurate model has low model uncertainty associated with it. Furthermore, based on available date, coefficients of variation in the range of 5-30% seem appropriate for beams in bending. For shear type of failure the modelling uncertainty can be expected to lie in the range of 10-40% (Schlune, Plos et al. 2012) Not only the way the model is build up, but even the software that is used can have mayor influence on the uncertainty of the calculation.

Based on the different uncertainties on material level it is expected that the physical uncertainties on structural level depend on whether the failure mode is governed by the concrete or the reinforcement, and expected to be particularly high if the failure mode is governed by the tensile strength of the concrete. This statement is supported in the work of (Ellingwood and Galambos) where the resistance of reinforced concrete beams failing in bending is found to have a lower coefficient of variation than beams failing in shear. (Engen, Hendriks et al. 2017)

The modelling uncertainty can be quantified by verification and validation (Roache 1998). Verification is related to how the equations of the mechanical model are solved, i.e. a quantification of the accuracy without questioning the relation between the equations and the physical problem at hand.
Validation, on the other hand, relates to how well the equations capture the true physical behaviour. “In the NLFEA context, validation thus relates to idealization of the geometry and the material behaviour. In other words, verification answers the question ‘are we solving the equations right?’, and validation answers the question ‘are we solving the right equations?’ “ (Engen, Hendriks et al. 2017)

2.6 Overview of methods used in this thesis

Level 0, I, II, III and IV are the possible reliability calculations. However, in this thesis only the reliability methods of level I, II and III are used as shown in Table 2. Furthermore, in this figure the combinations between the reliability levels and the structural level of approximation are shown. The crosses in the figure are representing the combinations which will be addressed in the thesis and the bold crosses are combinations which will be used in a calculation.

Table 2 combination of reliability method and approximation level for the reliability calculations

Reliability method Model approximation	I	II	III
I (Analytical)	**X**	X	**X**
II			
III			
IV (Numerical)	X		

In order to find an answer to the research question, basically the most optimal combination between the reliability method and the LoA has to be found. On one hand the accuracy is looked at. On the other hand the computation time is considered.

3 Experiment set-up

In this thesis an investigation of the reliability of ‘simple’ statically indeterminate structures is carried out. Monnier’s experiment is used as fundamental stepping stone. Moreover, for the experimental data about statically indeterminate reinforced concrete beams, this experiment is significant to this thesis. The fundamentals of the experiments are summaries in this chapter. Furthermore, the boundary conditions by Monnier are the same as for the experiment done in this thesis.
The laboratories of the Institute for Building Materials and Building Structures TNO-IBBC in Delft is been used for experiments to investigate the behaviour of continuous reinforced concrete beams. Between December 1967 and in January 1969 several tests concerning this behaviour have been carried out and these experiments are documented in TNO-reports [BI-65-1 (November 1965), BI-66-49 (July 1966), BI-67-106 (October 1967), BI-67-110 (December 1967)]. The reports of TNO together with other papers regarding M-kappa diagrams of reinforced concrete and computer-analyses were the building blocks for Monnier’s investigation of continuous beams in reinforced concrete. (Monnier 1970)

3.1 Monnier’s purpose of the experiment

The purpose of the experiment is to investigate the reinforcement requirements in the serviceability limit state (SLS), since there is a lot of freedom with respect to the reinforcement design in the ultimate limit state (ULS). The SLS is defined as the limit state is which function, comfort and aesthetical aspects are preserved. Therefore, in the SLS the design of the reinforcement must fulfil certain requirements with respect to crack width (aesthetical/function requirements) and maximum deflection (comfort/function requirements). In the paper both experimental and theoretical research is performed on continuous reinforced concrete beams.

3.2 Execution of Monnier’s experiment

The experimental tests are done on two-span beams with two-point loads per span. The loads and the spans are symmetrical with respect to the mid-support. An analysis-procedure is taken into consideration next, in this procedure the influence of the shear force can be considered. In the end, the calculated and measured results of the experiment are compared.

3.2.1 Properties of the tested beams

Firstly, the general information on the test beams is introduced. The beams which were investigated had an overall length of 4200mm and were tested as continuous beams on three supports, the two spans being each 2000mm in length. The cross-section has the following dimensions: width (denoted as ‘b’) of 150mm and total height (denoted as ‘ht') of 260mm. The effective depth both for the top and for the bottom reinforcement was 236mm. In all the test beams the longitudinal reinforcement consisted of 12mm diameter bars with steel grade QR 40 (Figure 3.1: Stress-strain diagram of the reinforcement bar). The beams were provided with stirrups of 8mm diameter, consisting of the same steel grade as the longitudinal reinforcement (Figure 3.2: The stirrup reinforcement).

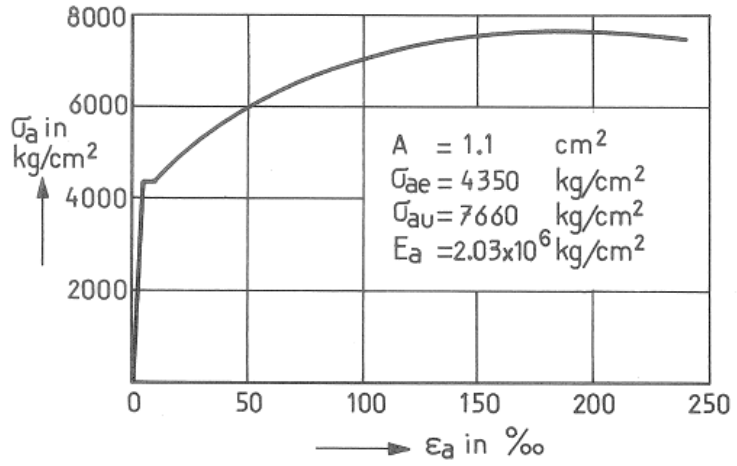

Figure 3.1: Stress-strain diagram of the reinforcement bar

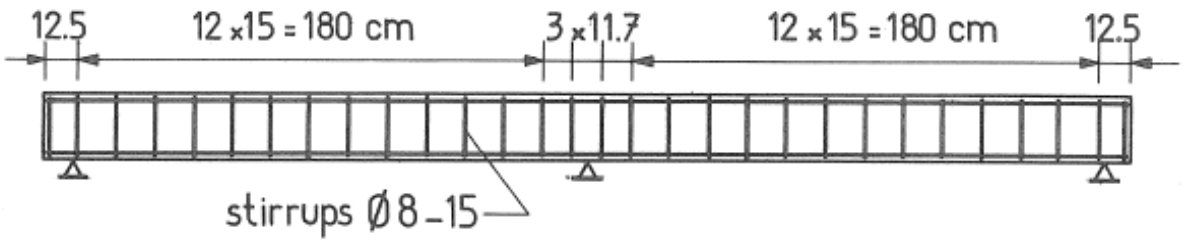

Figure 3.2: The stirrup reinforcement

Four different tests were done, on four different beams. These beams were denoted in Monnier's paper as respectively B1, B2, B3 and B4. The beam B1 had three re-bars in the top parts of the cross-section and two re-bars in the bottom part of the cross-section whereas the others (B2, B3 and B4) had two in the top part and three in the bottom. (see Figure 3.3: Typical detail of the test beams).

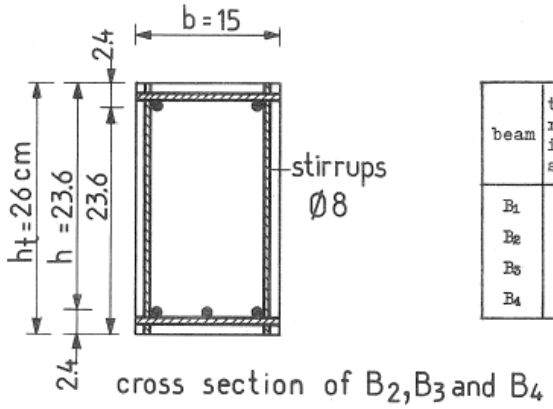

beam	tensile reinf. in the spans	tensile reinf. at the interior support	perc. of reinf. $\omega_o = \frac{100A}{bh}$
B_1	2Ø12	3Ø12	2Ø12 ≡
B_2	3Ø12	2Ø12	0.64%
B_3	3Ø12	2Ø12	3Ø12 ≡
B_4	3Ø12	2Ø12	0.96%

Figure 3.3: Typical detail of the test beams

3.2.2 Experiment set-up

As said before, the beams were tested as two-span continuous beams on three supports with 2000mm spans. The loading consisted of two-point loads applied to each span. In all experiments the load positions were the same, 500mm centre-to-centre and were symmetrical. (see Figure 3.4: Loading system and the actual areas of moment diagrams).

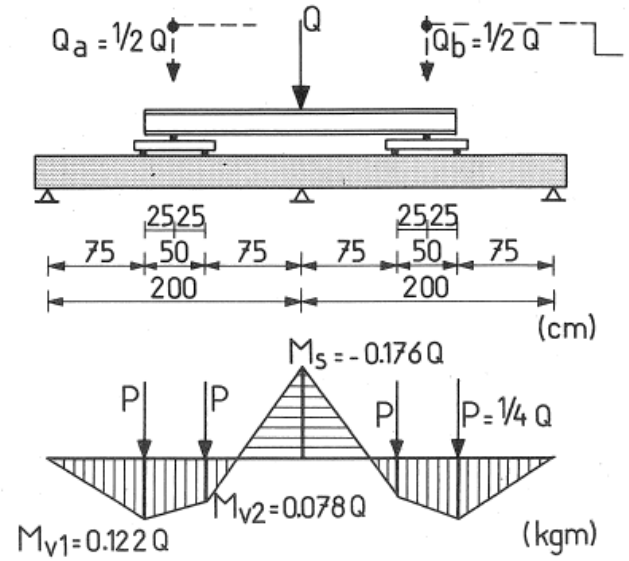

Figure 3.4: Loading system and the actual areas of moment diagrams

The third beam, B3, is characterised by its loading since the all the point loads, P, on the beams B1, B2 and B4 have the same magnitude. For B3 the load closest to the mid support is about 2.9 times higher than the other force but the collapse load is equal to the total magnitude of force acting on the beam (see Figure 3.5:Loading system and the actual areas of moment diagrams). The last beam B4 was solicited by a cyclic loading. The load was applied as a shake down analysis. This will not be explained further since it is not used in this report.

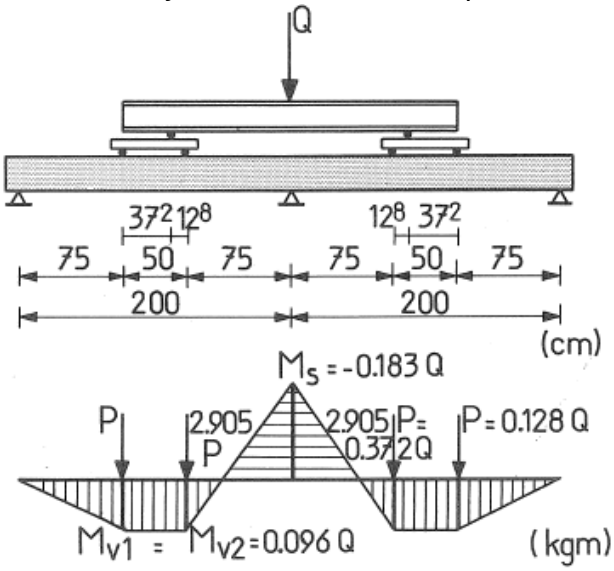

Figure 3.5:Loading system and the actual areas of moment diagrams

4 Analytical model for structural analyses

The fourth chapter of this thesis consists of two main parts; the analytical model of the structure and the probability calculations.

Starting with the analytical model of the structure. First, formulas for the analytical model are derived and assumptions with respect to the constitutive relations are made. Second, the numerical values of the geometrical and material parameters are introduced. Hence, these values will be used throughout the thesis and stem from Monnier's experiment discussed in the previous chapter. Third, the stochastic parameters are used to analyse the possible failure modes of the structure. Thereafter, a sensitivity study is performed on the resistance parameters. This sensitivity study will later be used for comparison with the sensitivity study of the numerical model (chapter 5).

The probabilistic part of this chapter includes three components. Firstly, a semi-probabilistic procedure is followed. The governing Eurocode provides this procedure. Secondly, a full-probabilistic calculation is done. Finally, the results of the semi- and full-probabilistic procedure are compared.

4.1 Structural formulas

This first paragraph of the fourth chapter describes the origin of the structural formulas of the analytical model. The assumptions made in the model are discussed first. A structural model is always an approximation of the reality; thus, assumptions have to be made. Thereafter, the analytical formulation of the bending resistance is derived. With the analytical formulation of the bending resistance, the failure load can be calculated. The same procedure holds for the shear force resistance capacity.

4.1.1 Assumptions

As said before, structural models are an approximation of reality. Simplifications are applied in order to make calculation time manageable. The first mayor simplification is the utilization of symmetry. The two-span beam (with symmetric loads in Figure 4.1) is reduced to a one span beam with one free and one clamped end (Figure 4.2). This simplification safes computation time.

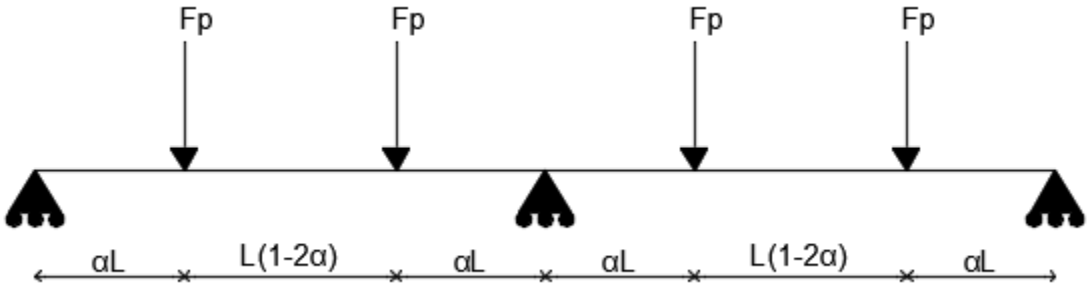

Figure 4.1: mechanical scheme of the structure that will be analysed.

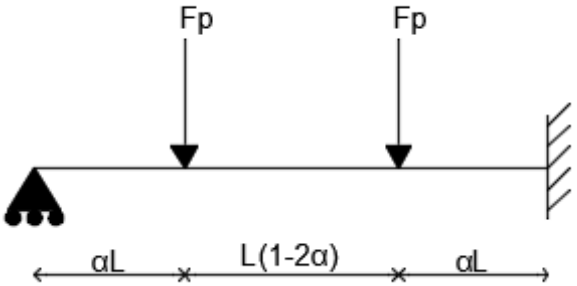

Figure 4.2: simplified mechanical scheme of the structure where symmetry is utilized.

In the analytical model it is assumed that the structure behaves as a beam, considering the height of the beam is not significant compared to its length. To determine the force flow in a membrane structure some constitutive conventions are important (NEN-EN 1992-2+C1:2011 nl):

1. Plane sections remain plane during bending;
2. Strain in bonded reinforcement, whether in tension or compression, is the same as the strain in concrete at the same level;
3. Tensile strength of concrete is ignored;
4. The stresses in the concrete in compression are given by the design stress-strain relationships;
5. The stresses in the reinforcement steel are given by the design stress-strain relationships.

Having said this, the beam properties are introduced as values which do not change along the beam. There can be a weak point in a material and this can influence the behaviour of the structure. There are more effects which can be of influence. The effects that can be considered for a more realistic simulation are for instance:

1. Damage and/or weak points in the structure;
2. Loading history and cyclic loading;
3. Parameter variation along the beam;
4. Corrosion of reinforcement steel;
5. Aging of concrete.

Even though these factors make the calculation more complicated, it gives the model a more realistic view. In this thesis these factors are not included. Instead, to account these simplifications a model uncertainty factor of 10% is considered.

4.1.2 Bending resistance formulas

In this subparagraph the bending resistance is derived by assuming a stress-strain relation when the structure is loaded. The cross-section of the beam consists of top and bottom reinforcement. The assumed stress and strain distribution in the cross-section is displayed in Figure 4.3.

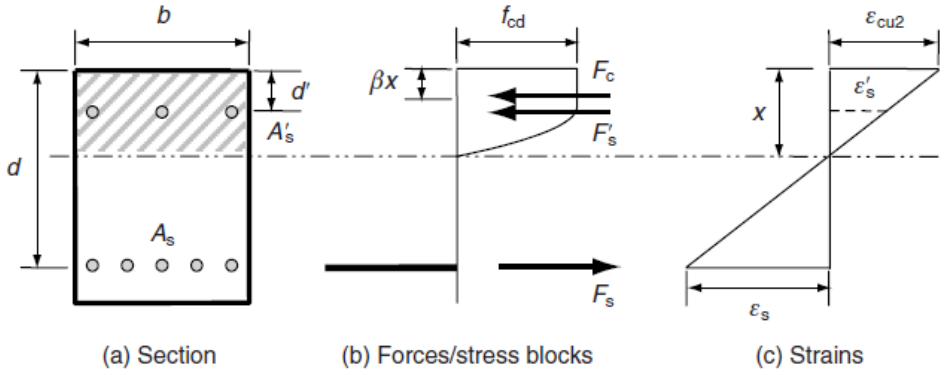

Figure 4.3 stresses and strain in the cross-section

Applying the five assumptions made in the Eurocode (as discussed in the previous section), the cross-sectional resistance can now be derived. In Appendix B.1, the full derivation of the cross-sectional resistance of a reinforced concrete beam with top and bottom reinforcement can be found. It turns out that whether or not the top reinforcement yields is decisive for the expression of the cross-sectional bending resistance. Because of this, a conditional expression is derived (equation (4.1)).

$$M_s = \begin{cases} f_{av} * b * x_u * (d - \beta_u * x_u) + A'_s * f_{yk} * (d - d') & \varepsilon_{cu2} * \left(1 - \frac{d'}{x_u}\right) \geq \frac{f_{yk}}{E_s} \\ f_{av} * b * x_u * (d - \beta_u * x_u) + A'_s * E_s * \varepsilon_{cu2} * \left(1 - \frac{d'}{x_u}\right) * (d - d') & \varepsilon_{cu2} * \left(1 - \frac{d'}{x_u}\right) < \frac{f_{yk}}{E_s} \end{cases} \quad (4.1)$$

With equation (4.1) the bending capacity of the cross-section can be determined. Now, it is possible to determine the theoretical maximum (deterministic) force on the beam. This method is used to determine which of the failure modes, introduced in paragraph 2.4.1 is the most probable to occur.

4.1.3 Shear resistance formulas

This section describes the formulation which is used to determine the shear resistance in the analytical model. Shear failure in concrete beams is a complex phenomenon. It is not possible to derive an analytical formula that will describe its behaviour perfectly. In the Model Code 1990 there are formulas presented which can be used to determine the design shear force resistance (eq. (4.2) and (4.3)). However, it cannot be used to determine probability of failure because it is a design formula. Therefore, the research that is done to derive this empirical design formula is studied. With these results, an expression is derived to determine the maximum force on the structure before shear failure occurs.

The design shear resistance of the cross-section with shear reinforcement is:

$$V_{rd_{max}} = 1.0 * b * (d - d') * 0.6 * \left(1 - \frac{f_{ck}}{250}\right) * \frac{f_{ck}}{1.5} \quad (4.2)$$

The design shear resistance of the structure without shear reinforcement is given as:

$$V_{rd_c} = 0.12 * k * (100 * \rho_l * f_{ck})^{\frac{1}{3}} * b * d$$
$$k = \min(1 + \sqrt{\frac{200}{d}}, 2) \quad (4.3)$$

$$V_{equivalent} = \min(V_{rd_{max}}, V_{rd_c}) * 10^{-3} \quad (4.4)$$

This design formula (4.3) for concrete beams without shear reinforcement is empirical derived from experiments which were done in 1995 by König and Fischer. From the data gathered in the experiment the 0.12 value in formula (4.3) was found. They started off with equation (4.5). This expression consists of four variables from which one is prescribed as an uncertainty parameter. This stochastic parameter has a probability density function with corresponding mean value and standard deviation. The formula for the shear resistance for concrete cross-sections without shear reinforcement stems from the following configuration:

$$V_u = c * \xi * (100 * \rho_l)^{\frac{1}{3}} * f_c^{\frac{1}{3}} \quad (4.5)$$

In this formula:

ξ the same as the variable k introduced in the design formulas
ρ_l the longitudinal reinforcement density
f_c the concrete compressive strength
c an uncertainty factor

Appendix B.2 discusses the experiment in more detail and focuses on the derivation of the uncertainty factor c. In this thesis, equation (4.5) will be used instead of equation (4.3) to determine “V equivalent”, therefore equation (4.6) is obtained.

$$V_{equivalent} = \min(V_{rd_{max}}, V_u) * 10^{-3} \quad (4.6)$$

In the end, it is the goal to establish what the governing failure mode is. Fact is that, it is not feasible to compare bending capacity with shear force capacity. Thus, the shear capacity of the cross-section is translated to an equivalent maximum load. If the shear capacity would be known, one can determine what the force could be to cause this shear force. This is performed by first constructing the shear force distribution to create an overview of the structure’s behaviour. From this visual representation of the force flow, the position of maximum shear force can be obtained. The shear force at the critical point can then be written as an expression of the external force. Finally, the information of the shear force capacity is used to calculate the maximum force on the structure before shear force occurs.

$$F_p = V_{equivalent} * \frac{2}{\max(|\{3 * \alpha^2 - 3 * \alpha + 2\}|, |\{6 - 3 * \alpha^2 - 3 * \alpha\}|)} \quad (4.7)$$

In Appendix B.2 the derivation of the formula for this equivalent force is given. For the bending formula, the same procedure is followed. This is done in paragraph 2.4.1. where the expression for the failure load of several mechanisms was derived.

4.2 Parameter study

The second paragraph of this fourth chapter gives more information about the numerical values of the geometrical and material parameters. Firstly, values are assigned to the parameters. Some parameters are stochastic, in this case probability density functions are attached. Secondly, with these properties the probabilities of failure in shear and bending are obtained. Thirdly, the most probable failure mode of the beam is computed. Finally, a sensitivity study gives insight in the dependency of the (geometrical and material) parameters on the cross-sectional capacity of the governing failure mode.

4.2.1 Properties of the parameters

11 parameters are introduced in Table 3. These parameters are fundamental for the calculation later in this chapter. Four of these 11 variables are stochastic and all of them are assumed to have a log-normal distribution. (Wiśniewski, Cruz et al. 2012) has concluded in his paper that a log-normal distribution is the best way to describe the behaviour of the concrete compressive strength. Furthermore, for the properties with respect to the reinforcement, log-normal or normal distributed variables work sufficiently. In this thesis is chosen for log-normal. For the geometrical parameter, a log-normal distribution is assumed as well.

The mean values of all the parameters stem from the experiment done by Monnier. This is done so the results of the experiment can be compared with the results of the analytical and numerical model. The numerical value for the coefficient of variation, V, is chosen after studying the papers of (Wiśniewski, Cruz et al. 2012) and (Schlune, Plos et al. 2012). Both use similar numbers for the coefficients of variation, therefore these numbers are used in this thesis.

Table 3 parameters used in the parameter study

Section	Definition	Parameter	Mean value	V	Distribution	Unit
Concrete	Compressive strength	f_c	30.9	15%	Lognormal	N/mm^2
	Maximum strain in compression	ε_{cu2}	0.0035	-		m/m
Steel	Yield strength	f_y	426.7	5%	Lognormal	N/mm^2
	Young's modulus	E_s	199143	8%	Lognormal	N/mm^2
	Cross-sectional area of top reinforcement	A'_s	227	-		mm^2
	Cross-sectional area of bottom reinforcement	A_s	340	-		mm^2
Geometry	Effective depth	d	236	-		mm
	Width	b	150	-		mm
	Span length	l	2000	-		mm

	Cover top	d'	24	20%	Lognormal	mm
	Length parameter	α	75/200	-		-

The reinforcement of a concrete beam often consists of stirrups. These stirrups are shear force reinforcement and at the same time they ensure the longitudinal reinforcement is connected to each other. As a result, the numerical value of d (effective depth of the bottom reinforcement) and d' (concrete cover of the top reinforcement) given in Table 3 are correlated. The distance between the top and bottom reinforcement is always the same. The two parameters are negative correlated with $\rho = -1$.

4.2.2 Bending capacity resistance versus shear capacity resistance

What is the most probable failure mode of the structure in Figure 4.1? This question will be answered in the section below. In order to do this, the two formulas for the cross-sectional capacity (for bending and shear resistance) and the values of the different parameters in Table 3, are necessary. Before the probability calculation can be performed, both the shear capacity and cross-sectional bending capacity need to be translated into a common variable. Here is chosen to use an equivalent force, Fp. In paragraph 2.4.1. this equivalent force has already been put in place. Namely, the failure load is written as a function of the moment resistance. Therefore, the only derivation that must be done is the equivalent force for the shear force resistance. This derivation was done in appendix B.2. The equivalent force for the shear force resistance is presented in equation (4.7) in paragraph 4.1.

In paragraph 2.4.1. the three possible failure mechanisms in bending were introduced. In Figure 4.4 the three-possible locations where a plastic hinge can develop is displayed. For a statically indeterminate structure as analysed in this thesis, two plastic hinges are necessary for the development of a failure mechanism. The three possible parallel systems are:

- Plastic hinges at a and c (Figure 2.7)
- Plastic hinges at b and c (Figure 2.8)
- Plastic hinges at a and b (Figure 2.9)

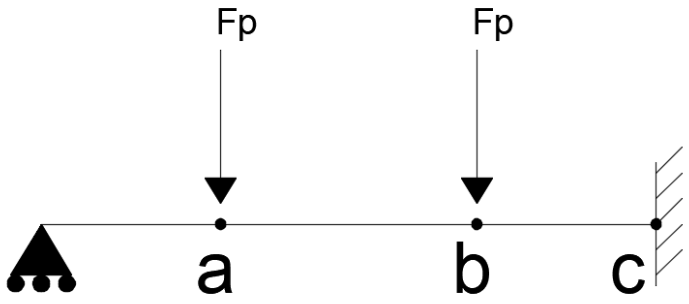

Figure 4.4 image of the structure with the possible locations for plastic hinges

Now that the numerical values are known, the most probable failure mode can be calculated. The following outcome can be obtained when the numerical values of **Table 3** are filled in: Starting with the ratio between the top and bottom reinforcement given as $\lambda = \frac{A_s}{A_s'}$ and its numerical value is therefore:

$$\lambda = \frac{A_s}{A_s'} = \frac{340}{227} = 1.5 \tag{4.8}$$

Bending mechanism 1 occurs when plastic hinges at point a and at point c are formed:

$$F_p = M_s * \left(\frac{\alpha + \lambda}{\alpha l}\right) = M_s * 2.5 \tag{4.9}$$

Bending mechanism 2 consists of plastic hinges at b and c:

$$F_p = M_s * \left(\frac{1 - \alpha + \lambda}{\alpha l}\right) = M_s * 2.83 \tag{4.10}$$

Bending mechanism 3 is caused by plastic hinges at a and b:

$$F_p = M_s * \left(\frac{\alpha - \alpha * \lambda + \lambda}{\alpha l * (1 - 2 * \alpha)}\right) = M_s * 7 \tag{4.11}$$

Equation (4.9) clearly shows the lowest failure load of the possible failure mechanisms in bending. Therefore, the failure load obtained from bending mechanism 1 is compared with the shear capacity. Thus, the most probable failure mode in bending is compared with the most probable failure mode in shear. The spread of the resistance parameters' failure modes are considered. "Python" simulates the bending- and shear force resistance during several random draws. The number of times that the shear force capacity is lower than the bending capacity is counted. The shear force capacity expression in equation (4.7) is used. This equation will be compared with the governing bending capacity formula. Continuing with the bending capacity, equation (4.9) consists of M_s which has been introduced in the previous paragraph in equation (4.1). By substituting eq.(4.1) in eq.(4.9), the following expression can be obtained:

$$F_p = \left(\frac{\alpha + \lambda}{\alpha l}\right) * \begin{cases} f_{av} * b * x_u * (d - \beta_u * x_u) + A_s' * f_y * (d - d') & \varepsilon_{cu2} * \left(1 - \frac{d'}{x_u}\right) \geq \frac{f_y}{E_s} \\ f_{av} * b * x_u * (d - \beta_u * x_u) + A_s' * E_s * \varepsilon_{cu2} * \left(1 - \frac{d'}{x_u}\right) * (d - d') & \varepsilon_{cu2} * \left(1 - \frac{d'}{x_u}\right) < \frac{f_y}{E_s} \end{cases} \tag{4.12}$$

The next step in determining the probability of failure in shear of the structure is to derive the limit state function of shear failure and exceeding the bending capacity. Using equation (4.7) and equation (4.12) the following limit state functions can be presented.

$$Z = M_s * \left(\frac{\alpha + \lambda}{\alpha l}\right) - F_p \tag{4.13}$$

$$Z = V_{equivalent} * \frac{2}{\max(|\{3 * \alpha^2 - 3 * \alpha + 2\}|, |\{6 - 3 * \alpha^2 - 3 * \alpha\}|)} - F_p \tag{4.14}$$

Both limit state functions (4.13) and equation (4.14) consist of conditional statements. Applying random draws, the probability of failure of a certain cross-sectional resistance can be determined. The Monte Carlo procedure is a common used-tool for simulation random draws. “Python” determines in every random draw of parameters which failure mode is dominant. Bending failure is dominant because in 10^7 draws none of them was failing in shear. The “Python” script is presented in Appendix A1 and the latter described procedure can be found in line 156 and 157.

The probability of shear failure is significantly small, therefore only bending failure will be considered in this thesis. During the discussion of the thesis it will be discussed whether it was a correct decision.

Monnier found a failure load of 60kN which is higher than the expected failure load (Figure 4.5). Monnier has observed that: The beam shows a considerable redistribution of the moments after the cracks has formed. Accordingly, in consequence of this redistribution, the yielding of the tensile reinforcement over the support occurred at a substantially higher load than that calculated according to the elastic theory. The bending moment at which yielding of the reinforcement began was in this case also higher than the calculated yield moment of the section concerned. The calculated collapse load was likewise exceeded. (Monnier 1970)

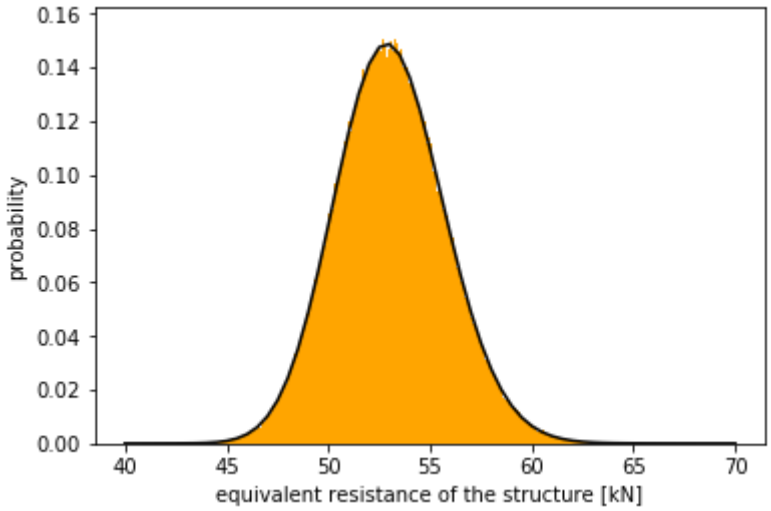

Figure 4.5 probability density function of the resistance of the structure.

4.2.3 Sensitivity study of the parameters

This subparagraph presents a sensitivity study of parameters. The sensitivity study will be performed as follows:

The resistance's distribution of the structure is constructed and there is looked at the spread or standard deviation. Every resistance distribution is constructed by varying one stochastic variable (using the numbers in Table 3). There is looked at the spread of the structure's resistance and large spread is interpreted as large sensitivity.

In the previous subparagraph it is concluded that shear failure is an unlikely event to occur, and the focus for the remainder of the thesis will be on bending failure. Diverse stochastic parameters have been varied during the Monte Carlo procedure. What is the influence of any parameters on the cross-sectional resistance? Later in this thesis finite element analyses will be done. This sensitivity study is used to compare the numerical model.

The sensitivity of the parameters is found by varying every stochastic parameter one at a time. More specifically, every single stochastic parameter is analysed while the other stochastic parameters are assumed to be deterministic. The deterministic values are equal to the mean value of the variable as presented in **Table 3**. To be noted that some parameters are appearing nonlinearly in the analytical expressions, therefore it is not possible to conclude on forehand what the sensitivity will be. This is also the reason why there has been chosen to use an equivalent load, rather than showing the probability density function of the given parameters and make decisions based upon these images.

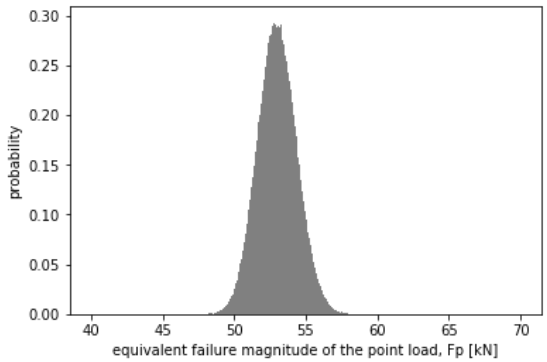

Figure 4.6: Varying the effective depth

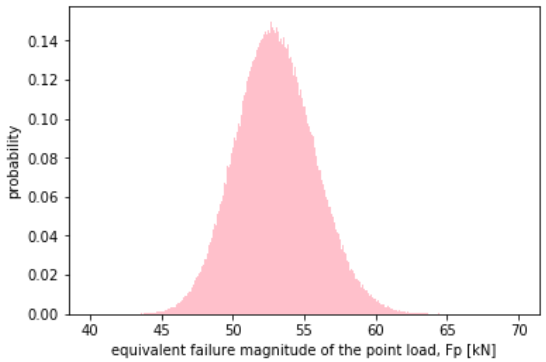

Figure 4.8: Varying the yield strength of the steel

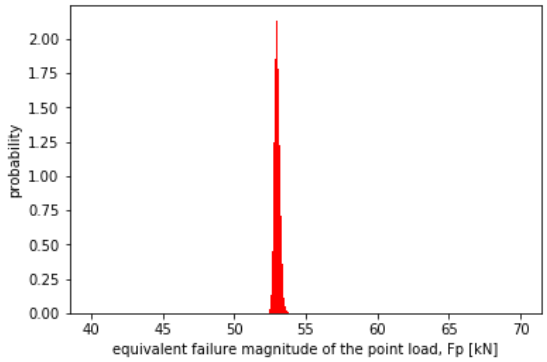

Figure 4.7: Varying the concrete compressive strength

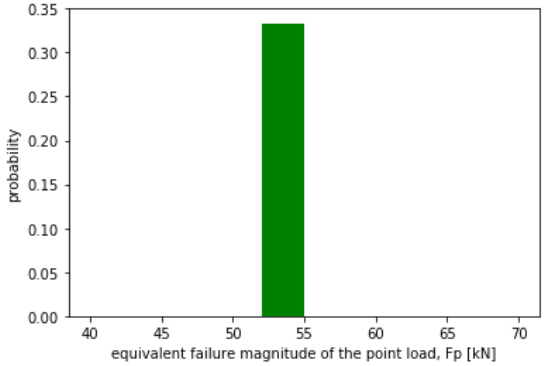

Figure 4.9: Varying the young's modulus of reinforcement

Presented in Figure 4.6 - Figure 4.9 is the cross-sectional bending resistance of the structure. It is clearly shown that the yield strength of the reinforcement steel is the most important factor

for the bending capacity. This is obvious because the reinforcement steel is the only part of the cross-section that can transfer tensile stress. A slight differentiation in this parameter can have a large influence on the cross-sectional resistance.

The variation of the effective depth has quite however not as large of an impact. This parameter regulates the arm between the internal cross-sectional forces. Consequently, this has a large influence on the resistance. Furthermore, the variation of the Young's modulus of the reinforcement steel has hardly any effect on the bending capacity. As a matter of fact, the Young's modulus is only influencing the compression reinforcement. However, the concrete only works in the compressive region for the compressive resistance in the cross-section. The concrete compressive strength has a small impact on the cross-sectional resistance. The concrete compressive region is changing when the concrete compressive strength changes.

Although the concrete compressive strength has a large coefficient of variation, its influence on the cross-sectional resistance is not significant. It can be conclude that a parameter with a small coefficient of variation (COV) can have a bigger influence on the spread of the failure load than one with a larger COV.

4.3 Semi-probabilistic calculation of the structure's analytical model

The third paragraph of the fourth chapter is the first paragraph that consists of reliability calculations. More specifically, semi-probabilistic calculations are done. This semi-probabilistic procedure is done by following the Eurocode design procedure. Furthermore, the structural scheme is statically indeterminate and therefore moment reduction is allowed in certain cases. This is explained in the last part of this paragraph. Finally, the design load per the semi-probabilistic calculation procedure is determined.

4.3.1 Calculation of design moment resistance

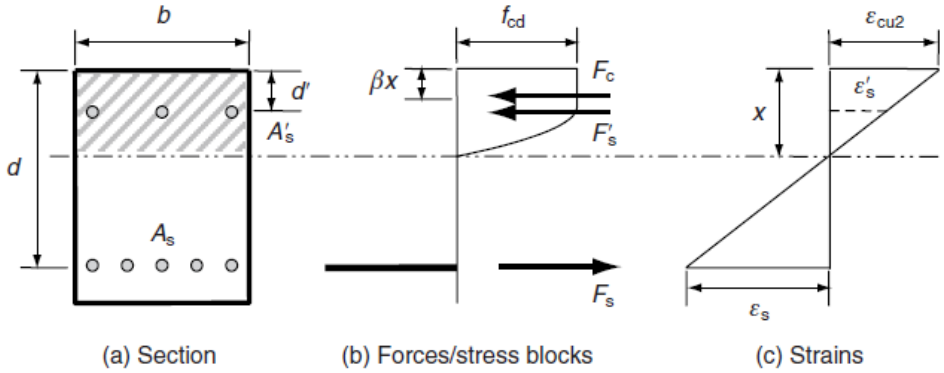

Figure 4.10 stress and strain distribution in the concrete cross-section

Keeping the assumptions discussed paragraph 4.1.1 in mind, with the Eurocode the cross-sectional resistance can be calculated. The constitutive relations in Figure 4.10 are valid for the derivation of the cross-sectional resistance. Using Appendix B.1 once again, the described procedure can be followed:

First the height of the concrete compressive zone is calculated. Within this calculation there is assumed that the reinforcement steel in the compressive zone is yielding.

$$x_u = \frac{fy_k}{\gamma_s} * \frac{As - A'_s}{f_{av} * b} \tag{4.15}$$

This assumption is checked in eq. (4.16).

$$\varepsilon'_s \geq \varepsilon_{s_{yield}} \leftrightarrow \varepsilon_{cu2} * (1 - \frac{d'}{x_u}) \geq \frac{f_{yk}}{\gamma_s * E_s} \tag{4.16}$$

When inequality (4.16) holds the design moment capacity can be calculated in the following way:

$$M_{rd} = F_c * (d - \beta_u * x_u) + F'_s * (d - d')$$

$$F_c = f_{av} * b * x_u \tag{4.17}$$

$$F'_s = \frac{fy_k}{\gamma_S} * A'_s$$

However, when the inequality does not hold, the design moment capacity has to be determined by making use of the strain compatibility method. The method is consisting of the following equations to determine the internal forces:

$$F_c = f_{av} * b * x_u \tag{4.18}$$

$$F_s' = E_s * \varepsilon_s' * A_s'$$
$$\varepsilon_s' = \varepsilon_{cu2} * \left(1 - \frac{d'}{x_u}\right) \tag{4.19}$$

Using horizontal equilibrium of force gives expression (4.20). Thereafter equation(4.18) and (4.19) can be substituted.

$$F_c + F_s' = F_s$$

$$f_{av} * b * x_u + E_s * \varepsilon_s' * A_s' = \frac{fy_k}{\gamma_S} * A_s$$

$$f_{av} * b * x_u^2 + \left(E_s * \varepsilon_{cu2} * A_s' - \frac{fy_k}{\gamma_S} * A_s\right) * x_u - d' * E_s * \varepsilon_{cu2} * A_s' = 0 \tag{4.20}$$

Solving the quadratic equation for x by using the ABC-formula. It turns out that there is only one physically possible answer:

$$x_u = -\frac{\left(E_s * \varepsilon_{cu2} * A_s' - \frac{fy_k}{\gamma_S} * A_s\right)}{2 * f_{av} * b} + \frac{\sqrt{\left(\frac{E_s * \varepsilon_{cu2} * A_s' - \frac{fy_k}{\gamma_S} * A_s}{f_{av} * b}\right)^2 + \frac{4 * d' * E_s * \varepsilon_{cu2} * A_s'}{(f_{av} * b)^2}}}{2} \tag{4.21}$$

With this value for height of the concrete compressive zone the last step can be made. The cross-sectional moment capacity is calculated by using eq. (4.22).

$$M_{rd} = F_c * (d - \beta_u * x_u) + F_s' * (d - d') \tag{4.22}$$

To see what the recommendations of the Eurocode are, the numerical values are filled in. The Eurocode makes use of the characteristic values of the stochastic variables. For the resistance part of the limit state function this characteristic value is the 5-quantile of the probability density function. The characteristic value of the solicitation part of the limit state function is the 95-quantile of the probability density function of its variable.
Using the information state above, the height of the concrete compressive zone is calculated. First with the assumption that the reinforcement steel in the compressive zone is yielding.

$$x_u = \frac{391.6}{1.15} * \frac{\frac{3-2}{4} * \pi * 12^2}{0.6 * 0.69 * 23.28 * 150} = 26.6[\text{mm}]$$

With this height of the concrete compressive zone, the assumption of the yielding reinforcement in the compressive zone can be checked.

$$3.5 * 10^{-3} * (1 - \frac{24}{26.6}) \geq \frac{391.7}{1.15 * 199 * 10^3}$$

$$3.4 * 10^{-4} \geq 1.7 * 10^{-3}$$

The assumption was not correct, and the strain compatibility method must be used. Thus:

$$x_u = -\frac{\left(1.73 * 3.5 * 10^3 * \frac{3}{4} * \pi * 12^2 - \frac{391.6}{1.15} * \frac{2}{4} * \pi * 12^2\right)}{2 * 0.69 * 0.6 * 23.28 * 150} + \sqrt{\left(\frac{1.73 * 3.5 * 10^3 * \frac{3}{4} * \pi * 12^2 - \frac{391.6}{1.15} * \frac{2}{4} * \pi * 12^2}{4 * 0.69 * 0.6 * 23.28 * 150}\right)^2 + \frac{24 * 1.73 * 3.5 * 10^3 * \frac{3}{4} * \pi * 12^2}{0.69 * 0.6 * 23.28 * 150}} = 28.95 \text{ [mm]}$$

Now the height of the compressive zone is known, the magnitude of the internal forces can be calculated. Thereafter the design bending moment resistance can be determined.

$$F_c = 0.6 * 0.69 * 23.28 * 150 * 28.95 = 41.8 * 10^3 \text{ [N]}$$

$$F_s' = 173 * 3.5 * \left(1 - \frac{24}{28.95}\right) * \frac{3}{4} * \pi * 12^2 = 35.1 * 10^3 \text{ [N]}$$

$$M_{rd} = 41.8 * 10^3 * (236 - 0.39 * 28.95) + 35.1 * 10^3 * (236 - 24) = 16.8 * 10^6 \text{ [Nmm]}$$

For statically determinate structures this would be the end of the design resistance calculation with respect to bending failure. However, thesis deals with statically indeterminate structures. As explained earlier, plastic hinges can develop in the structure and by allowing more deformation. The force on the structure can be increased further. In the Eurocode this is partly allowed, in paragraph 4.3.3 the moment reduction will be calculated. Before this calculation will be executed, rotation capacity should be checked.

4.3.2 Rotation capacity calculation

In paragraph 2.4.2, rotation capacity is introduced quite extensively. In this part of the thesis the verification whether the rotation capacity is sufficient will be done. Bending mechanism 1 is used because this mechanism is most likely to occur. In the latter mentioned paragraph the following expression for the required rotation capacity was derived. As a reminder, the α symbol is a length parameter and λ is the ratio between the bending and hogging moment resistance.

$$\Delta\varphi_b = -\frac{M_s * l}{3 * EI} + \frac{\Delta F_p * l^2}{2 * EI} * \left((1 - \alpha) - (1 - \alpha)^2\right)$$

$$\Delta Fp = Fp_{collapse} - Fp_{first\ plastic\ hinge}$$

$$Fp_{collapse} = \frac{Ms * (\alpha + \lambda)}{\alpha * l} \qquad (4.23)$$

$$Fp_{first\ plastic\ hinge} = \frac{2 * Ms}{3 * (1 - \alpha) * \alpha * l}$$

By filling in the numerical value, the following can be obtained:

$$Fp_{collapse} = \frac{21.2 * (0.375 + 1.5)}{0.375 * 2} = 53 \text{ [kN]}$$

$$Fp_{first\ plastic\ hinge} = \frac{2 * 21.2}{3 * (1 - 0.375) * 0.375 * 2} = 30.15 \text{ [kN]}$$

$$\Delta Fp = 53 - 30.15 = 22.85 \text{ [kN]}$$

The required rotation capacity is:

$$\Delta\varphi_b = abs\left(-\frac{21.2 * 2}{3 * 7070} + \frac{22.85 * 2^2}{2 * 7070} * \left((1 - 0.375) - (1 - 0.375)^2\right)\right) = 0.00048 \text{ [rad]}$$

To determine the available rotation capacity the method developed by, A. Bigaj and explained in paragraph 2.4.2 is used. Therefore, first the material reinforcement ratio must be determined:

$$c = \omega * \frac{f_y}{f_c'} = 0.96 * 10^{-2} * \frac{426}{30.9 * 0.8} = 0.25$$

By making use of Figure 2.14 empirical relation between the material reinforcement ratio and the plastic rotation capacity of a beam with a slenderness (a/h) of 12 on page 28, the $\Delta\varphi_{12}$ value can be determined. It turns out that in this case: $\Delta\varphi_{12} = 0.009$.

The last value that needs to be clarified is the value ‘a’ which is used in the final empirical equation. The definition for this parameter is: the distance between the points of the structure where the bending moment is equal to zero. This is shown on the right-hand side of Figure 2.14. The numerical value in this case is: $a = 0.667\ [m]$. Now all the numerical values are known, the available rotation capacity can be calculated.

$$\Delta\varphi_{a/h} = \left[\frac{\frac{a}{h}}{12}\right]^{0.85} * \Delta\varphi_{12} \qquad (4.24)$$

$$\Delta\varphi_{0.667/0.260} = \left[\frac{\frac{0.667}{0.260}}{12}\right]^{0.85} * 0.009 = 0.0024 \text{ [rad]}$$

The required rotation capacity is smaller than the available capacity, redistribution of the external forces is possible. The redistribution is done by reduction of the peak moment located at the middle support.

4.3.3 Moment reduction

There is enough rotation capacity available in the structure, therefore moment reduction is applied. Since hyper static beams are considered, linear elastic analysis with limited redistribution can be used. Because the Eurocode states; for the structural safety of hyper static beams it is always possible, in structural design, to refer to forces deduced from a linear

analysis that use the elastic characteristics of the section. It is also possible to refer the structural design to different stress diagrams, obtained with a redistribution of internal forces that keep equilibrium with the external forces. This can only be done as moments close enough are to the elastic one.

The characteristic concrete compressive strength is lower than 50 MPa, therefore the following redistribution can be used according to the Eurocode:

$$\delta \geq k_1 + k_2 * \xi \geq 0.7 \qquad (4.25)$$

Where:

$$k_1 = 0.44$$
$$k_2 = 1.25$$

$$\xi = \frac{x_u}{d} = \frac{29.24}{236} = 0.124$$

The numerical values for k1 and k2 are given in the fib MC2010. ((fib) 2012)

Therefore:

$$\delta \geq 0.44 + 1.25 * 0.124 = 0.59 \geq 0.7$$

Thus:

$$\delta = 0.7$$

4.3.4 Calculations of the design forces

The calculation of the design is performed in this subparagraph. The previous section has shown that the structure has enough rotation capacity and thus moment reduction is allowed. The maximum hogging bending moment at the mid-support can be reduced to 70% of its magnitude. Therefore, a larger design force will be calculated for the structure. This is beneficial from an economical prospective. The design force can have a maximum magnitude of:

$$M_{rd} \geq \delta * M_{ED} \tag{4.26}$$

$$M_{ED} \leq \frac{M_{rd}}{\delta} = \frac{16.8}{0.7} = 24.0\ [\mathrm{kNm}]$$

With linear elastic theory, the maximum hogging moment can be translated to a deterministic load. Figure 2.10 forget me nots; simply supported beam with a moment acting at one side and simply supported beam with one vertical point at distance 'a' from the left-hand side.
Figure 2.10, in which some forget-me-nots were introduced, gives the tools to do this. Together with Figure 2.12 and Figure 2.13 in which the support position of 3 forget-me-nots is shown graphically, the following derivation can be done:

$$\frac{M_{ED} * l}{3 * EI} = \frac{F_p * l^2}{6 * EI} * \left(2 * \frac{a}{l} - 3 * \frac{a^2}{l^2} + \frac{a^3}{l^3} + \frac{a}{l} - \frac{a^3}{l^3}\right)$$

$$a = l * (1 - \alpha) \tag{4.27}$$

$$F_p = \frac{2 * M_{ED}}{3 * l * (1 - \alpha) * \alpha}$$

$$F_p = 34.4[\mathrm{kN}]$$

The force $F_p = 34.4[\mathrm{kN}]$ is derived from the Eurocode procedure. The target reliability of the Eurocode is $\beta = 3.8$. This value is rather low compared to the experiment outcome of $60\ [\mathrm{kN}]$. As explained earlier: Monnier found a failure load of $60\ [\mathrm{kN}]$ which is higher than the expected failure load. Monnier has observed that: The beam shows a considerable redistribution of the moments after the cracks has formed. Accordingly, in consequence of this redistribution, the yielding of the tensile reinforcement over the support occurred at a substantially higher load than that calculated according to the elastic theory. The bending moment at which yielding of the reinforcement began was in this case also higher than the calculated yield moment of the section concerned. The calculated collapse load was likewise exceeded. (Monnier 1970)

4.4 Full-probabilistic calculation of the structure's analytical model

The fourth paragraph of this chapter represents a full-probabilistic calculation procedure. Full-probabilistic calculations differ from semi-probabilistic calculations in the use of the limit state function, whereas semi-probabilistic calculations make use of characteristic values and partial factors. In this paragraph, first a procedure for the full-probabilistic calculation is chosen. Together with this choice certain assumption are made to reduce the calculation time. In the last section of this chapter, the properties of the limit state function are used to determine the design load.

4.4.1 Calculation method and assumptions

The full-probabilistic calculation methods (level III) were introduced in paragraph 2.3.1 and the limit state functions used were derived in paragraph 2.4.1. The full-probabilistic calculation procedure that will be used is called "explicit calculation". This method is the least time-consuming method and therefore preferred. It consists of one single expression to calculate the reliability index, equation(4.9). Within this procedure the assumption is that the stochastic variables of the limit state function are independent and normally distributed. Under these assumptions the reliability index can be calculated in the following way:

$$\beta = \frac{\mu(Z)}{\sigma(Z)} \tag{4.28}$$

And thus, the probability of failure:

$$P(F) = \Phi(-\beta) \tag{4.29}$$

Remark: In the second paragraph, Monte Carlo simulation is used to determine the probability of failure in shear. Even though the Monte Carlo simulation is a full-probabilistic method, there was deliberately chosen to use another procedure for the determination of the design load. It would have been better to use the Monte Carlo procedure again in this section for the determination of the failure probability. This was not done, due to limited time for the process, the alternative procedure which is explained below, was continued.

In state, the cross-sectional resistance is approximated by a normal distributed variable, consequently a small error should be accepted and the computation time is significantly smaller. Additionally, Monte Carlo simulation will not give an exact reliability index representation. Monte Carlo simulation counts the number of successes (or failures) to determine a probability of failure. One could not translate this directly to a reliability index.

The limit state function and the properties of the random variables are known. The force parameter F_p is assumed to be deterministic, as the correlation between the bending moment resistance is assumed to be independent of each other. The reason is: one bending moment is resistance of a negative (field) moment and the other bending moment is the resistance of a positive (support) moment. Thus, these moment resistances are completely different from each other.

Let us recall the necessary information before proceeding the calculations. As mentioned in the paragraph 2.4.1. there are three possible failure mechanisms within the assumptions in this thesis. “Table 1 limit state functions of the failure mechanisms” on page 17 has given all the information about the three limit state functions. In paragraph 4.2.2 a Monte Carlo simulation was done to establish the distribution of the moment resistance. In the remark this was explained by choosing time reduction for an approximation of the moment resistance of the cross-section. The mean value and standard deviation of the resistance of the plastic hinges is approached by:

$$\mu_{M_s} = 21.23$$
$$\sigma_{M_s} = 1.07$$
$$V_M = \frac{\sigma_{M_s}}{\mu_{M_s}} = 0.05$$

And

$$\mu_{M_f} = 31.85$$
$$\sigma_{M_f} = 1.61$$
$$V_M = \frac{\sigma_{M_f}}{\mu_{M_f}} = 0.05$$

These values are extracted from “Python” by analysing the outcome of the Monte Carlo simulation. The mean values and the standard deviations of the moment capacity can be obtained. This is the approximation of the probability density function of the cross-sectional capacity. See also appendix A1 where the “Pyhton” script is displayed. Another point of attention, the value of the external force on the structure is assumed to be deterministic. This means that the standard deviation of the force is equal to zero.

$$V_F = 0$$

4.4.2 Derivation of the design load

Table 4 and Table 5 represent the mean values and standard deviations of the three limit state functions. With this information the reliability index can be calculated according to equation (4.9). The result is presented, together with the numerical evaluation in Table 6 deterministic value of failure load of all possible failure mechanisms.

Table 4 mean values of the limit state functions

Case:	Mean value:
1	$\mu(Z) = \mu_{M_s} * \left(\frac{\alpha + \lambda}{1 - \alpha}\right) - F_p * \alpha l * \left(\frac{1}{1 - \alpha}\right)$
2	$\mu(Z) = \mu_{M_s} * \left(\frac{1 - \alpha + \lambda}{\alpha}\right) - F_p * \alpha l * \left(\frac{1}{\alpha}\right)$
3	$\mu(Z) = \mu_{M_s} * \left(\frac{\alpha - \alpha * \lambda + \lambda}{1 - 2 * \alpha}\right) - F_p * \alpha l$

Table 5 standard deviations of the limit state functions

Case:	Standard deviation:
1	$\sigma(Z)^2 = \left(\mu_{M_s} * \left(\frac{\alpha}{1-\alpha}\right) * V_M\right)^2 + \left(\mu_{M_f} * \left(1 + \frac{\alpha}{1-\alpha}\right) * V_M\right)^2$
2	$\sigma(Z)^2 = \left(\mu_{M_s} * \frac{1-\alpha}{\alpha} * V_M\right)^2 + \left(\mu_{M_f} * \left(\frac{1}{\alpha}\right) * V_M\right)^2$
3	$\sigma(Z)^2 = \left(\mu_{M_s} * \left(\frac{\alpha}{1-2*\alpha}\right) * V_M\right)^2 + \left(\mu_{M_f} * \left(1 + \frac{\alpha}{1-2*\alpha}\right) * V_M\right)^2$

Table 6 deterministic value of failure load of all possible failure mechanisms

Case	Deterministic F_p
1	$F_p * \alpha l * \left(\frac{1}{1-\alpha}\right) =$ $= M_s * \left(\frac{\alpha+\lambda}{1-\alpha}\right) - \beta * \left(\left(M_s * \left(\frac{\alpha}{1-\alpha}\right) * V_M\right)^2 + \left(M_f * \left(1 + \frac{\alpha}{1-\alpha}\right) * V_M\right)^2\right)^{1/2}$ $F_p * 1.2 = 63.69 - \beta * 2.63$
2	$F_p * \alpha l * \left(\frac{1}{\alpha}\right) =$ $= M_s * \left(\frac{1-\alpha+\lambda}{\alpha}\right) - \beta * \left(\left(M_s * \frac{1-\alpha}{\alpha} * V_M\right)^2 + \left(M_f * \left(\frac{1}{\alpha}\right) * V_M\right)^2\right)^{1/2}$ $F_p * 2.00 = 120.30 - \beta * 4.60$
3	$F_p * \alpha l =$ $= M_s * \left(\frac{\alpha - \alpha * \lambda + \lambda}{1-2*\alpha}\right) - \beta *$ $* \left(\left(M_s * \left(\frac{\alpha}{1-2*\alpha}\right) * V_M\right)^2 + \left(M_f * \left(1 + \frac{\alpha}{1-2*\alpha}\right) * V_M\right)^2\right)^{1/2}$ $F_p * 0.75 = 111.46 - \beta * 4.29$

Finally, with the information obtained from Table 6, the reliability index of the three bending mechanisms is calculated. As solicitation the same force as found in the semi-probabilistic calculation is used.

Table 7: reliability index of the bending mechanisms.

Case	**Force**	**Reliability index**
1	$F_p = 34.4$[kN]	$\beta = 8.5$
2	$F_p = 34.4$ [kN]	$\beta = 11.2$
3	$F_p = 34.4$ [kN]	$\beta = 20.0$

Bending mechanism 1 is most likely to occur, however the reliability index is still rather high. Thus is this case the semi-probabilistic calculation is very conservative. To give clear idea about the difference, the equivalent force to a reliability index of $\beta = 3.8$ would be:

$$F_p = 44.75[\mathrm{kN}]$$

And the failure load according the full-probabilistic calculation would have been:

$$F_p = 53.08[\mathrm{kN}]$$

This value is still conservative since it is known that the actual failure load is:

$$F_p = 60.00[\mathrm{kN}]$$

Once again: Monnier found a failure load of $60\ [\mathrm{kN}]$ which is higher than the expected failure load. Monnier has observed that: The beam shows a considerable redistribution of the moments after the cracks has formed. Accordingly, in consequence of this redistribution, the yielding of the tensile reinforcement over the support occurred at a substantially higher load than that calculated according to the elastic theory. The bending moment at which yielding of the reinforcement began was in this case also higher than the calculated yield moment of the section concerned. The calculated collapse load was likewise exceeded. (Monnier 1970)

However, it can be concluded that the semi-probabilistic calculation compared to the full-probabilistic calculation is conservative. The reason for this is probably the type of cross-section which is used during the experiment by Monnier. This cross-section had a rather unusual distribution of reinforcement. Due to this extraordinary choice the standard code have difficulty in determination of design forces.

4.5 Comparison between the results of full-probabilistic and semi-probabilistic calculations

The previous paragraph has shown that a full-probabilistic calculation presents much higher design values then the semi-probabilistic calculation according to the Eurocode. In this paragraph the reason for this rather extensive difference will be discussed.

4.5.1 Comparison in case of much redistribution of forces

First, the location of the reinforcement is discussed. The cross-section of the beam as used in this thesis does not change along its length. This is rather strange for a statically indeterminate structure. The way in which engineers design such beams is done by reinforcing the peak moments. The cross-section of this beam has the least reinforcement at the side of the peak moment (at the mid-support) (Figure 4.11). However, the total amount of reinforcement is enough to let the beam develop all its plastic hinges without local failure. For ULS calculations this is not an issue. Moreover, engineers should design their structures in SLS. The restrictions with respect to the SLS are much stricter, because comfort is considered. Therefore, large displacements are not allowed according these requirements.

Second, the results of the semi and full-probabilistic calculation summarised in Table 8. As discussed before, engineers can design with the theory of plasticity in the ULS. However, the semi-probabilistic calculation procedure using the Eurocode does not allow full redistribution of forces. Instead, only the peak moment (at mid-support) might be reduced to 70% of its value. This is the main reason that the differences between the semi-probabilistic and full-probabilistic calculations have such a disagreement.

Table 8 results of the semi-probabilistic and full-probabilistic calculations in one table

Method	Force	Reliability index
Semi-probabilistic	$F_p = 34.4[\text{kN}]$	$\beta = 3.8$
Full-probabilistic	$F_p = 44.8[\text{kN}]$	$\beta = 3.8$
Full-probabilistic	$F_p = 53.1[\text{kN}]$	$\beta = 0.0$
experiment	$F_p = 60.0[\text{kN}]$	-

In this thesis SLS is touched upon, however this would be a great extension for this thesis. As to show that the redistribution of force is indeed the cause of this difference, a different cross-section will be used in in the next paragraph. The goal is to see if the differences between the semi-probabilistic and full-probabilistic calculation with respect to statically indeterminate structures will decrease.

4.5.2 Comparison in case of no redistribution of forces

It has been noticed that when large displacements are necessary to activate the entire capacity of a structure, it will cause large difference between the semi-probabilistic and the full-probabilistic calculations. Therefore, a case study has been done with the same structure, but a different cross-section. The only two things that have changed are the reinforcement ratios (top and bottom). They are swapped; meaning, three longitudinal reinforcement bars as top reinforcement and two longitudinal reinforcement bars are bottom reinforcement. The cross-section is displayed in Figure 4.12. The full calculation is done in Appendix C.

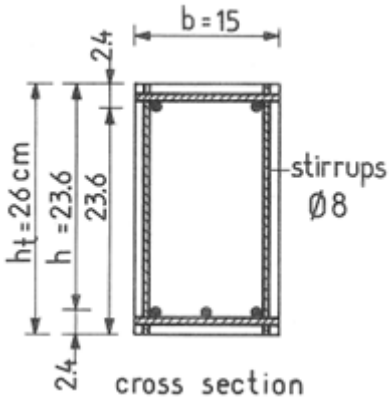

Figure 4.11 cross-section 1

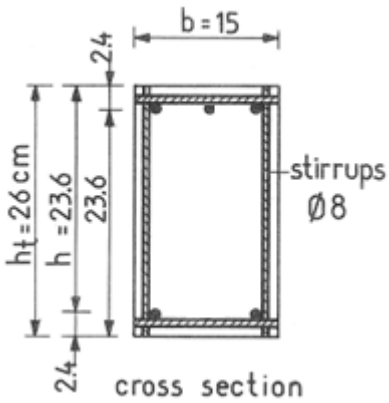

Figure 4.12 cross-section 2

Table 9 results of the case study with no redistribution of forces in a statically indeterminate structure, of the Eurocode and the level III reliability calculations in one table.

Method	Force	Reliability index
Semi-probabilistic	$F_p = 34.8[\text{kN}]$	$\beta = 3.8$
Full-probabilistic	$F_p = 38.0\ [\text{kN}]$	$\beta = 3.8$
Full-probabilistic	$F_p = 42.3\ [\text{kN}]$	$\beta = 0.0$
experiment	$F_p = 46.6[\text{kN}]$	-

The results are shown in Table 9. It is striking that the results are much more in agreement. Due to the new design of the cross-section, less redistribution of force is necessary. The semi-probabilistic calculation in the Eurocode is limited with regards to redistribution. This is not a bad thing, however it can cause an overcapacity in a structure that is not taken into account.

The expected failure load determined through the full-probabilistic method is still lower than the actual failure load. However the difference between the two outcomes is smaller than the previous case.

5 Numerical model for structural analyses

In this chapter a finite element model is build up to evaluate the experiment by Monnier, introduced in chapter 3. This finite element model will be used to utilise a sensitivity study. The sensitivity study will show the influences of nonlinear effects on the maximum bending capacity of the structure. It is very inconvenient to take nonlinear effects into account with hand calculations. However, finite element programme “DIANA” gave the possibility to deal with physical and geometric nonlinear properties in a convenient way.

In paragraph 5.1, the verification of the finite element model is executed. Before the finite element model can be used to perform the sensitivity study, the finite element model need to be calibrated. This is done by making use of the, in chapter 4 introduced, analytical model of the structure. Firstly, a one-dimensional finite element model is made, and the force-displacement relation of the analytical model and the finite element model are compared. By doing this check, the finite element model is verified. However, this is an in-between step to keep track of the discretisation of the model. Secondly, the same procedure must be done for a two-dimensional approximation of the structure. A two-dimensional model is necessary to use because “DIANA” does not provide all the nonlinear properties in one-dimensional models.

Paragraph 5.2 presents the results of the sensitivity analyses of the nonlinear effects. The following nonlinear effects are investigated in the sensitivity study:

- Tensile strength of the concrete;
- Ultimate tensile strength of the reinforcement steel;
- Bond slip relation between the reinforcement steel and the concrete.

The aim of this chapter is to give a brief overview of the influences of these nonlinear effects, when considered. There are no reliability calculations performed in combination with the finite element model.

5.1 Verification of finite element models

In this paragraph the numerical models used for the sensitivity discussed in paragraph 5.2 is studied. The numerical schemes for the finite element models are introduced and discussed. Furthermore, the mesh, load scheme and convergence norm will be examined.

The evaluation of the models will be done by making use of the mean values given in “Table 3 parameters used in the parameter study”. Firstly, a one dimensional model is evaluated because the hand-calculation uses theory of plasticity and is based on one dimensional approximations. Secondly, after the verification of the one-dimensional model a two-dimensional model is set up. As a matter of fact, not all of the nonlinear properties that are studied in the sensitivity study are supported in one dimensional finite element models.

In Table 10 the numerical schemes for the finite element analyses are presented. The mesh density is courser in the two-dimensional model than the one-dimensional. The number of elements in a two-dimensional model is considerably higher and on top of that they have more degrees of freedom. Consequently, the tangential stiffness matrix of a two-dimensional structure is much larger. In every load step a larger system of equations must be solved. However, the accuracy of a finer mesh is in most cases larger than the accuracy of a courser mesh. The balance between the computation time and accuracy is a point of attention. In this specific model there is chosen for a courser mesh to safe computation time.

Important to note, for the one-dimensional model (Figure 5.1), beam elements are applied. This choice tries to make the best approximation of the analytical model as introduced in chapter 4. In the two-dimensional model is made use of plane stress elements. This type of elements provides the possibility to include the nonlinear effects mentioned earlier.

Table 10 Numerical analyses schemes for finite element models

Dimensions	Element size	Load	Convergence		Iteration		
			Norm	Tol	#	Method	Converge scheme
1D	5 mm	Force	Displa Force	1e-2 1e-2	25	Newton-Raphson	Line search
2D	25 mm	Force	Displa Force	1e-2 1e-2	25	Newton-Raphson	Line search

Path following techniques
In finite element model there are two ways to apply loads one the model:

- Prescribed forces (force control)
- Prescribed displacements (displacement control)

Path following method is another (according to some better) name for arc-length control. The path following method is a modification of the force and displacement control methods. The force control method increases the magnitude of load with a prescribed value and by solving a system of equation the corresponding displacement are found. Moreover, the displacement control method does the same however the displacements are increased by a fixed value and the corresponding forces are determined. In addition to these two methods, the path following method does not increases or decreases the magnitude of just one unit. Both force and displacement units are modified in every load step, and the length of the force displacement step is prescribed. Therefore, the magnitude of the force increment, and the displacement increment can very every load step, although the total arc-length of the load increment in the force displacement space stays the same. (prof.dr.ir. R. de Borst 2015)

To analyse the numerical models, arc length control is used. The advantage of arc length control is that the load step does not have to have a fixed value beforehand. In state, the arc length algorithm determines during the load step what the load and displacement will become. The disadvantage is however that it costs more time to execute an analysis. In general, is displacement control preferred, because it costs less computation time, it is a pretty stable method, and most experiments are displacement controlled performed.

Having said that, in case of the experiment used in this thesis, one of the boundary conditions is that the two forces acting on the structure have the same magnitude. This means that the experiment was performed as a force control loading procedure. This is very hard to model with displacement control, on top of that force control can become numerically unstable very quick. Therefore, the path following method is used.

Figure 5.1 geometry of the one-dimensional model

5.1.1 Load step

The nonlinear analyses are executed by making use of load steps. There is chosen for arc-length load steps of 0.8. It turns out that this choice of load step is very efficient, because the nonlinear effects are visible and there are no problems with convergence. There is only looked at bending failure of the beam, there were no large errors obtained during calculation. Furthermore, there were numerous step sizes tried, but 0.8 seems the most efficient.

5.1.2 Convergence norm

The convergence norm is the following:

- Force <1%
- Displacement <1%

Both criteria must hold at the same time. In most load steps the critical factor was the force convergence. The force convergence is in this case the most important since the loading is force based.

5.1.3 Comparison of the one-dimensional numerical model with experiment and the hand calculations

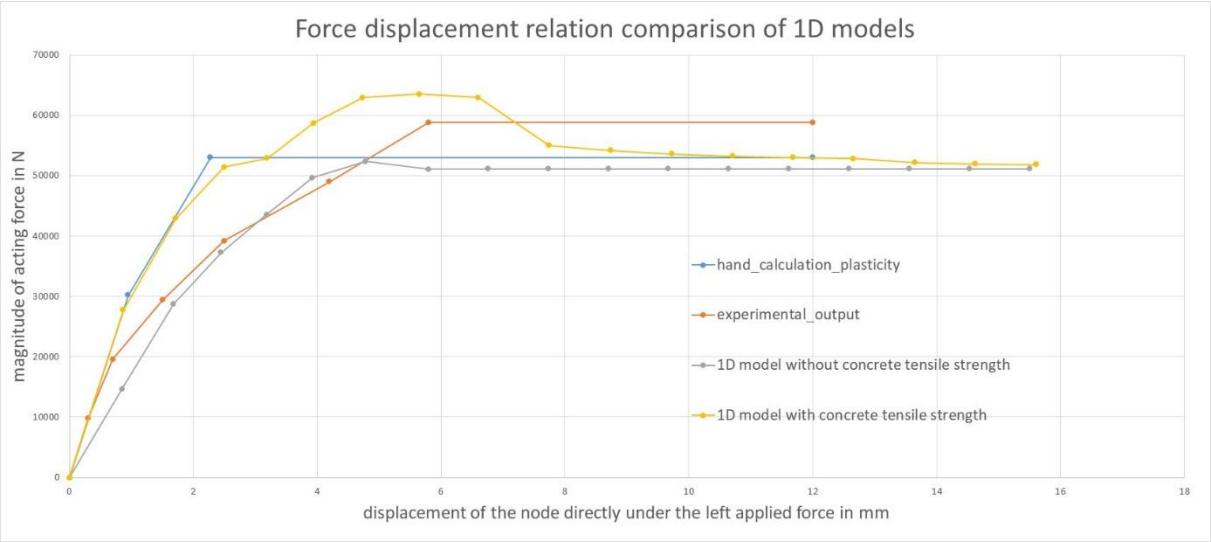

Figure 5.2 Force displacement diagram of two different one-dimensional models, one hand calculation and the experimental results presented in one graph

Figure 5.2 shows four different force displacement relations in one graph. There is chosen to present the force-displacement relation because it gives a good global impression of the behaviour of the structure. It is striking that the one-dimensional model which include the tensile strength looks very much like the hand calculation. Different is the peak value of the one-dimensional model, however this difference is explained by the fact that tensile strength is not considered in the hand calculation. Hence, the one-dimensional model without concrete tensile strength does not quite look like the hand calculation's output. Another assumption done in the hand calculation can clarify this variance. Namely, the cross-section that is used for the hand calculation remains the same throughout the whole calculation procedure. The one-dimensional model is done with a nonlinear loading procedure and the constitutive is therefore also update every load step. Because of this the cross-sectional area changes during the load execution and explains the difference in output.
Moreover, without concrete tensile strength, the concrete beam starts to crack from the very first load step. Therefore, the elastic responds of the beam is less stiff. Vis-à-vis the result that came from the laboratory experiment by Monnier is slightly different. Keeping in mind that a one-dimensional model of the beam is not a flatness approximation. In the next section, the two-dimensional models are compared with experiment results. These models are more sophisticated and ergo the expectation is that the force displacement relations are more similar.

5.1.4 Comparison of the two-dimensional numerical model with experiment and the hand calculations

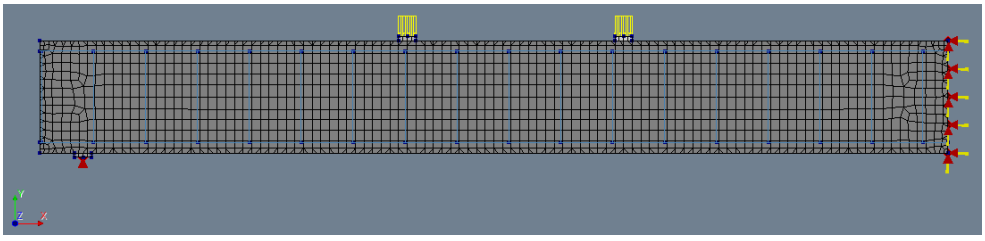

Figure 5.3 geometry and mesh of the two-dimensional model

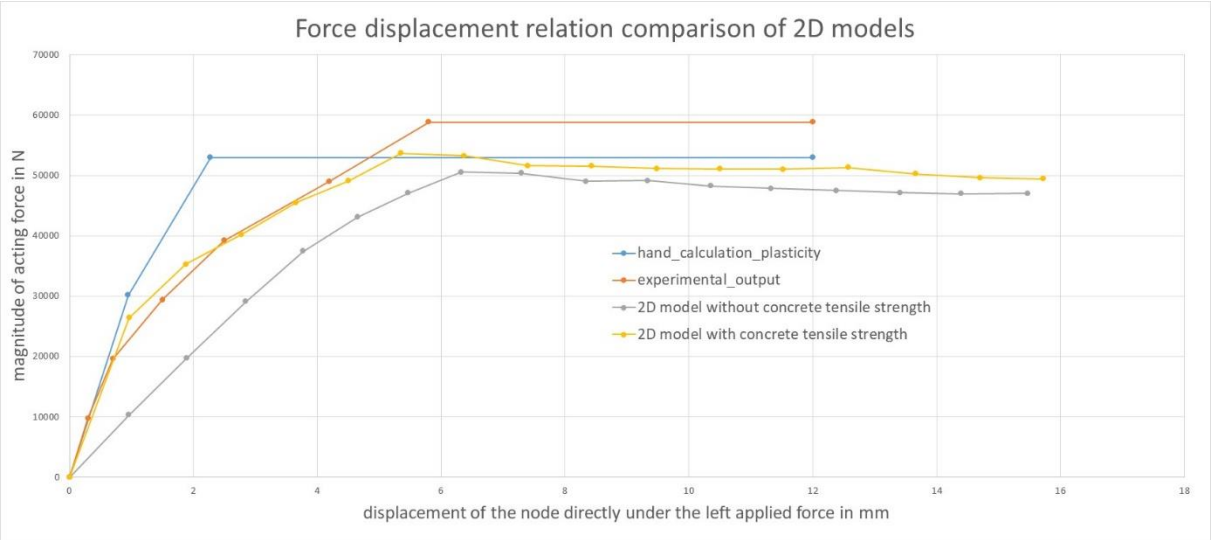

Figure 5.4 Force displacement diagram of two different two-dimensional models, one hand calculation and the experimental results presented in one graph

The force displacement relation of the two-dimensional models together with the experimental results and the hand calculation out is presented in Figure 5.4. Notably is the line which represents the force displacement relation of the two-dimensional model without concrete tensile strength. This line shows a very ductile behaviour. Due to the very low tensile strength of the concrete, cracks develop rapidly. Consequently, the cross-sectional area decreases and so does the stiffness of the structure. The other line that represent the two-dimensional model with concrete tensile strength shows behaviour that is like the one of the experiment. Noticeable is the peak value of the experiment compared to the simulation done with the finite element model. The peak in the experiment is higher, this difference is extensive discussed in the previous chapter. The two-dimensional model with concrete tensile strength will be used as cornerstone of the sensitivity study.
To note, the boundary conditions at the right hand side of the 2D-model (Figure 5.3) is **incorrect**. The vertical constrain should only be applied at the bottom, however it is applied over the entire height. This mistake is not expected to have a mayor effect on the results found in this thesis.

5.1.5 Sensitivity of the yield stress of the reinforcement

Now the calibration of the two-dimensional model is complete, the sensitivity is compared. As said in the previous chapter, the sensitivity of the parameters will be checked as well. In order to do this another approach is used than in case of the analytical model. 15 random draws out of the yield stress' distribution are taken. Numbers are generated from the probability density function. As introduced in the previous chapter, the mean value of the yield stress is 426.7 N/mm^2 with a coefficient of variation of 5%. The distribution of all the random variables is log-normal. The random draws are done from this distribution and the 15 draws are found in ascending order in Table 11.

Keeping all the material and geometrical properties the same and varying the yield stress of the reinforcement steel, Figure 5.5 can be obtained. Thereafter the comparison of the yield stress sensitivity of the reinforcement's yield stress is displayed. Figure 5.6 shows that the numerical sensitivity is equal to the sensitivity shown by the analytical model.

Table 11 random draws from the log-normal distribution of the yield strength of the reinforcement steel

Number of sensitivity simulation	Reinforcement yield stress $[N/mm^2]$
1	388.85
2	399.73
3	406.06
4	410.95
5	415.15
6	418.97
7	422.61
8	426.17
9	429.76
10	433.48
11	437.48
12	441.95
13	447.28
14	454.35
15	467.07

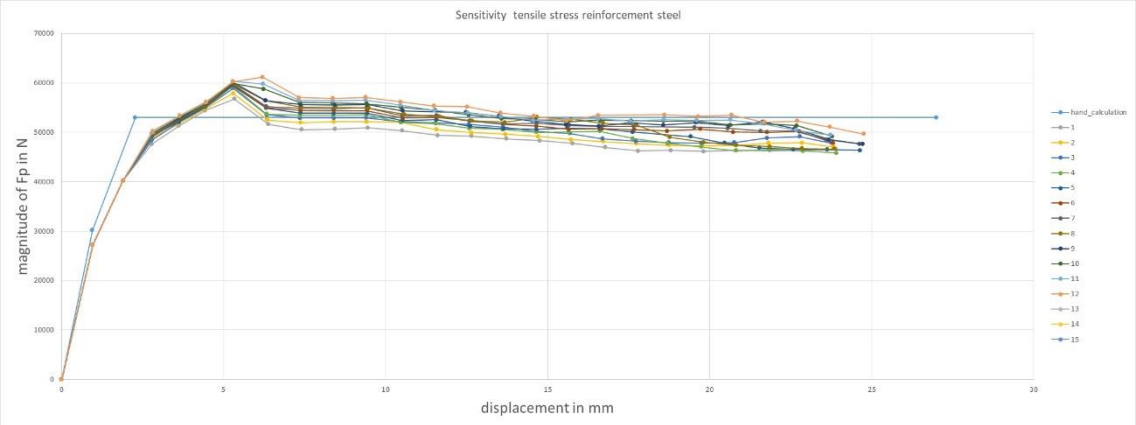

Figure 5.5 force displacement relation of the sensitivity analysis with the given parameters in Table 11.

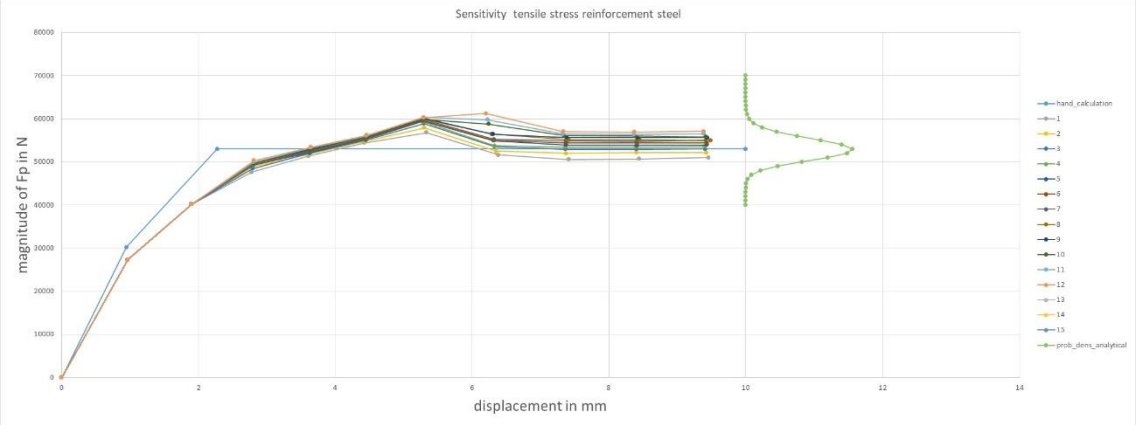

Figure 5.6 comparison of the sensitivity of the reinforcement's yield stress

In order to keep track of the correctness of the execution of the calculation procedure, the stress in the reinforcement is monitored. In Figure 5.7 the force displacement diagram is shown. The Roman numbers in Figure 5.7 are corresponding with the screenshots in Figure 5.8. The 5 screenshots displayed below (Figure 5.8) are taken from the 8th simulation with a yield stress of the reinforcement of 426.17 N/mm^2. It is clearly visible the first plastic hinge develops on the right hand side of the beam in the top region. This is the place where this was expected. From the 2nd screenshot, the development of the 2nd plastic hinge is started. This confirms the expectations with respect to this analysis and therefore is accepted as a good simulation.

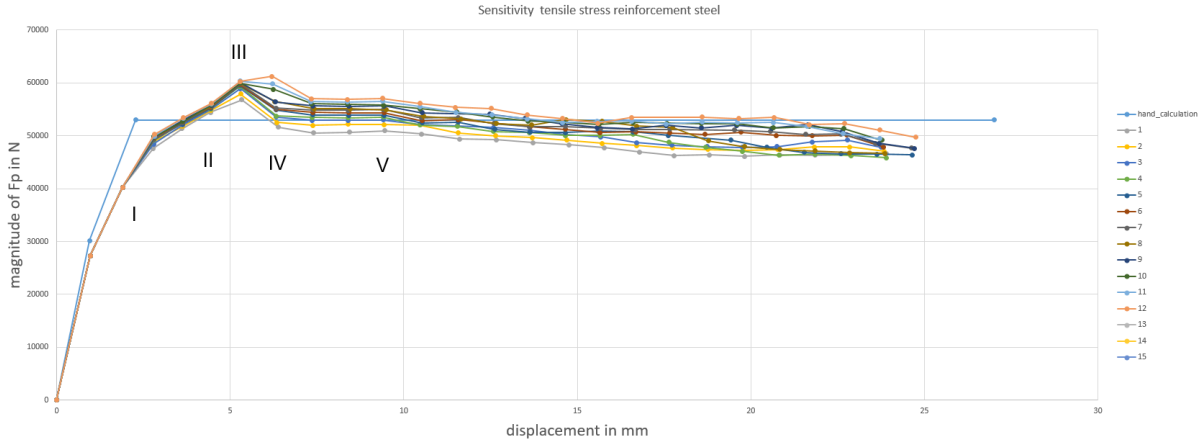

Figure 5.7 the five stages which are investigated for one simulation

I

II

III

IV

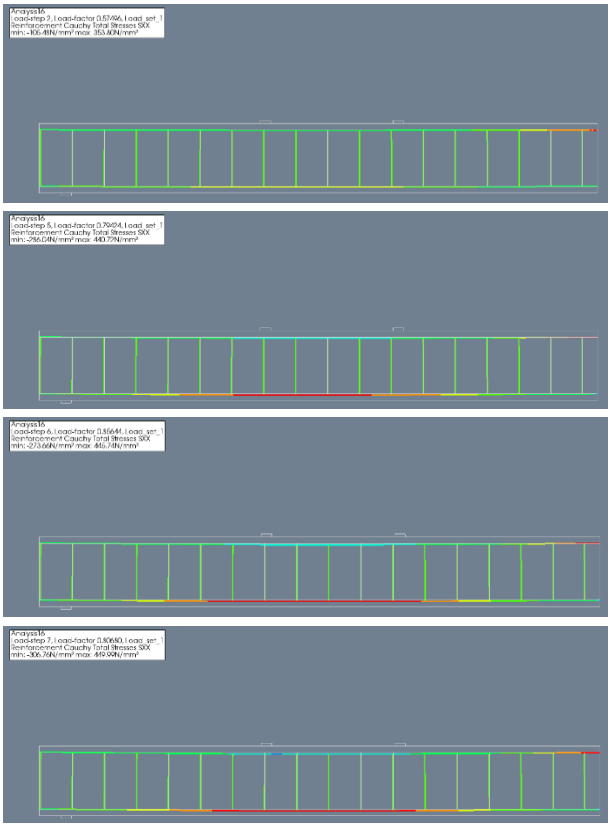

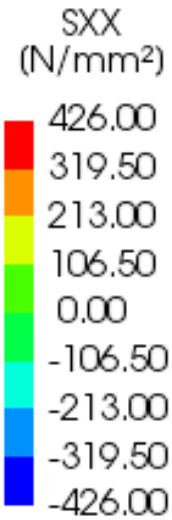

V

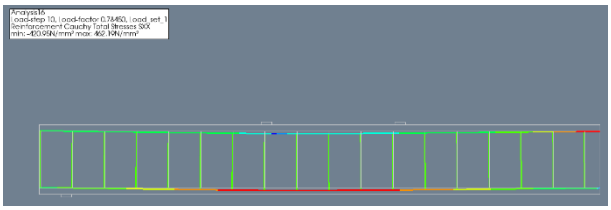

Figure 5.8 The stress diagrams in the 5 stage as displayed in Figure 5.7

Figure 5.8 displays the stresses in the reinforcement of the beam during the loading process. In the very first stage already the development of the first plastic hinge is visible. The location of the peak stress in the reinforcement is exactly where it was expected. The second, third and fourth stage show the stress increase of the second plastic hinge. This second plastic hinge is formed at the same position as found in the analytical calculation. The fifth and last stage shows some large compressive stress in the reinforcement. At the location on the force-displacement graph, where this stage was taken, the displacement is already considerably large. Thus the compressive strain at the top of the cross-section just under the left load is large. All in all, the results in Figure 5.8 show results that were expected.

5.2 Sensitivity of nonlinear constitutive parameters

The sensitivity study is documented in this paragraph. This documentation starts off with the initial model properties. These initial properties come from the previous paragraph in which the one- and two-dimensional models were compared. As concluded earlier there is made use of two-dimensional numerical models.
One of the nonlinear constitutive parameters is the concrete tensile strength with tensile softening. Also, the ultimate tensile strength of the reinforcement steel will be varied. The influences of this variation will be discussed as second nonlinear effect. The last nonlinear effect that is looked at is bond-slip relation between the reinforcement steel and the concrete. In general, the bond between the reinforcement and the concrete is taken as fully embedded. Moreover, in the second chapter is showed that in this specific case the bond is not a critical factor.

5.2.1 Initial situation

The zero or initial situation is the start point of the sensitivity study. The initial parameters are presented below in Table 12 and Figure 5.9 shows the force displacement relation of this initial model.

Table 12 Initial model properties for nonlinear sensitivity study

Properties	Symbol	Magnitude	Unit
Concrete tensile strength	f_{ctm}	2	N/mm^2
Fracture energy	G_f	1.135	N/mm
Concrete compressive strength	f_c	30.9	N/mm^2
Yield strength reinforcement steel	f_y	426.7	N/mm^2
Young's modulus (steel)	E_s	199143	N/mm^2
Young's modulus (concrete)	E_c	32176	N/mm^2

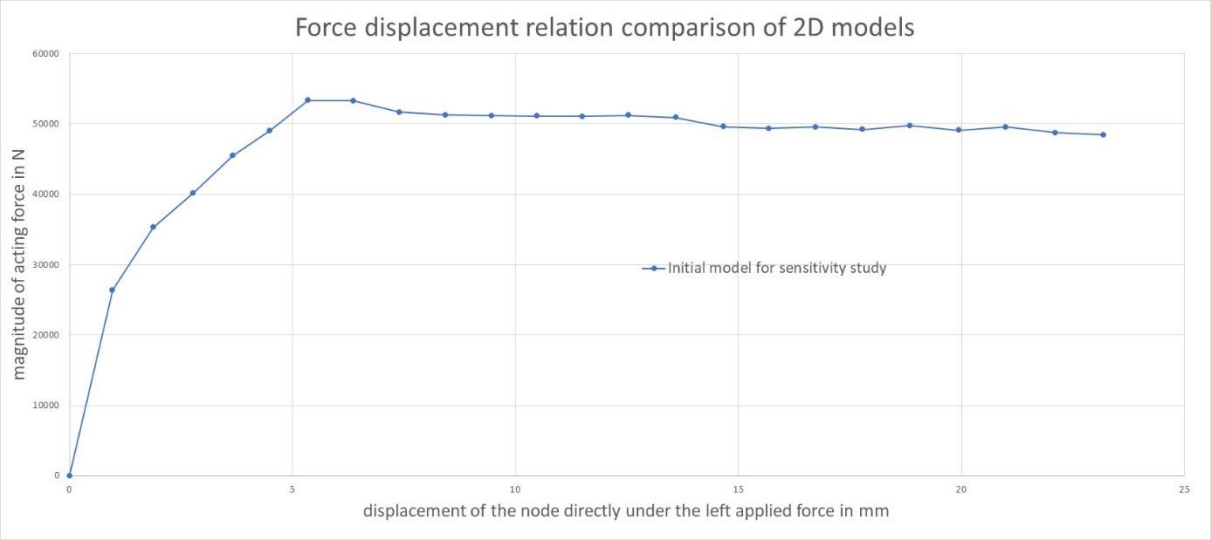

Figure 5.9 initial force displacement relation based upon the properties given in Table 12

5.2.2 Sensitivity of concrete tensile strength

The sensitivity of the concrete tensile strength starts with a simulation in which the concrete tensile strength is close to zero. Exactly zero is not possible in the finite element programme and therefore is chosen for a very small number. In the hand-calculation that is discussed in the previous chapter, does not account for concrete tensile strength and that is the reason to investigate this value. The process continues by a concrete tensile strength that is risen gradually (shown in Table 13), first to 2 N/mm^2 which is the actual value obtained during the tests before the laboratory experiment. Note, there is not made use of any probabilistic approach for generating these numbers.

On top of that the behaviour of the structure is simulated with even a higher concrete tensile strength. As one can conclude from Figure 5.10 a simulation with a concrete tensile strength higher than 0.3 N/mm^2 does not increase the failure load significantly. The response of the structure is stiffer when the concrete tensile strength increases. Despite that the maximum force during the plastic deformation of the structure is more or less the same as that of the latter mentioned value.

Table 13 the magnitude of the different concrete tensile strength in the sensitivity study

Number of sensitivity simulation	Concrete tensile strength [N/mm^2]
1	1*e-7
2	0.2857
3	0.5714
4	0.8571
5	1.1429
6	1.4286
7	1.7143
8	2
9	2.2857
10	2.5714
11	2.8571
12	3.1429
13	3.4286
14	3.7143
15	4

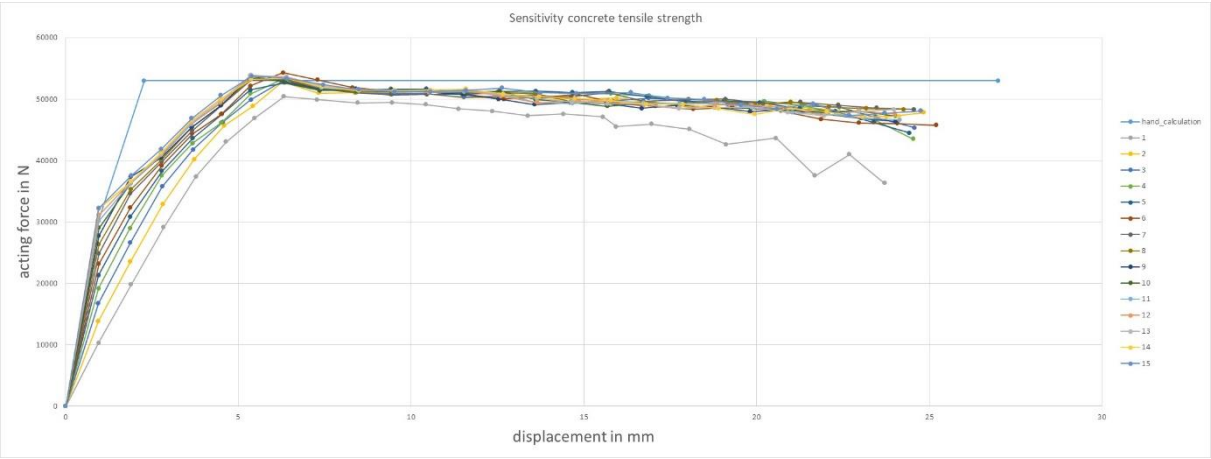

Figure 5.10 force displacement relation of the different sensitivity simulations based on the values in Table 13

To show what is happening in the material during the loading procedure, the stresses and strains in the concrete are monitored. In Figure 5.11 the force displacement relation of the sensitivity study in concrete tensile strength is shown. The Roman numbers in Figure 5.11 are corresponding with the screenshots in Figure 5.12. Four screenshots are displayed in Figure 5.12 are taken from the 8th simulation with a concrete compressive strength of 2 N/mm^2. It is clearly visible the first plastic hinge develops on the right hand side of the beam in the top region. Cracks develop in that region to activate the reinforcement steel. This is the place where cracks were expected. From the 5th screenshot, the development of the 2nd plastic hinge is started. This confirms the expectations with respect to this analysis and therefore is accepted as a good simulation.

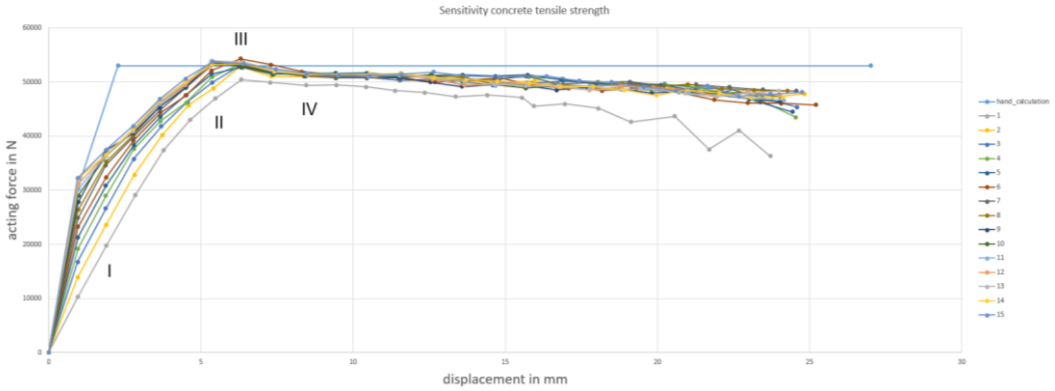

Figure 5.11 The force displacement relation of the concrete tensile strength sensitivity with indicated locations to check the stresses and strain during the simulation.

I

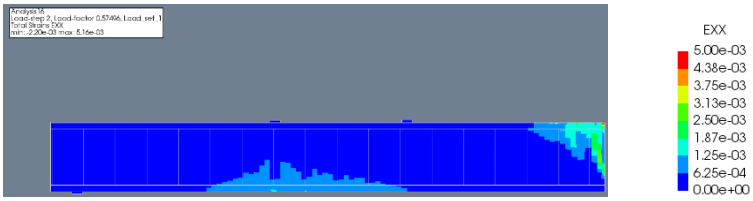

II

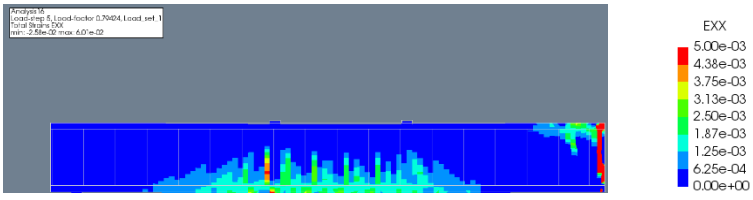

III

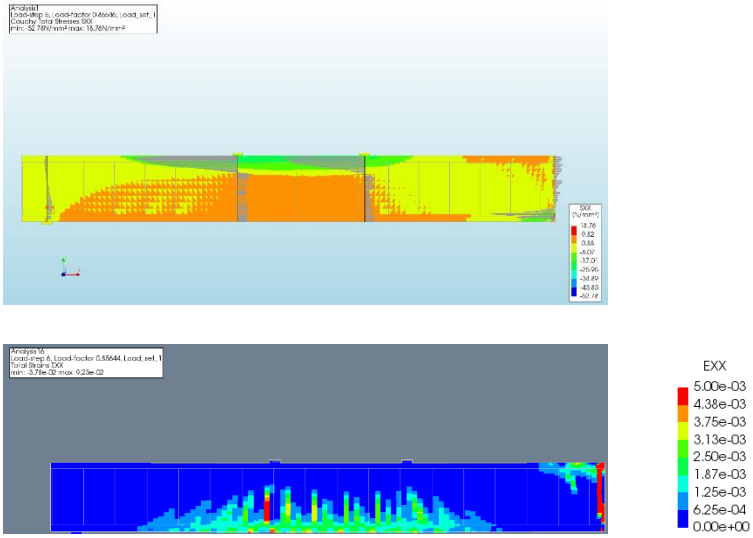

IV

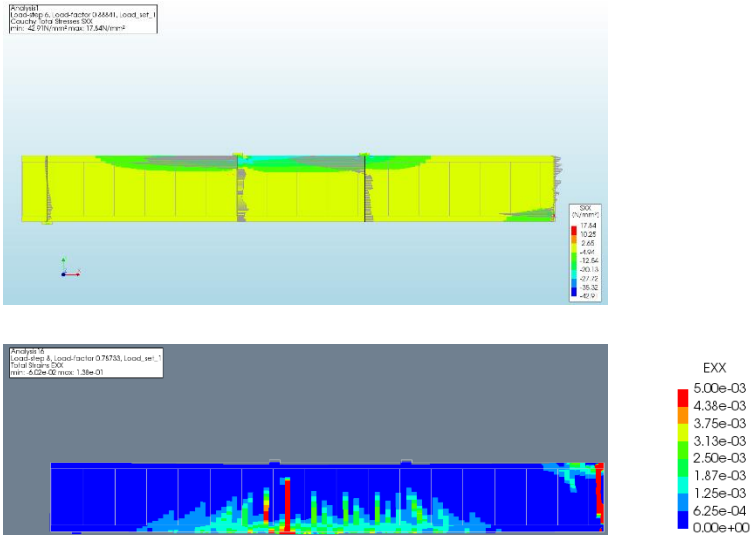

Figure 5.12 The four check stress and strain distributions

Figure 5.12 displays four stages during the loading process. More precisely the stress and strain distribution of the concrete is shown. The stain distribution shows only the positive strains. The locations at which cracks develop are then easy to spot.
The first stage that is displayed shows crack development at the upper right hand side. The same behaviour was found when the reinforcement was evaluated. At the same time is it clearly visible that the strains start to develop at the bottom region of the beam. The Second, third and fourth stage show further development of the strain and thus cracks in the beam.

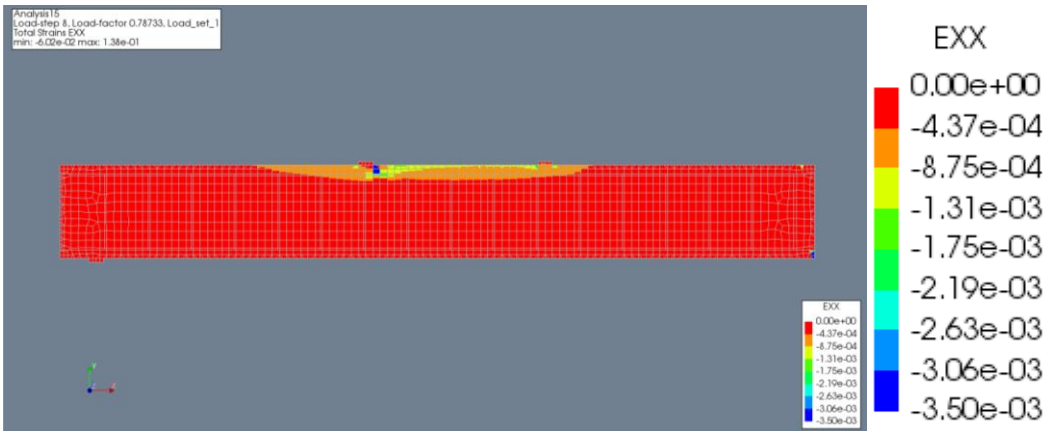

Figure 5.13 concrete compressive strains in the IV stage as given in Figure 5.11

The thing that is not shown here is the concrete compressive strain. It could be that the concrete compressive strength is decisive as well. A quick hand calculation shows:

$$\varepsilon = \frac{\sigma}{E} = \frac{30.9}{32176} = 9{,}6 * 10^{-4}\ [-]$$

A compressive strain of 9.6‰ would be a possible problem for concrete crushing. Figure 5.13 shows that the concrete compressive strength does not have significant influence. There are some peak strains visible underneath the applied forces. This could be a numerical singularity. Although, the concrete crushing could happen very locally, it would not be a significant effect to consider.

5.2.3 Ultimate tensile strength of reinforcement

The next non-linear properties that is considered in the sensitivity study is the ultimate tensile strength of the reinforcement. The numbers used for this sensitivity study are chosen without probabilistic background. To allow the structure to develop plastic hinges a yield plateau is required. In every simulation initial stiffness similar and the length of the yield plateau as well. Difference is in the actual ultimate stress when hardening starts. One example is shown in Figure 5.14. All the points in this figure are changed in ratio with each other so that the shape keeps the same.

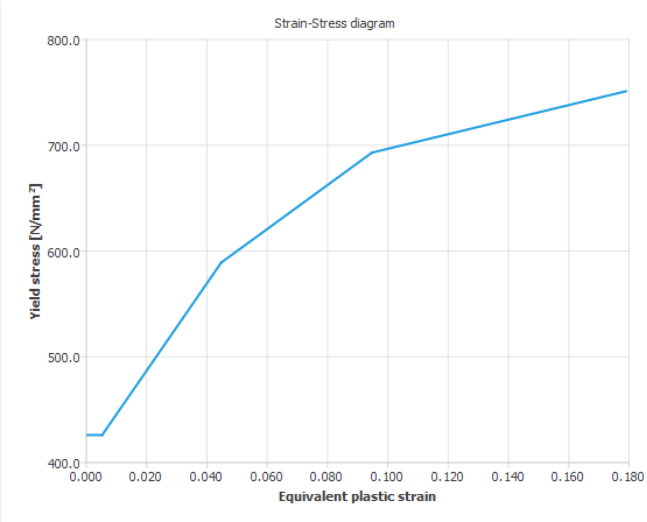

Figure 5.14 example of stress-plastic strain relationship

Table 14 the magnitude of the different ultimate tensile strength of the reinforcement steel in the sensitivity study

Number of sensitivity simulation	Ultimate tensile strength of reinforcement $[N/mm^2]$
1	540
2	555
3	570
4	585
5	600
6	615
7	630
8	645
9	660
10	675
11	690
12	705
13	720
14	735
15	750

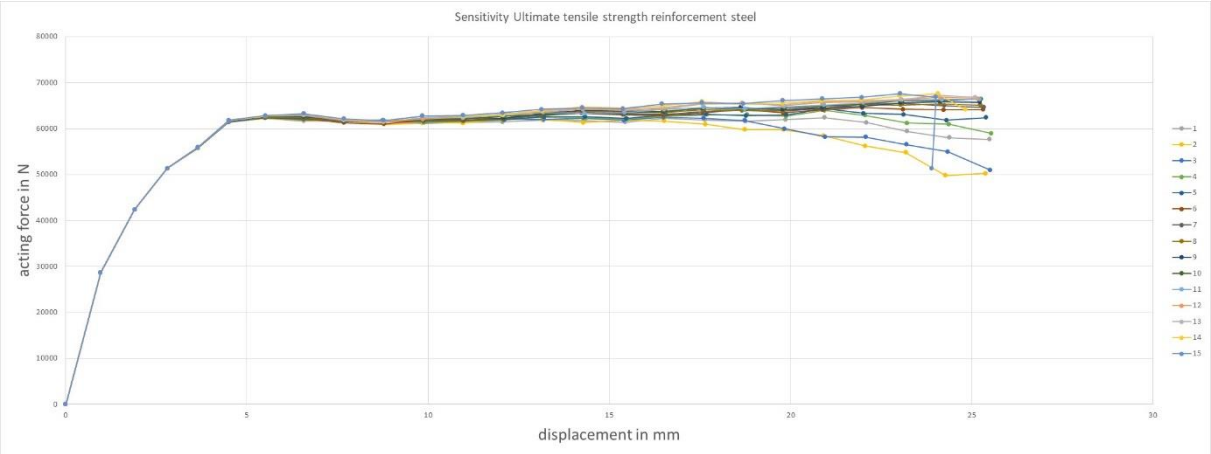

Figure 5.15 force displacement relation of the different sensitivity simulations based on the values in Table 14

The influence of the ultimate tensile strength of reinforcement steel is not very large. The variation of maximum value is quite large as shown in Table 14, however, Figure 5.15 displays very small difference in maximum force. The effect of the ultimate tensile strength of the reinforcement is only visible far beyond the point where the failure mechanism has developed. The ultimate tensile strength starts to work when plastic strain develops. It turns out that the plastic strain in the first plastic hinge starts to develop when full failure mechanism has formed.

5.2.4 Bond-slip relation

As mentioned in the second chapter, bond-slip is not an issue which would cause problems in the specific structure that is investigated in this thesis. Nonetheless, its effect is investigated to get an idea what the possible effects are when it becomes critical. Table 15 gives an overview of the values that are tried as normal and shear stiffness modulus of the bond between the concrete and the reinforcement steel.

Table 15 the magnitude of the different normal stiffness modulus in the sensitivity study

Number of sensitivity simulation	Normal stiffness modulus $[N/mm^3]$	shear stiffness modulus $[N/mm^3]$
1	20	20
2	40	40
3	60	60
4	80	80
5	100	100
6	200	200
7	300	300
8	400	400
9	500	500
10	600	600
11	700	700
12	800	800
13	900	900
14	1000	1000
15	1100	1100

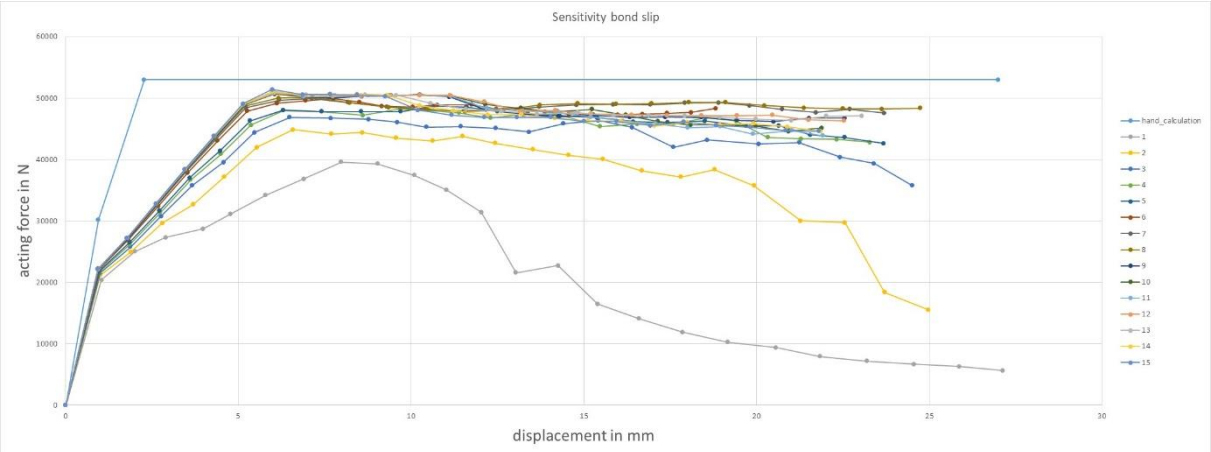

Figure 5.16 force displacement relation of the different sensitivity simulations based on the values in Table 15

It turns out that the very low values (under 100 $[\mathrm{N/mm^3}]$) have a large scatter. In contrast the normal stiffness modulus larger than 100 $[\mathrm{N/mm^3}]$ do not have a large bias.
When the shear stiffness modulus is very low, the bond between the reinforcement steel and the concrete is weak. The concrete has difficulty in transferring the tensile strength to the reinforcement. Usually a cracking pattern with a lot of small crack will occur. However, when the bonding is weak the cracking pattern will not occur instead a few crack will develop due to exceeding the concrete tensile strength. These cracks will have a large crack width. The grey line in Figure 5.16 shows the force displacement relationship of a model with a low shear stiffness modulus.

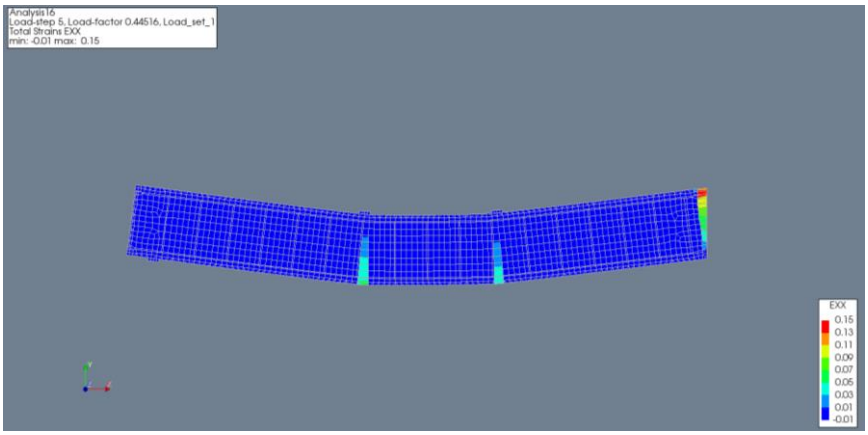

Figure 5.17 strain distribution in a concrete beam with a low bond between the concrete and the reinforcement steel.

The reason that force-displacement relation of structure with a low bond between the concrete and the reinforcement steel differs is explained by using Figure 5.17. This figure was taken from the “DIANA” analysis with the lowest bond-slip relation in the fifth load step.
The concrete has to deform first to activate the reinforcement. The tensile strength of concrete is low compared to its compressive strength and this is the reason that reinforcement steel is used. When the structure is loaded, the tensile stressed regions of the concrete starts to crack. Now the reinforcement is activated and the reinforcement bar is elongated. Due to the elongation the reinforcement bar it could transfer tensile stresses to other parts of the concrete to create a crack pattern. When the bond between the concrete and the reinforcement steel is low problems occur. The steel cannot transfer the force easily. Consequently, large cracks occur. When the load is increased the little number of cracks have to increase to handle more load that is applied on the structure. Therefore the crack width is large compared to a structure with perfect bond between concrete and reinforcement steel. In Figure 5.17 it is clearly visible this is happening.

5.3 Conclusion

In the previous paragraph, the results of the sensitivity analysis of the nonlinear constitutive parameters was presented. As mentioned earlier, the goal of the sensitivity study to see the influence of the nonlinear parameters on the failure load. Neither of the three-investigated nonlinear parameter has mayor influence on the failure load. Though it is striking that the concrete tensile strength has most influence on the elastic stage of the failure process. Whereas the bond-slip and ultimate yield strength have more influences later in the failure process. The bond-slip causes a variation in the stage just after the formation of the first plastic hinge. The final stage of the failure process scatters largely if the ultimate tensile strength of the reinforcement is varied.

In case of a statically indeterminate reinforced concrete beam with a symmetric two span geometry, neither bond-slip nor ultimate tensile strength variation of the reinforcement steel is significate to the bending capacity. However, concrete tensile strength can be considered when finite element is evaluated. Without this tensile strength a slightly lower maximal bending capacity will be found.

In this thesis there is no probability analysis done in combination with finite element models. A logic continuation would be to perform such an analysis. The nonlinear effects investigated in this chapter will not have a large influence on this probability analysis. Having said that, the values used in the analytical hand calculation will be quite interesting to test in combination with finite elements. Full probabilistic analyses require a lot (and in most cases too much) computation time. However, the partial factors according to the EN 1992-1-1 were established for the component check, according to the classic design approach. Nevertheless, they can also be used in combination with non-linear analysis. (Schlune, Plos et al. 2012)

6 Conclusion

The research question that this thesis has tried to answer is as follows: *"How does a semi-probabilistic compare to a full-probabilistic safety assessment for a statically indeterminate beam structure?"*

To answer this question, the components of a reliability model have been investigated. The levels of model approximation (LoA) as stated in the model code 2010 together with the level of reliability calculations (Steenbergen 2011) were used. Two combinations between LoA and reliability methods have been analysed to assess their strengths and weaknesses. These two reliability analyses were both were based on an analytical model (LoA I). The reliability level I and III, the so called semi-probabilistic and full-probabilistic, calculations were used.

In conclusion, the full-probabilistic reliability calculation is all cases applicable to determine the probability of failure of a statically indeterminate structure. However, semi-probability reliability are useful as well but it does allow only partly redistribution of forces. In case of statically indeterminate structures this can have significant impact on the failure load. The best reliability method for a statically indeterminate structure is dependent on the amount of redistribution of forces.
The semi-probabilistic calculations treat structures, where a lot of redistribution can occur, conservatively. For instance, the semi-probabilistic calculation procedure that is used in this thesis allows for only partly redistribution of forces. The full-probabilistic calculation procedure is therefore beneficial to use for structures where a lot of redistribution can occur in the ultimate limit state.

It turned out that the full-probabilistic calculation determines a higher reliability of the structure. In the full-probabilistic analysis, the limit state function is used in its analytical form. Whereas in the semi-probabilistic analysis is made with the use of approximations of the limit state function. However, when the cross-section of a statically indeterminate structure is designed in such a way that little redistribution will take place, the difference between the full- and semi-probabilistic is insignificant.

Numerical analyses in the form of nonlinear finite element analysis have been investigated. With a sensitivity study is looked at the influence of certain parameters on nonlinear analyses. These parameters were; concrete tensile strength, yield stress of the reinforcement steel and the bond-slip relation between the concrete and the reinforcement steel.
The sensitivity study showed that, the influence of the reinforcement's yield stress has the same sensitivity as in the analytical model. The other parameters are only used in the nonlinear analyses, since it is very hard to implement in an analytical model. Besides, the numerical calculation showed that, the influence of the non-linear parameters is not significant on the failure load. It is expected that non-linear effects will not generate significant different results from the analytical simulations without these effects.

The stochastic parameters used in the reliability analysis were investigated in the fourth chapter. In regards to the analytical model, it turns out that a stochastic parameter with a small coefficient of variation (COV) can have a bigger influence on the spread of the resistance than one with a larger COV. Not all parameters occur linearly in the analytical expression and therefore it is not obvious what the effect on the cross-sectional capacity is. After preforming a

Monte Carlo simulation, it turned out that parameters with a small COV can have a large influence on the cross-sectional resistance.
Examples are:

- Concrete compressive strength (COV = 15%)
- Reinforcement's yield stress (COV = 5%)

Figure 6.1 displays the spread of the cross-sectional resistance when the concrete compressive strength is varied. Figure 6.2 does the same for the variation of the reinforcement's yield stress. It is seen that the difference is significant.

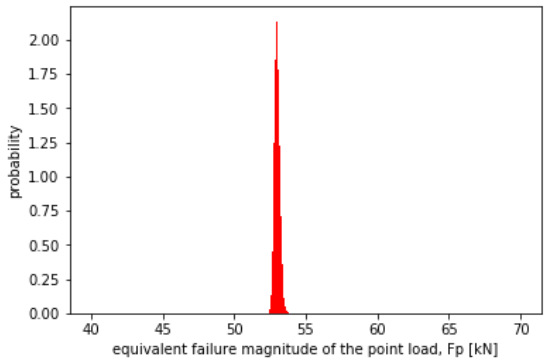

Figure 6.1 spread of the structural resistance when concrete compressive strength is varied

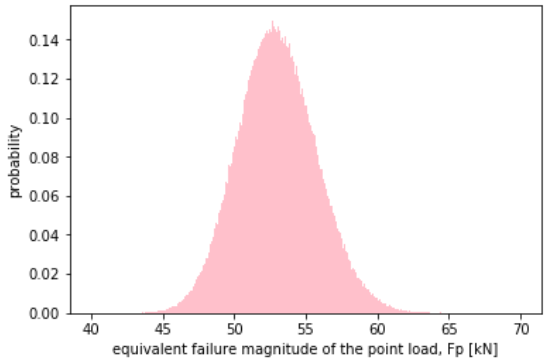

Figure 6.2 spread of the structural resistance when the reinforcement's yield stress is varied

7 Recommendation for future work

This paragraph lists recommendations for future work:

All the analyses done in this thesis are based on the ultimate limit state, a useful part to add would be the service ability limit state. The redistribution of forces would become less of importance and therefore the outcome of the full-probabilistic and semi-probabilistic calculations would become closer.

There is looked at only one specific statically indeterminate beam with equal spans. Due to this symmetry the calculation is simplified. When one looks at a statically indeterminate beam structure without a symmetry axis, the interaction between the span could causes interesting effects.

Another possible statically indeterminate structure that would be interesting to analyse is a frame structure. A frame structure is mostly statically indeterminate with a degree of 3 or even more, depending on the supports and existence of cross bars.

In this thesis, the loading scheme and the reinforcement in the structure clearly states that the structure fails in bending. With respect to reliability calculations and failure modes, it would be interesting to look at a different loading scheme. More specifically, look at a structure where the failure mode is not obvious. This could be achieved by a small modification in the location of the force.

This thesis provides only two reliability calculations. There are 12 combinations between a reliability method and a model approximation. One of these 12 combinations is not feasible due to computation time. That leaves 9 other reliability calculations possible to investigate.
With respect to the stochastic variables, not all the parameters used in the analyses are stochastic. A possibility is to evaluate the reliability calculation with all the parameters stochastic.

Bibliography

(fib), t. I. F. f. S. C. (2012). "Model Code 2010 - Final draft, Volume 2." **2**: 370.

(NEN), N. N. I. (2011). *Eurocode 2: Ontwerp en berekening van betonconstructies - Betonnen bruggen - Regels voor ontwerp, berekening en detaillering*. Delft, The Netherlands, Author.

Ellingwood, B. and T. V. Galambos (1982). "Probability-based criteria for structural design." Structural Safety **1**(1): 15-26.

Engen, M., et al. (2017). "A quantification of the modelling uncertainty of non-linear finite element analyses of large concrete structures." Structural Safety **64**: 1-8.

Hartsuijker, C. and H. Welleman (2003). Toegepaste mechanica: Deel 3: Statisch onbepaalde constructies en Bezwijkanalyse, Academic Service.

Janssen, L., et al. (2006). Welvaart en leefomgeving: een scenariostudie voor Nederland in 2040: achtergronddocument, Centraal Planbureau.

Jonkman, S., et al. (2015). "Probabilistic Design: Risk and Reliability Analysis in Civil Engineering." Lecture Notes CIE4130. Delft University of Technology.

König, G. and J. Fischer (1995). "Model Uncertainties concerning Design Equations for the Shear Capacity of Concrete Members without Shear Reinforcement."

Monnier, T. (1970). The Behaviour Continous Beams in Reinforced Concrete, Stevin-Laboratory of the Department of Civil Engineering, Delft University of Technology; Reijswik (ZH): Institute TNO for Building Materials and Building Structures.

prof.dr.ir. R. de Borst, P. d. i. L. J. S. (2015). "Computational methods in non-linear solid mechanics."

Roache, P. J. (1998). "Verification of codes and calculations." AIAA journal **36**(5): 696-702.

Schlune, H., et al. (2012). "Safety formats for non-linear analysis of concrete structures." Magazine of Concrete Research **64**(7): 563-574.

Wells, G. N. (2006). "The finite element method: An introduction." CT5123 Lecture Notes, Delft University of Technology: 10.

Wiśniewski, D. F., et al. (2012). "Probabilistic models for mechanical properties of concrete, reinforcing steel and pre-stressing steel." Structure and Infrastructure Engineering **8**(2): 111-123.

List of figures

List of tables

Appendices

A. Python scripts:
    1. Reliability calculation analytical model
    2. Run multiple projects in DIANA

B. Derivation structural formulas:
    1. Bending capacity formulas
    2. Shear force capacity formulas

C. Case study reliability calculation without redistribution of forces.

A. Python scripts

A.1. Reliability calculation analytical model

```
# Importing the Python packages
import numpy as np
import matplotlib.pyplot as plt
import time
import statistics
import math
from scipy.optimize import fsolve
from scipy.integrate import quad
from sympy import *
from mpl_toolkits.mplot3d import Axes3D
time_start_calculation = time.clock()

# Introducing the variables
n=10**8                          # number of samples in the parameter study
f_ck=315.*9.81/100.              # concrete compressive strength
cov_f_ck = 0.15                  # coefficient of variation of the concrete
compressive strength
sigma_bu=0.6*f_ck                # reduced concrete compressive strength
f_yk=4350.*9.81/100.             # yield strength of the bottom reinforcement steel
cov_f_yk = 0.05                  # coefficient of variation of theyield strength of
the reinforcement steel
Es=2.03*10.**6.*9.81/100.        # young's modulus of the reinforcement steel
cov_Es= 0.08                     # coefficient of variation of the young's modulus of
the reinforcement steel
d=236.                           # effective depth of the cross-section
cov_d_= 0.2                      # coefficient of variation of the cover of the
cross-section
d_=24.                           # effective depth of the top reinforcement
b=150.                           # width of the cross-section
w0_=0.64                         # top reinforcement ratio
w0=0.96                          # bottom reinforcement ratio
epsilon_cu2=3.5*10.**-3.         # maximum strain at the top of the concrete
cross-section
f_yk_=f_yk                       # yield strength of the top reinforcement steel
l=2000.                          # length of the field
alpha=75./200.                   # factor for the distance between the forces acting
on the beam
beta = 0.39                      # parameter for the arm of the force in the concrete
compressive zone

f_av=sigma_bu*0.69               # average stress in the concrete compressive zone

As_=w0_/100.*b*d                 # the area of top reinforcement in the cross-section
As=w0/100.*b*d                   # the area of bottom reinforcement in the
cross-section
rho_l=np.sqrt(w0_**2+w0**2)      # the total percentage of reinforcement steel in the
cross-section
a1=(3.*alpha**2.-3.*alpha+2.)/2. #  parameter to help with shear force calculation

# Definition of the structural calculations
# shear capacity according to the Eurocode
def Shearcapacity(b,d,d_,f_ck,rho_l,z):
    V_rd_max=1.0*b*(d-d_)*0.6*(1-f_ck/250.)*f_ck/1.5
    k=min(1.+np.sqrt(200./d),2.)
    V_rd_c=0.15/z*k*(100*rho_l*f_ck)**(1./3.)*b*d
    V=min(V_rd_max,V_rd_c)*10**-3
    return V

# bending capacity according to the Eurocode
def bendingcapacity(d_,d,As_,b,As,sigma_bu,epsilon_cu2,Es,f_yk,f_yk_,f_av,beta):

    f_av=sigma_bu*0.69
    B=(As_*Es*epsilon_cu2-f_yk*As)/(f_av*b)
    C=-(d_*As_*Es*epsilon_cu2)/(f_av*b)
    x=-B/2.+np.sqrt(B**2.-4.*C)/2.
    sigma_s=epsilon_cu2*Es*(1-d_/x)

    if sigma_s<f_yk_:
        Mu=(f_av*b*x*(d-beta*x)+As_*Es*epsilon_cu2*(1-d_/x)*(d-d_))*10**(-6)

    else:
        sigma_s=f_yk_
        x=(As-As_)/(f_av*b)*f_yk_
```

```
65          Mu=(f_av*b*x*(d-beta*x)+As_*f_yk*(d-d_))*10**(-6)
66
67      return Mu
68
69  # translate the maximum shear capacity into an equivalent pointload
70  def Shearcapacity_to_pointload(b,d,d_,f_ck,rho_l,z,alpha):
71      V_capacity=Shearcapacity(b,d,d_,f_ck,rho_l,z)
72      V_max=max(a1,(2-a1))
73      V=V_capacity*1./V_max
74      return V
75
76  # translate the maximum moment capacity into an equivalent pointload
77  def
    Bendingmoment_to_pointload(d_,d,As_,b,As,sigma_bu,epsilon_cu2,Es,f_yk,f_yk_,f_av,beta,
    alpha):
78
        Mu_support=bendingcapacity(d_,d,As,b,As_,sigma_bu,epsilon_cu2,Es,f_yk,f_yk_,f_av,b
        eta)
79      lambda_=As/As_
80      Fp=Mu_support*(alpha+lambda_)/(alpha*l*10**-3)
81      return Fp
82
83  # Definition of the probabilistic calculation
84  def mean_and_standard(cov,mean):
85      m,s= math.log(mean)-0.5*math.log(1+cov**2),np.sqrt(math.log(1+cov**2))
86      ret=([m,s])
87      return ret
88
89  def rand_var(f_ck,f_yk,Es):
90
91      m1,s1= mean_and_standard(cov_f_ck,f_ck)
92      m2,s2= mean_and_standard(cov_f_yk,f_yk)
93      m3,s3= mean_and_standard(cov_Es,Es)
94
95      v1 = np.random.lognormal(m1, s1,1)
96      v2 = np.random.lognormal(m2, s2,1)
97      v3 = np.random.lognormal(m3, s3,1)
98
99      R=([v1[0],v2[0],v3[0]])
100
101     return R
102
103 def rand_var2(d_):
104
105     m4,s4= mean_and_standard(cov_d_,d_)
106
107     v4 = np.random.lognormal(m4, s4,1)
108
109     R=(v4[0])
110
111     return R
112
113 def rand_var3(z):
114     m5,s5= mean_and_standard(cov_z,z)
115     v5 = np.random.lognormal(m5, s5,1)
116
117     R=(v5[0])
118
119     return R
120
121 ## Calculation with varying the parameters
122 time_start = time.clock()
123 list1=np.zeros(n)
124 list2=np.zeros(n)
125 list3=np.zeros(n)
126 list4=np.zeros(n)
127 count=0
128
129 for i in range(n):
130     f_ck=315.*9.81/100.
131     f_yk=4350.*9.81/100.
132     Es=2.03*10.**6.*9.81/100.
133     d_=24.
```

```
        d=236.
        var=rand_var(f_ck,f_yk,Es)
        f_ck=var[0]
        f_yk=var[1]
        Es=var[2]
        var2=rand_var2(d_)
        d_=var2
        d=236-(24-d_)
        sigma_bu=0.6*f_ck
        f_yk_=f_yk
        z=0.91
        cov_z=0.11
        z=rand_var3(z)

        V_shear=Shearcapacity_to_pointload(b,d,d_,f_ck,rho_l,z,alpha)

        V_bending=Bendingmoment_to_pointload(d_,d,As_,b,As,sigma_bu,epsilon_cu2,Es,f_yk,f_
        yk_,f_av,beta,alpha)

        list1[i-1]=V_shear
        list2[i-1]=V_bending
        list3[i-1]=Shearcapacity(b,d,d_,f_ck,rho_l,z)

        list4[i-1]=bendingcapacity(d_,d,As,b,As_,sigma_bu,epsilon_cu2,Es,f_yk,f_yk_,f_av,b
        eta)

        if V_shear<V_bending:
            count=count+1

    shear_failure = count/n
    print (list1)
    print (list2)
    print ('ratio of shear failure =',shear_failure)
    time_elapsed = (time.clock() - time_start)
    print('computation time lists =',time_elapsed,'sec')

    time_start = time.clock()

    count, bins, ignored = plt.hist(list3, 1000, normed=True, align='mid', color='blue')
    plt.xlabel('shear capacity[kN]')
    plt.ylabel('probability')
    plt.show()
    print('maximum shear capacity before failure')
    count, bins, ignored = plt.hist(list4, 1000, normed=True,align='mid', color='orange')
    plt.xlabel('bending capacity [kNm]')
    plt.ylabel('probability')
    plt.show()
    print('maximum bending capacity before failure')

    count, bins, ignored = plt.hist(list1, 1000, normed=True, align='mid', color='blue')
    plt.xlabel('equivalent failure magnitude of the point load, Fp [kN]')
    plt.ylabel('probability')
    plt.show()
    print('maximum shear capacity before failure')
    count, bins, ignored = plt.hist(list2, 1000, normed=True,align='mid', range=[40,70],
    color='orange')
    plt.xlabel('equivalent failure magnitude of the point load, Fp [kN]')
    plt.ylabel('probability')
    plt.show()
    print('maximum bending capacity before failure')
    count, bins, ignored = plt.hist(list1, 1000, normed=True, align='mid', color='blue')
    count, bins, ignored = plt.hist(list2, 1000, normed=True, align='mid', color='orange')
    plt.xlabel('equivalent failure magnitude of the point load, Fp [kN]')
    plt.ylabel('probability')
    plt.show()
    print('maximum capacity in bending and shear together')

    time_elapsed = (time.clock() - time_start)
    print('computation time images =',time_elapsed,'sec')


```

A.2. Run multiple projects in DIANA

```
1  ##########################################################################
2  # DianaIE 10.2 update 2017-09-22 08:09:41
3  # Python  3.6.1
4  # Session recorded at 2017-11-04 00:22:36
5  ##########################################################################
6  A=["Analysis1","Analysis2","Analysis3","Analysis4","Analysis5","Analysis6","Analysis7"
   ,"Analysis8","Analysis9","Analysis10","Analysis11","Analysis12","Analysis13","Analysis
   14","Analysis15"]
7  B=[0,0,0,0,0,0,0,0,0,0,0,0,0,0,0]
8  B[0]="C:/Users/Gebruiker/Documents/TU
   Delft/Master/Thesis/DIANA/model_dat_files/tensile_stress_rebar/1.dat"
9  B[1]="C:/Users/Gebruiker/Documents/TU
   Delft/Master/Thesis/DIANA/model_dat_files/tensile_stress_rebar/2.dat"
10 B[2]="C:/Users/Gebruiker/Documents/TU
   Delft/Master/Thesis/DIANA/model_dat_files/tensile_stress_rebar/3.dat"
11 B[3]="C:/Users/Gebruiker/Documents/TU
   Delft/Master/Thesis/DIANA/model_dat_files/tensile_stress_rebar/4.dat"
12 B[4]="C:/Users/Gebruiker/Documents/TU
   Delft/Master/Thesis/DIANA/model_dat_files/tensile_stress_rebar/5.dat"
13 B[5]="C:/Users/Gebruiker/Documents/TU
   Delft/Master/Thesis/DIANA/model_dat_files/tensile_stress_rebar/6.dat"
14 B[6]="C:/Users/Gebruiker/Documents/TU
   Delft/Master/Thesis/DIANA/model_dat_files/tensile_stress_rebar/7.dat"
15 B[7]="C:/Users/Gebruiker/Documents/TU
   Delft/Master/Thesis/DIANA/model_dat_files/tensile_stress_rebar/8.dat"
16 B[8]="C:/Users/Gebruiker/Documents/TU
   Delft/Master/Thesis/DIANA/model_dat_files/tensile_stress_rebar/9.dat"
17 B[9]="C:/Users/Gebruiker/Documents/TU
   Delft/Master/Thesis/DIANA/model_dat_files/tensile_stress_rebar/10.dat"
18 B[10]="C:/Users/Gebruiker/Documents/TU
   Delft/Master/Thesis/DIANA/model_dat_files/tensile_stress_rebar/11.dat"
19 B[11]="C:/Users/Gebruiker/Documents/TU
   Delft/Master/Thesis/DIANA/model_dat_files/tensile_stress_rebar/12.dat"
20 B[12]="C:/Users/Gebruiker/Documents/TU
   Delft/Master/Thesis/DIANA/model_dat_files/tensile_stress_rebar/13.dat"
21 B[13]="C:/Users/Gebruiker/Documents/TU
   Delft/Master/Thesis/DIANA/model_dat_files/tensile_stress_rebar/14.dat"
22 B[14]="C:/Users/Gebruiker/Documents/TU
   Delft/Master/Thesis/DIANA/model_dat_files/tensile_stress_rebar/15.dat"
23 for i in range(len(A)):
24     newProject( "./Untitled/Untitled", 10 )
25     setModelAnalysisAspects( [ "STRUCT" ] )
26     setModelDimension( "2D" )
27     setDefaultMeshOrder( "QUADRATIC" )
28     setDefaultMesherType( "HEXQUAD" )
29     setDefaultMidSideNodeLocation( "LINEAR" )
30     importModel( B[i], "", True )
31     saveProjectAs( "C:/Users/Gebruiker/Documents/TU
       Delft/Master/Thesis/DIANA/model_dat_files/tensile_stress_rebar/experiment_with_ten
       sile_stress_rebar.dpf" )
32     addAnalysis( A[i] )
33     addAnalysisCommand(  A[i], "NONLIN", "Structural nonlinear" )
34     addAnalysisCommandDetail(  A[i], "Structural nonlinear", "TYPE/GEOMET" )
35     setAnalysisCommandDetail(  A[i], "Structural nonlinear", "TYPE/GEOMET", True )
36     addAnalysisCommandDetail(  A[i], "Structural nonlinear", "EXECUT(1)/LOAD/LOADNR" )
37     setAnalysisCommandDetail(  A[i], "Structural nonlinear",
       "EXECUT(1)/LOAD/LOADNR", 1 )
38     setAnalysisCommandDetail(  A[i], "Structural nonlinear",
       "EXECUT(1)/LOAD/STEPS/EXPLIC/SIZES", "0.8(24)" )
39     addAnalysisCommandDetail(  A[i], "Structural nonlinear",
       "EXECUT(1)/LOAD/STEPS/EXPLIC/ARCLEN" )
40     setAnalysisCommandDetail(  A[i], "Structural nonlinear",
       "EXECUT(1)/LOAD/STEPS/EXPLIC/ARCLEN", True )
41     setAnalysisCommandDetail(  A[i], "Structural nonlinear",
       "EXECUT(1)/ITERAT/MAXITE", 10 )
42     setAnalysisCommandDetail(  A[i], "Structural nonlinear",
       "EXECUT(1)/ITERAT/CONVER/SIMULT", True )
43     addAnalysisCommandDetail(  A[i], "Structural nonlinear",
       "EXECUT(1)/ITERAT/LINESE" )
44     setAnalysisCommandDetail(  A[i], "Structural nonlinear",
       "EXECUT(1)/ITERAT/LINESE", True )
45     setAnalysisCommandDetail(  A[i], "Structural nonlinear",
```

```
        "EXECUT(1)/ITERAT/CONTIN", True )
46      setAnalysisCommandDetail(  A[i], "Structural nonlinear",
        "EXECUT(1)/ITERAT/MAXITE", 25 )
47      setAnalysisCommandDetail(  A[i], "Structural nonlinear",
        "EXECUT(1)/ITERAT/CONVER/DISPLA/NOCONV", "CONTIN" )
48      setAnalysisCommandDetail(  A[i], "Structural nonlinear",
        "EXECUT(1)/ITERAT/CONVER/FORCE/NOCONV", "CONTIN" )
49      runSolver( A[i] )
50      showView( "RESULT" )
51      setResultPlot( "contours", "Displacements/node", "TDtY" )
52      saveProject(  )
53
```

B. Derivation structural formulas

B.1. Bending capacity formulas

In this appendix, the Monnier approach and the current Eurocode are derived. To clearly distinguish between Monnier's approach and the current Eurocode, the assumptions in the Eurocode need to be introduced as well. The stress-strain relation that is showed in Figure B.0.1 was used by Monnier together with the parameters Table 16.

Stress-strain relation used by Monnier:

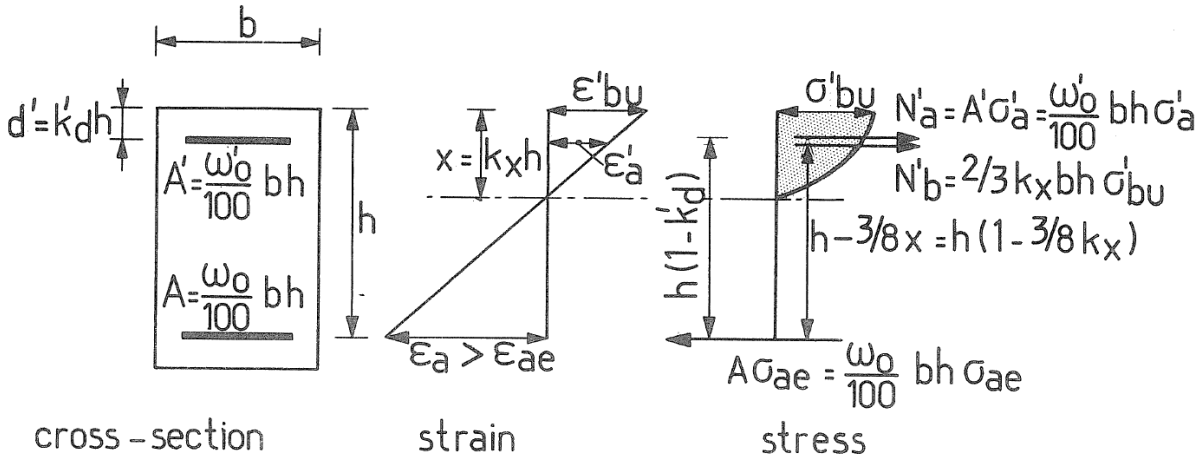

Figure B.0.1 stress-strain relation used in the analytical derivation in Monnier's report about his experiment

The following parameters are used:

Table 16 parameters with units as they were used in the derivation in Monnier's report about his experiment

variable	unit	definition
b	cm	width of the cross-section
h	cm	effective depth of the bottom reinforcement
d'	cm	effective depth of the top reinforcement
ω'0	%	reinforcement ration (top)
ω0	%	reinforcement ration (bottom)
εa	-	strain in bottom reinforcement
ε'a	-	strain in top reinforcement
ε'bu	-	strain at the top of the cross-section
σ'bu	kg/cm^2	stress at the top of the cross-section
σae	kg/cm^2	yield stress of the bottom reinforcement
σ'ae	kg/cm^2	yield stress of the top reinforcement
σ'a	kg/cm^2	stress in the top reinforcement
εae	-	yield strain
k'd	-	ratio between the effective depth of the top reinforcement and the effective depth of the bottom reinforcement (k'd=d'/h)
kx	-	ratio between the concrete compressive zone and the effective depth of the bottom reinforcement (kx=x/h)

With this information given one could derive the formula for the bending moment capacity in the ULS. To start off the strain distribution.

From the strain distribution:

$$\varepsilon'_a = \varepsilon'_{bu} * \frac{x - d'}{x} = \varepsilon'_{bu} * (1 - \frac{k'_d}{k_x}) \tag{B.1}$$

And thus

$$\sigma'_a = \varepsilon'_{bu} * E_a * \left(1 - \frac{k'_d}{k_x}\right) \leq \sigma'_{ae} \tag{B.2}$$

From horizontal equilibrium follows:

$$N'_b + N'_a - N_a = 0 \tag{B.3}$$

The known formulas depending on the variables introduced earlier are replaced. The assumption here is that the bottom reinforcement is yielding.

$$\frac{2}{3} * k_x * \sigma'_{bu} * b * h + \frac{\omega'_0}{100} * \varepsilon'_{bu} * E_a * \left(1 - \frac{k'_d}{k_x}\right) * b * h - \frac{\omega_0}{100} * \sigma_{ae} * b * h = 0 \tag{B.4}$$

Now the width and the depth of the cross-section can be cancelled out and the formula can be rearranged into a quadratic equation.

$$k_x^2 + k_x * \frac{3 * \omega_0}{200 * \sigma'_{bu}} * \left(\frac{\omega'_0}{\omega_0} * \varepsilon'_{bu} * E_a - \sigma_{ae}\right) - \frac{3 * \omega_0}{200 * \sigma'_{bu}} * \left(\frac{\omega'_0}{\omega_0} * \varepsilon'_{bu} * E_a * k'_d\right) = 0 \tag{B.5}$$

This quadratic formula can be solve using the ABC-formula which gives two possible answers. Please note that the value of kx has to be in the range of (0-0.6] otherwise the bottom reinforcement is not yielding. Therefore there is only one solution to this formula.

$$\begin{aligned} A &= 1 \\ B &= \frac{3 * \omega_0}{200 * \sigma'_{bu}} * \left(\frac{\omega'_0}{\omega_0} * \varepsilon'_{bu} * E_a - \sigma_{ae}\right) \\ C &= -\frac{3 * \omega_0}{200 * \sigma'_{bu}} * \left(\frac{\omega'_0}{\omega_0} * \varepsilon'_{bu} * E_a * k'_d\right) \\ k_x &= \frac{-B + \sqrt{B^2 - 4 * C}}{2} \end{aligned} \tag{B.6}$$

When kx is known the bending moment capacity of the cross-section can be calculated.

$$M_u = \left(N'_b * h * \left(1 - \frac{3}{8} * k_x\right) + N'_a * h * (1 - k'_d)\right) \tag{B.7}$$

Now all the known expressions of the internal forces can be substituted in.

$$M_u = \left(\frac{2}{3} * k_x * \sigma'_{bu} * \left(1 - \frac{3}{8} * k_x\right) + \frac{\omega'_0}{100} * \varepsilon'_{bu} * E_a * \left(1 - \frac{k'_d}{k_x}\right) * (1 - k'_d)\right) * b * h^2 \quad (B.8)$$

After finding the expression for the moment capacity, one should check whether or not the top reinforcement yields. So the following check has to be done.

$$\varepsilon'_{bu} * \left(1 - \frac{k'_d}{k_x}\right) * E_a \geq \sigma'_{ae} \quad (B.9)$$

If this inequality holds the expression for Mu has to be replaced by:

$$M_u = \left(\frac{2}{3} * k_x * \sigma'_{bu} * \left(1 - \frac{3}{8} * k_x\right) + \frac{\omega'_0}{100} * \sigma'_{ae} * (1 - k'_d)\right) * b * h^2 \quad (B.10)$$

Since

$$\sigma'_a = \sigma'_{ae} = \sigma_{ae} \quad (B.11)$$

Thus

$$\frac{2}{3} * k_x * \sigma'_{bu} - \frac{\sigma_{ae}}{100} * (\omega_0 - \omega'_0) = 0 \quad (B.12)$$

And

$$k_x = \frac{3 * (\omega_0 - \omega'_0)}{200} * \frac{\sigma_{ae}}{\sigma'_{bu}} \quad (B.13)$$

In the Eurocode the assumptions are little bit different but not entirely. Stress-strain relation according to the Eurocode are showed in Figure B.0.2.

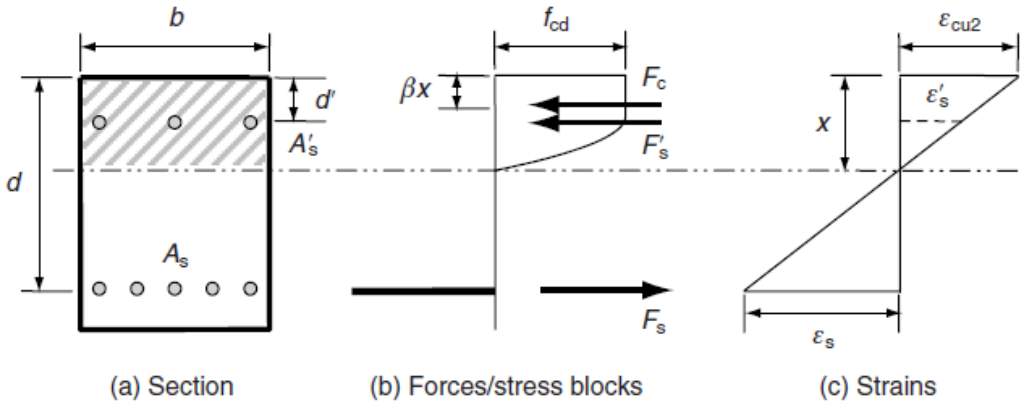

Figure B.0.2 Stress-strain relation as used in the Eurocode

The following parameters are used:

Table 17 variables and corresponding units used in the Eurocode to determine the bending moment resistance of a reinforced concrete beam.

variable	unit	definition
b	mm	width of the cross-section
d	mm	effective depth of the cross-section
d'	mm	effective depth of the top reinforcement
As'	mm^2	cross-sectional area of the top reinforcement
As	mm^2	cross-sectional area of the bottom reinforcement
β	-	ratio ≈ 0,39
Es	N/mm^2	youngs'modulus of the reinforcement steel
εs	-	strain in the bottom reinforcement
x	mm	depth of the concrete compressive zone
fav	N/mm^2	averaged stress in the concrete compressive zone above the neutral axis
fyk	N/mm^2	characteristic yield strength
γs	-	partial factor yield strength
ε's	-	strain in the top reinforcement
εcu2	-	maximum strain at the top of the cross-section

With this information given in Table 17 one could derive the formula for the bending moment capacity in the ULS. To start off the strain distribution.

From the strain distribution:

$$\varepsilon'_s = \varepsilon_{cu2} * \left(1 - \frac{d'}{x}\right) \qquad (B.14)$$

The next step in finding out what the maximum moment capacity is of the cross-section, the internal forces need to be calculated.

$$F_c = f_{av} * b * x$$
$$F_s' = A_s' * E_s * \varepsilon_s' = A_s' * E_s * \varepsilon_{cu2} * \left(1 - \frac{d'}{x}\right) \quad \text{(B.15)}$$
$$F_s = \frac{f_{yk}}{\gamma_s} * A_s$$

With horizontal equilibrium an equation can be derived to find an expression for the height of the concrete compressive zone.

$$F_c + F_s' - F_s = 0 \quad \text{(B.16)}$$

Now substitute the known expressions.

$$f_{av} * b * x + A_s' * E_s * \varepsilon_{cu2} * \left(1 - \frac{d'}{x}\right) - \frac{f_{yk}}{\gamma_s} * A_s = 0 \quad \text{(B.17)}$$

The formula can be rewritten in the form of a quadratic equation.

$$x^2 + \frac{\left(A_s' * E_s * \varepsilon_{cu2} - \frac{f_{yk}}{\gamma_s} * A_s\right)}{f_{av} * b} * x - \frac{d' * A_s' * E_s * \varepsilon_{cu2}}{f_{av} * b} = 0 \quad \text{(B.18)}$$

This quadratic formula can be solve using the ABC-formula which gives two possible answers. Please note that the value of x has to be in the range of (0-0.6] times h, otherwise the bottom reinforcement is not yielding. Therefore there is only one solution to this formula.

$$A = 1$$
$$B = \frac{\left(A_s' * E_s * \varepsilon_{cu2} - \frac{f_{yk}}{\gamma_s} * A_s\right)}{f_{av} * b} \quad \text{(B.19)}$$
$$C = -\frac{d' * A_s' * E_s * \varepsilon_{cu2}}{f_{av} * b}$$
$$x = \frac{-B + \sqrt{B^2 - 4 * A * C}}{2 * A}$$

With this information the maximum moment capacity of the cross-section can almost be calculated. But first, one check has to be done. The check whether or not the top reinforcement is yielding or not.

$$\varepsilon_{cu2} * \left(1 - \frac{d'}{x}\right) \geq \frac{f_{yk}}{\gamma_s * E_s} \quad \text{(B.20)}$$

If this is true then:

$$F_c + F_s' - F_s = 0 \quad \text{(B.21)}$$

Gives:

$$f_{av} * b * x - (A_s - A'_s) * \frac{f_{yk}}{\gamma_s} = 0$$
$$x = \frac{(A_s - A'_s)}{f_{av} * b} * \frac{f_{yk}}{\gamma_s} \quad (B.22)$$

And finally:

$$M_{ED} = f_{av} * b * x * (d - \beta * x) + A'_s * \frac{f_{yk}}{\gamma_s} * (d - d') \quad (B.23)$$

And if:

$$\varepsilon_{cu2} * \left(1 - \frac{d'}{x}\right) < \frac{f_{yk}}{\gamma_s * E_s} \quad (B.24)$$

Then:

$$M_{ED} = f_{av} * b * x * (d - \beta * x) + A'_s * E_s * \varepsilon_{cu2} * \left(1 - \frac{d'}{x}\right) * (d - d') \quad (B.25)$$

The different parameters which are used in the two calculations make it confusing to understand both. The parameter h, in Monnier his assumption, is call d in the Eurocode calculation. Also, the units as mentioned before are different. The resemblance between both calculations is that both procedures have a conditional statement, whether or not the top reinforcement is yielding. It is also striking that both expression look very similar in their final form.

The Eurocode expression for the maximum moment capacity has two partial factors in it. These factors will be set equal to one when the reliability calculation will be done. The expression with respect to the allowable stress level in the concrete and the steel are therefore set equal to the characteristic values. The partial factors are a result of a Level I reliability calculation, in this thesis the goal is to perform a Level II or Level III reliability calculation. During the reliability calculations the reliability will be expressed into a beta value, the normal inverse of the probability of failure. When this assumption is done, one could prove that the two expressions (Monnier's expression and the Eurocode expression for the bending moment capacity) give the same result when:

$$f_{av} = \frac{2}{3} * \sigma'_{bu} \quad (B.26)$$

And

$$\beta = \frac{3}{8} \quad (B.27)$$

In the Eurocode is a parameter beta (this is not the reliability value of beta) given as approximately $\beta = 0.39$ and $f_{av} \approx 0.69 * \sigma_{cd}$ which stated that Monnier's and the Eurocode

expressions are very close to each other. For the convenience of the rest of the thesis, from this point on the Eurocode expression will be used.

The evaluation of the analytical model is done in the following way: Firstly, the expression introduced at the top of this page is used to determine the maximum moment capacity of the cross-section. Moreover, not only the bending, also shear is briefly touched upon. It is done to show that in this specific case shear is not the most probable failure mechanism. Secondly, the geometry of the beam is evaluated. With the given load case one could determine where the maximum bending moment will occur, when the load is increased. Thereafter, the maximum bending moment in the structure can be expressed in terms of the load on the structure. This relation is calculated by making use of the theory of plasticity. Thirdly, the same procedure is done for the maximum shear load. The highest shear force value in the structure can be expressed in terms of the load solicited on the structure. Finally, When there are expressions for both the maximum bending moment and the maximum shear force in terms of the same variable (the force acting on the structure), they can be compared. This comparison will be done in the next paragraph.

In order to prove that shear has very little influence on the failure mode of this specific beam, the conservative Eurocode expression for shear is used. The goal is not to use a very realistic formulation for the shear behaviour, but the target is to show that bending is the main failure mode. Shear failure in concrete is a very complex process. This is not the main focus of the thesis and therefore this approach is taken. For bending the expression of the Eurocode without partial factors is used and for shear the Eurocode expression with partial factors is used.

B.2. Shear force capacity formulas

The shear formulation of the Eurocode NEN-EN 1990 is as follows.

The maximum allowable shear force in a structure with shear reinforcement is:

$$V_{rd_{max}} = 1.0 * b * (d - d') * 0.6 * \left(1 - \frac{f_{ck}}{250}\right) * \frac{f_{ck}}{1.5} \quad (B.28)$$

The maximum allowable shear force in a structure without shear reinforcement is:

$$V_{rd_c} = 0.12 * k * (100 * \rho_l * f_{ck})^{\frac{1}{3}} * b * d$$
$$k = \min(1 + \sqrt{\frac{200}{d}}, 2) \quad (B.29)$$

And

$$V_{equivalent} = \max(V_{rd_{max}}, V_{rd_c}) * 10^{-3} \quad (B.30)$$

This design formula (B.29) for concrete beams without shear reinforcement is empirical derived from experiments which are done in 1995 by König and Fischer. From the data gathered in the experiment the 0.12 value in formula (4.3) was found. They started off with equation (B.31). This expression consists of four variables from which one is prescribed as an uncertainty parameter. This stochastic parameter has a probability density function with corresponding mean value and standard deviation. The formula for the shear resistance for concrete cross-sections without shear reinforcement stems from the following configuration:

$$V_u = c * \xi * (100 * \rho_l)^{\frac{1}{3}} * f_c^{\frac{1}{3}} \quad (B.31)$$

In this formula:
ξ is the same as the variable k introduced in the design formulas
ρ_l is the longitudinal reinforcement density
$f_c$is the concrete compressive strength
c is an uncertainty factor

As introduced earlier (König and Fischer 1995) has done an investigation to the behaviour of concrete beams without shear reinforcement together with Fischer. They tested 176 beams with different concrete compressive strengths (varying from 20 Mpa to 110 Mpa). As a matter of fact, this investigation has covered a lot of information in different situations. Therefore, the results of this investigations are used in this thesis. (Konig and Fischer) aspire to find the behaviour of the uncertainty factor c. In the Eurocode and Model Code, the numerical value for the uncertainty factor is 0.12. Moreover, this is result of the work done by König and Fischer.

They have found a distribution which approximately matches the behaviour of the uncertainty factor. They transformed the formula into the following form which consists of random variables.

$$V_u = \frac{c}{z}\xi * (100 * \rho_l)^{\frac{1}{3}} * f_{cm}^{\frac{1}{3}} \quad (B.32)$$

In which:
c is a scalar

z is a lognormal random variable
f_{cm} is a lognormal random variable

They found a value for c equal to 0.15 and for normal strength concrete (≤60MPa according to König and Fischer) the z values are as follows:

$$\mu_z = 0.92$$
$$\sigma_z = 0.12$$

These values in combination with eq. (B.32) will be used in chapter 4 to determine the shear capacity of the beam.

All the expressions necessary to determine the maximum resistances in the different failure modes are known. The next step is to set up an expression for failure in bending in terms of the maximum bending moment. Note that the bending moment capacity for the field moment and the support moment have different values but, there is taken care of later on. In the previous chapter is shown that when the maximum shear force is exceeded anywhere in the structure, failure occurs immediately. However, for bending failure this is slightly more complicated.

To start off, the expression for the maximum shear force occurring in the structure is derived. Starting with an elastic situation in which symmetry is assumed, the shear force distribution can be derived quite easily.

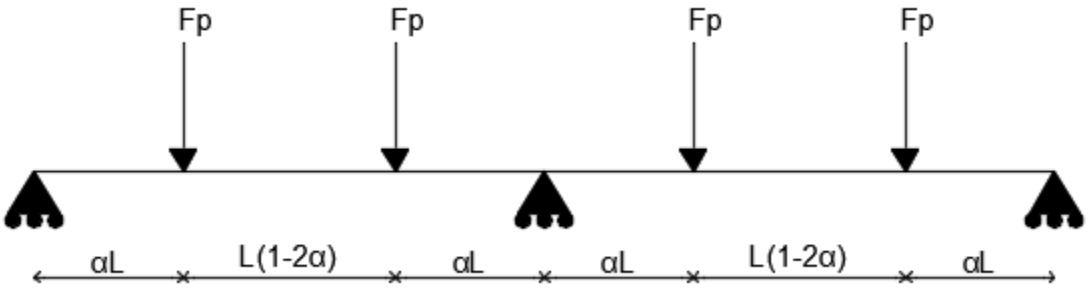

Figure B.0.3 geometry of the structure

In Figure B.0.3 geometry of the structure, one could see that the structure has a clear symmetry. In order to make use of this simplification, half of the structure is removed and the one of the supports should be replaced by a clamped end. In Figure B.0.4 the structure after making use of symmetry, it is visible that there is chosen to just look at the left hand side of the structure.

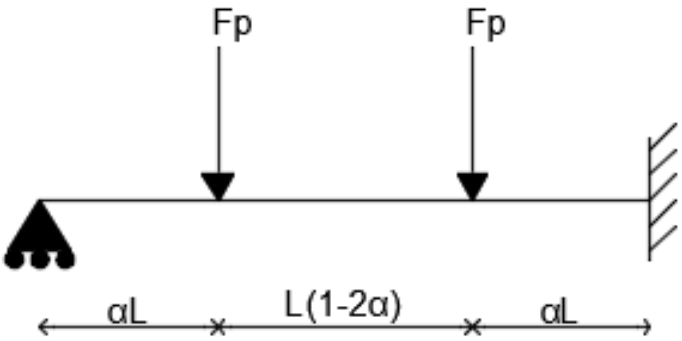

Figure B.0.4 the structure after making use of symmetry

Now the simplification is done, the shear force distribution can be drawn. In Figure B.0.5 shear force distribution of the structure, the values of the shear force in the specific parts of the structure. Please note that in theory it is not known on beforehand whether the line between two external forces is above or under the zero line. However, it will be proven later on that the line between the external forces is drawn on the correct side. Furthermore, since both of the external forces have the same value, the maximum shear force is equal to the reaction force in point B.

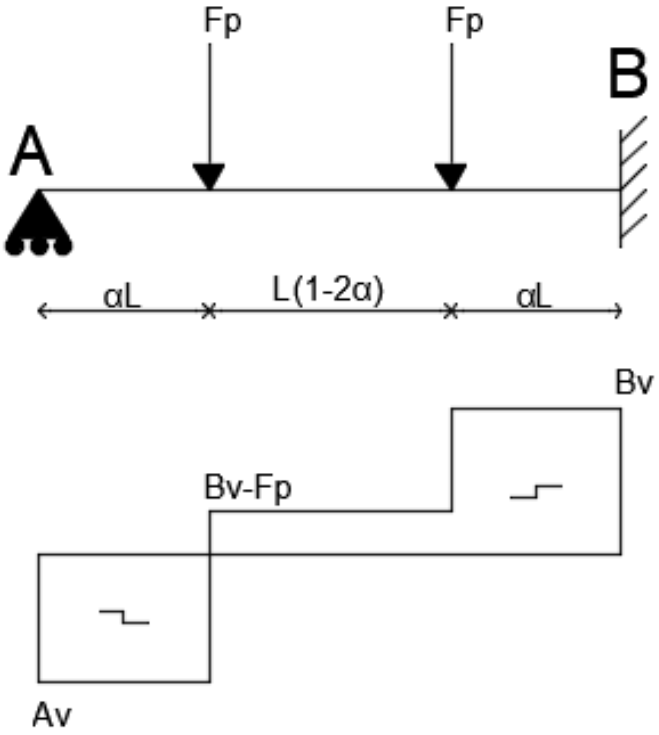

Figure B.0.5 shear force distribution of the structure

Since there still has to be dealt with a statically indeterminate structure, therefore is made use of the “forget me nots”. By using these formulas, the force flow can be determined entirely. The requirement chosen to use is the deflection in point A has to be zero. This means that the support in point A will be replaced by a force which is denoted as Av (Figure

B.0.6 support of A replaced by a force). The magnitude of Av needs to have a value which satisfice the requirement of zero displacement in A.

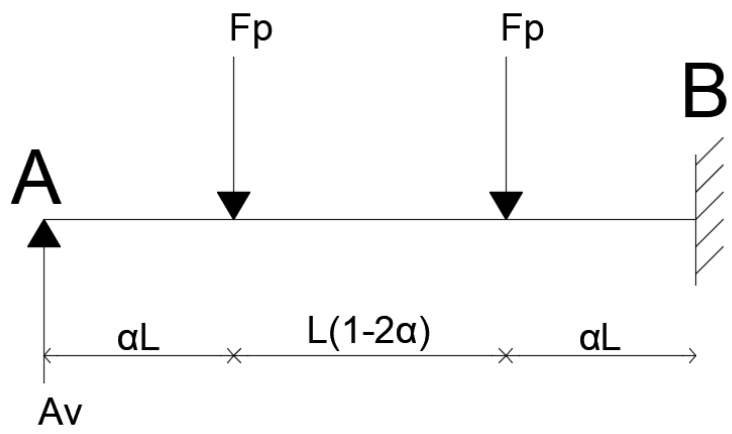

Figure B.0.6 support of A replaced by a force

The formulation for the deflection in point A is as follows:

$$\delta_A = \frac{A_v * L^3}{3 * EI} - \left(\frac{F_p * L^3\{\alpha^3 + (1-\alpha)^3\}}{3 * EI} + \frac{F_p * L^3\{\alpha^2 * (1-\alpha) + (1-\alpha)^2 * \alpha\}}{2 * EI} \right) = 0 \quad (B.33)$$

This expression can be rewritten as an equation for Av, namely.

$$A_v = \frac{F_p}{2} * \{2 * (\alpha^3 + (1-\alpha)^3) + 3 * (\alpha^2 * (1-\alpha) + (1-\alpha)^2 * \alpha)\}$$

$$A_v = \frac{F_p}{2} * \{3 * \alpha^2 - 3 * \alpha + 2\} \quad (B.34)$$

This automatically means that:

$$B_v = 2 * F_p - A_v = \frac{F_p}{2} * \{6 - 3 * \alpha^2 - 3 * \alpha\} \quad (B.35)$$

Thus the maximum shear force that occurs in the structure is:

$$V_{max} = \max(|A_v|, |B_v|) \quad (B.36)$$

Now the maximum value of the force that occurs in the structure is known and the Eurocode expression is introduced, the next step can be taken. One could now derive an expression for the maximum force allowed on the structure before failure occurs. The V equivalent is now replaced by the Vu from the experiment introduced earlier.

A quick summary of the two formulas that are derived:

$$V_{equivalent} = V_u \tag{B.37}$$

And

$$V_{max} = \max(|A_v|, |B_v|) \tag{B.38}$$

For the maximum load the following condition holds:

$$V_{equivalent} = V_{max} \tag{B.39}$$

Note that both Av and Bv are functions of the Fp in which the final function has to be expressed. When a closer look is taken on the expressions for Av and Bv is taken one could Vmax write in a different form.

$$\begin{aligned} A_v &= \frac{F_p}{2} * \{3 * \alpha^2 - 3 * \alpha + 2\} \\ B_v &= \frac{F_p}{2} * \{6 - 3 * \alpha^2 - 3 * \alpha\} \\ V_{max} &= \max(|A_v|, |B_v|) \end{aligned} \tag{B.40}$$

Thus:

$$V_{max} = \frac{F_p}{2} * \max(|\{3 * \alpha^2 - 3 * \alpha + 2\}|, |\{6 - 3 * \alpha^2 - 3 * \alpha\}|) \tag{B.41}$$

Therefore it could be said that:

$$F_p = V_{equivalent} * \frac{2}{\max(|\{3 * \alpha^2 - 3 * \alpha + 2\}|, |\{6 - 3 * \alpha^2 - 3 * \alpha\}|)} \tag{B.42}$$

C. Case study reliability calculation without redistribution of forces

C.1. Semi-probabilistic calculation of the structure's analytical model

Keeping the assumptions discussed paragraph 4.1.1 in mind, with the Eurocode the cross-sectional resistance can be calculated. Using Appendix B.1 once again, the described procedure can be followed:

First the height of the concrete compressive zone is calculated. Within this calculation there is assumed that the reinforcement steel in the compressive zone is yielding.

$$x_u = \frac{fy_k}{\gamma_s} * \frac{As - A'_s}{f_{av} * b} \tag{C.43}$$

This assumption is checked in eq. (C.44).

$$\varepsilon'_s \geq \varepsilon_{s_{yield}} \leftrightarrow \varepsilon_{cu2} * (1 - \frac{d'}{x_u}) \geq \frac{f_{yk}}{\gamma_s * E_s} \tag{C.44}$$

When inequality (C.44) holds the design moment capacity can be calculated in the following way:

$$M_{rd} = F_c * (d - \beta_u * x_u) + F'_s * (d - d')$$
$$F_c = f_{av} * b * x_u \tag{C.45}$$
$$F'_s = \frac{fy_k}{\gamma_S} * A'_s$$

However, when the inequality does not hold, the design moment capacity has to be determined by making use of the strain compatibility method. The method is consisting of the following equations to determine the internal forces:

$$F_c = f_{av} * b * x_u \tag{C.46}$$

$$F'_s = E_s * \varepsilon'_s * A'_s$$
$$\varepsilon'_s = \varepsilon_{cu2} * \left(1 - \frac{d'}{x_u}\right) \tag{C.47}$$

Using horizontal equilibrium of force gives expression (4.20). Thereafter equation(4.18) and (4.19) can be substituted.

$$F_c + F'_s = F_s \tag{C.48}$$

$$f_{av} * b * x_u + E_s * \varepsilon'_s * A'_s = \frac{fy_k}{\gamma_S} * A_s$$

$$f_{av} * b * x_u^2 + \left(E_s * \varepsilon_{cu2} * A'_s - \frac{fy_k}{\gamma_S} * A_s\right) * x_u - d' * E_s * \varepsilon_{cu2} * A'_s = 0$$

Solving the quadratic equation for x by using the ABC-formula. It turns out that there is only one physically possible answer:

$$x_u = -\frac{\left(E_s * \varepsilon_{cu2} * A'_s - \frac{fy_k}{\gamma_S} * A_s\right)}{2 * f_{av} * b} + \frac{\sqrt{\left(\frac{E_s * \varepsilon_{cu2} * A'_s - \frac{fy_k}{\gamma_S} * A_s}{f_{av} * b}\right)^2 + \frac{4 * d' * E_s * \varepsilon_{cu2} * A'_s}{(f_{av} * b)^2}}}{2} \qquad (C.49)$$

With this value for height of the concrete compressive zone the last step can be made. The cross-sectional moment capacity is calculated by using eq. (4.22).

$$M_{rd} = F_c * (d - \beta_u * x_u) + F'_s * (d - d') \qquad (C.50)$$

To see what the recommendations of the Eurocode are, the numerical values are filled in. The Eurocode makes use of the characteristic values of the stochastic variables. For the resistance part of the limit state function this characteristic value is the 5-quantile of the probability density function. The characteristic value of the solicitation part of the limit state function is the 95-quantile of the probability density function of its variable.
Using the information state above, the height of the concrete compressive zone is calculated. First with the assumption that the reinforcement steel in the compressive zone is yielding.

$$x_u = \frac{391.6}{1.15} * \frac{\frac{3-2}{4} * \pi * 12^2}{0.6 * 0.69 * 23.28 * 150} = 26.6[mm]$$

With this height of the concrete compressive zone, the assumption of the yielding reinforcement in the compressive zone can be checked.

$$3.5 * 10^{-3} * (1 - \frac{24}{26.6}) \geq \frac{391.7}{1.15 * 199 * 10^3}$$

$$3.4 * 10^{-4} \geq 1.7 * 10^{-3}$$

The assumption was not correct, and the strain compatibility method needs to be used. Thus:

$$x_u = -\frac{\left(1.73 * 3.5 * 10^3 * \frac{2}{4} * \pi * 12^2 - \frac{391.6}{1.15} * \frac{3}{4} * \pi * 12^2\right)}{2 * 0.69 * 0.6 * 23.28 * 150} + \sqrt{\left(\frac{1.73 * 3.5 * 10^3 * \frac{2}{4} * \pi * 12^2 - \frac{391.6}{1.15} * \frac{3}{4} * \pi * 12^2}{4 * 0.69 * 0.6 * 23.28 * 150}\right)^2 + \frac{24 * 1.73 * 3.5 * 10^3 * \frac{2}{4} * \pi * 12^2}{0.69 * 0.6 * 23.28 * 150}} = 38.64\ [mm]$$

Now the height of the compressive zone is known, the magnitude of the internal forces can be calculated. Thereafter the design bending moment resistance can be determined.

$$F_c = 0.6 * 0.69 * 23.28 * 150 * 38.64 = 55.8 * 10^3\ [N]$$

$$F_s' = 173 * 3.5 * \left(1 - \frac{24}{36.64}\right) * \frac{2}{4} * \pi * 12^2 = 59.9 * 10^3\ [N]$$

$$M_{rd} = 55.8 * 10^3 * (236 - 0.39 * 28.95) + 59.9 * 10^3 * (236 - 24) = 25.0 * 10^6\ [Nmm]$$

For statically determinate structures this would be the end of the design resistance calculation with respect to bending failure. However, in this thesis must be dealt with statically indeterminate structures. As explained earlier, plastic hinges can develop in the structure and by allowing more deformation. The force on the structure can be increased further. In the Eurocode this is partly allowed, in paragraph 4.3.3 the moment reduction will be calculated. Before this calculation will be executed, rotation capacity must be checked. It turns out that there is no moment reduction possible.

$$M_{rd} \geq M_{ED} \qquad (C.51)$$

With linear elastic theory, the maximum hogging moment can be translated to a deterministic load. Figure 2.10 forget me nots; simply supported beam with a moment acting at one side and simply supported beam with one vertical point at distance ‘a’ from the left-hand side.), gives the tools to do this. Together with Figure 2.12 and Figure 2.13 in which the use of the forget-me-nots is shown graphically, the following derivation can be done:

$$\frac{M_{ED} * l}{3 * EI} = \frac{F_p * l^2}{6 * EI} * \left(2 * \frac{a}{l} - 3 * \frac{a^2}{l^2} + \frac{a^3}{l^3} + \frac{a}{l} - \frac{a^3}{l^3}\right)$$

$$a = l * (1 - \alpha) \qquad (C.52)$$

$$F_p = \frac{2 * M_{ED}}{3 * l * (1 - \alpha) * \alpha}$$

$$F_p = 34.8[kN]$$

C.2. Full-probabilistic calculation of the structure's analytical model

The full-probabilistic calculation methods (level III) in this appendix is basically the same as done in paragraph 4.4. The limit state functions used are slightly. The full-probabilistic calculation procedure "explicit calculation" is still used. This method is the least time-consuming method and therefor preferred. It consists of one single expression to calculate the reliability index, equation (C.53). Within this procedure there is assumed that the stochastic variables of the limit state function are independent and normal distributed. Under these assumptions the reliability index can be calculated in the following way:

$$\beta = \frac{\mu(Z)}{\sigma(Z)} \qquad (C.53)$$

And thus, the probability of failure:

$$P(F) = \Phi(-\beta) \qquad (C.54)$$

The limit state functions and the properties of the random variables are known. Moreover, the force parameter F_p is still assumed to be deterministic. Also, the correlation between the bending moment resistance is assumed to be independent of each other. The reason for this is: one bending moment is resistance of a negative (field) moment and the other bending moment is the resistance of a positive (support) moment. Thus, these moment resistances are completely different from each other.

Let us now recall the necessary information before moving on to the calculations. As mentioned in the paragraph 2.4.1. there are three possible failure mechanisms within the assumptions in this thesis. Table 1 limit state functions of the failure mechanisms) on page 17 has given all the information about the three limit state functions. In paragraph 4.2.2 a Monte Carlo simulation is done to find out what the distribution is of the moment resistance. In the remark is explained that because of time reduction is chosen for an approximation of the moment resistance of the cross-section. The mean value and standard deviation of the resistance of the plastic hinges is approached by:

$$\mu_{M_s} = 31.85$$
$$\sigma_{M_s} = 1.61$$
$$V_M = \frac{\sigma_{M_s}}{\mu_{M_s}} = 0.05$$

And

$$\mu_{M_f} = 21.23$$
$$\sigma_{M_f} = 1.07$$
$$V_M = \frac{\sigma_{M_f}}{\mu_{M_f}} = 0.05$$

Another point of attention, the value of the external force on the structure is assumed to be deterministic. This means that the standard deviation of the force is equal to zero. The difference however is that the value for lambda has changed.

$$V_F = 0$$
$$\lambda = \frac{2}{3}$$

Derivation of the design load:

Table 18 and Table 19 present the mean values and standard deviations of the three limit state functions. With this information the reliability index can be calculated according equation (C.51). The result is presented, together with the numerical evaluation in Table 20 deterministic value of failure load of all possible failure mechanisms

Table 18 mean values of the limit state functions

Case:	Mean value:
1	$\mu(Z) = \mu_{M_s} * \left(\frac{\alpha + \lambda}{1 - \alpha}\right) - F_p * \alpha l * \left(\frac{1}{1 - \alpha}\right)$
2	$\mu(Z) = \mu_{M_s} * \left(\frac{1 - \alpha + \lambda}{\alpha}\right) - F_p * \alpha l * \left(\frac{1}{\alpha}\right)$
3	$\mu(Z) = \mu_{M_s} * \left(\frac{\alpha - \alpha * \lambda + \lambda}{1 - 2 * \alpha}\right) - F_p * \alpha l$

Table 19 standard deviations of the limit state functions

Case:	Standard deviation:
1	$\sigma(Z)^2 = \left(\mu_{M_s} * \left(\frac{\alpha}{1-\alpha}\right) * V_M\right)^2 + \left(\mu_{M_f} * \left(1 + \frac{\alpha}{1-\alpha}\right) * V_M\right)^2$
2	$\sigma(Z)^2 = \left(\mu_{M_s} * \frac{1-\alpha}{\alpha} * V_M\right)^2 + \left(\mu_{M_f} * \left(\frac{1}{\alpha}\right) * V_M\right)^2$
3	$\sigma(Z)^2 = \left(\mu_{M_s} * \left(\frac{\alpha}{1-2*\alpha}\right) * V_M\right)^2 + \left(\mu_{M_f} * \left(1 + \frac{\alpha}{1-2*\alpha}\right) * V_M\right)^2$

Table 20 deterministic value of failure load of all possible failure mechanisms

Case	Deterministic F_p
1	$F_p * \alpha l * \left(\frac{1}{1-\alpha}\right) =$ $= M_s * \left(\frac{\alpha+\lambda}{1-\alpha}\right) - \beta * \left(\left(M_s * \left(\frac{\alpha}{1-\alpha}\right) * V_M\right)^2 + \left(M_f * \left(1 + \frac{\alpha}{1-\alpha}\right) * V_M\right)^2\right)^{1/2}$ $F_p * 1.2 = 53.08 - \beta * 1.96$
2	$F_p * \alpha l * \left(\frac{1}{\alpha}\right) =$ $= M_s * \left(\frac{1-\alpha+\lambda}{\alpha}\right) - \beta * \left(\left(M_s * \frac{1-\alpha}{\alpha} * V_M\right)^2 + \left(M_f * \left(\frac{1}{\alpha}\right) * V_M\right)^2\right)^{1/2}$ $F_p * 2.00 = 109.69 - \beta * 3.91$
3	$F_p * \alpha l =$ $= M_s * \left(\frac{\alpha - \alpha * \lambda + \lambda}{1-2*\alpha}\right) - \beta *$ $* \left(\left(M_s * \left(\frac{\alpha}{1-2*\alpha}\right) * V_M\right)^2 + \left(M_f * \left(1 + \frac{\alpha}{1-2*\alpha}\right) * V_M\right)^2\right)^{1/2}$ $F_p * 0.75 = 100.84 - \beta * 3.60$

Finally, with the information obtained from Table 21, the deterministic failure load in the three different cases can be determined. There is chosen to show the deterministic failure load in case of a consequence class 2 and a service period of 50 years ($\beta = 3.8$). The following design load can be calculated:

Table 21: deterministic numerical value of the full-probabilistic calculation procedure for a consequence class 2 and a service period of 50 years.

Case	Deterministic F_p
1	$F_p = 38.01\ kN$
2	$F_p = 47.41\ kN$
3	$F_p = 116.22\ kN$